

310  
6-16-75

Dr-1375

BNWL-1903  
UC-70

---

# Impact Testing of Vitreous Simulated High-Level Waste in Canisters

---

May 1975

Prepared for the U.S. Energy  
Research and Development Administration  
under Contract AT(45-1):1830

MASTER

MASTER

 **Battelle**  
Pacific Northwest Laboratories

MASTER

BNWL-1903

DISTRIBUTION OF THIS DOCUMENT UNLIMITED

## NOTICE

This report was prepared as an account of work sponsored by the United States Government. Neither the United States nor the United States Energy Research and Development Administration, nor any of their employees, nor any of their contractors, subcontractors, or their employees, makes any warranty, express or implied, or assumes any legal liability or responsibility for the accuracy, completeness or usefulness of any information, apparatus, product or process disclosed, or represents that its use would not infringe privately owned rights.

### PACIFIC NORTHWEST LABORATORY

*operated by*

**BATTELLE**

*for the*

**U.S. ENERGY RESEARCH AND DEVELOPMENT ADMINISTRATION**

*Under Contract AT(45-1)-1830*

*On January 19, 1975, research and development programs of the U.S. Atomic Energy Commission (AEC) became part of the newly formed Energy Research and Development Administration (ERDA). In this report, since it refers to work done in 1974, most references are to AEC programs.*

Printed in the United States of America

Available from

National Technical Information Service

U.S. Department of Commerce

5285 Port Royal Road

Springfield, Virginia 22151

Price: Printed Copy \$5.45; Microfiche \$2.25

## **DISCLAIMER**

**This report was prepared as an account of work sponsored by an agency of the United States Government. Neither the United States Government nor any agency Thereof, nor any of their employees, makes any warranty, express or implied, or assumes any legal liability or responsibility for the accuracy, completeness, or usefulness of any information, apparatus, product, or process disclosed, or represents that its use would not infringe privately owned rights. Reference herein to any specific commercial product, process, or service by trade name, trademark, manufacturer, or otherwise does not necessarily constitute or imply its endorsement, recommendation, or favoring by the United States Government or any agency thereof. The views and opinions of authors expressed herein do not necessarily state or reflect those of the United States Government or any agency thereof.**

## **DISCLAIMER**

**Portions of this document may be illegible in electronic image products. Images are produced from the best available original document.**

IMPACT TESTING OF VITREOUS SIMULATED  
HIGH-LEVEL WASTE IN CANISTERS

by T. H. Smith and W. A. Ross

May 1975

**NOTICE**

This report was prepared as an account of work sponsored by the United States Government. Neither the United States nor the United States Energy Research and Development Administration, nor any of their employees, nor any of their contractors, subcontractors, or their employees, makes any warranty, express or implied, or assumes any legal liability or responsibility for the accuracy, completeness or usefulness of any information, apparatus, product or process disclosed, or represents that its use would not infringe privately owned rights.

Battelle  
Pacific Northwest Laboratories  
Richland, Washington 99352

**MASTER**

DISTRIBUTION OF THIS DOCUMENT UNLIMITED

*fy*

## ACKNOWLEDGMENTS

Significant contributions by the following people to the test program and/or this report are gratefully acknowledged: S. L. Sutter removed the particles from the canisters, sieved the particles, and contributed to Sections 8.0 and 9.0. L. C. Schwendiman and M. O. Cloninger contributed to Section 11.0.

## CONTENTS

ACKNOWLEDGMENTS . . . . .	ii
LIST OF FIGURES . . . . .	v
LIST OF TABLES . . . . .	vii
1.0 SUMMARY. . . . .	1
2.0 INTRODUCTION . . . . .	3
Management of High-Level Nuclear Waste . . . . .	3
Waste Fixation Program . . . . .	3
Safety and Systems Evaluation Task of the Waste Fixation Program. . . . .	3
Need for Impact Data . . . . .	5
3.0 REVIEW OF PREVIOUS WORK. . . . .	7
Canister Impact Behavior . . . . .	7
Data for Post-Impact Particle Size Distribution. . . . .	8
Scaling Laws . . . . .	9
4.0 TEST PROGRAM RATIONALE . . . . .	11
Objectives . . . . .	11
Approach . . . . .	11
Selection of Test Conditions . . . . .	12
5.0 SPECIMEN DESCRIPTION . . . . .	15
Glass Description . . . . .	15
Canister Description . . . . .	17
Canister Filling and Heat-Treating Procedures . . . . .	20
Imposed Devitrification. . . . .	22
Comparison of Glass Processing of Specimens with Proposed Large-Scale Processing . . . . .	25
6.0 TESTING PROCEDURES AND CONDITIONS . . . . .	27
Large Specimens. . . . .	27
Small Specimens. . . . .	27
7.0 IMPACT EFFECTS ON THE CANISTERS. . . . .	31
Small Canisters . . . . .	31
Large Canisters. . . . .	38
8.0 CANISTER OPENING AND PARTICLE REMOVAL PROCEDURES . . . . .	45
Large Canisters. . . . .	45

Small Canisters. . . . .	51
Errors Introduced by the Particle Removal Procedures . . . . .	56
9.0 PARTICLE SIZING PROCEDURES . . . . .	59
Large Canisters. . . . .	59
Small Canisters. . . . .	60
Size Sampling with Microscope . . . . .	60
Sieving Accuracy . . . . .	61
10.0 GLASS IMPACT RESULTS . . . . .	63
Fraction of Inventory Broken . . . . .	63
Particle Size Distribution . . . . .	70
Representative Particle Shape; Surface Area Increase . . . . .	77
11.0 USE OF THE RESULTS IN ANALYSIS OF RADIOLOGICAL HAZARDS . . . . .	87
Considerations in Analysis of the Airborne Pathway . . . . .	87
Considerations in Analysis of the Groundwater Pathway . . . . .	90
REFERENCES . . . . .	93
APPENDIX A: Particle Size Distribution Table . . . . .	A.1
APPENDIX B: Data from Size Sampling with Microscope . . . . .	B.1

## LIST OF FIGURES

1	Representative Year-2000 Waste Management System	4
2	Risk Analysis Methodology	5
3	Dependence of Failure Velocity of Filled Cylinders on Length/Diameter Ratio	8
4	Typical Pre-Impact Dimensions of Small Specimens	17
5	Typical Pre-Impact Dimensions of Large Specimens	18
6	Reference High-Level Waste Canister	19
7	Small Canisters Before Impact Testing	24
8	Specimen 15 After Edge-On Impact at 117 fps	31
9	Specimens 23 and 14 After Edge-On Impact at 117 and 114 fps, Respectively	32
10	Specimen 6 After End-On Impact at 117 fps	32
11	Specimen 8 After Edge-On Impact at 66 fps	33
12	Specimen 18 After Edge-On Impact at 44 fps	33
13	Specimen 21 After Edge-On Impact at 25 fps	34
14	High-Speed Photographic Coverage of 30-ft Drop Impact	39
15	High-Speed Photographic Coverage of Side-On Penetration Test	40
16	Large Canister 2 After 44 fps Edge-On Impact	43
17	Wall Removal Scheme for Large Canisters in Edge-On Impact	45
18	Wall Removal Scheme for Large Canister in Side-On Impact	46
19	Large Canister 1 After Opening	47
20	Large Canister 2 After Opening	48
21	Large Canister 3 After Opening	49
22	Large Canister 4 After Opening	49
23	Large Canister 5, Edge Area, After Opening	50
24	Large Canister 5, Mid-Region, After Opening	50
25	Large Canister 6 After Opening	51
26	Small Canister 8 After Opening, Top View	53
27	Small Canister 8 After Opening, Inverted	53
28	Small Canister 11 After Opening, Top View	54
29	Small Canister 11 After Opening, Inverted	54

30	Small Canister 14 After Opening, Top View	55
31	Small Canister 14 After Opening, Inverted	55
32	Small Canister 19 After Opening and Longitudinal Sectioning	56
33	Fraction of Glass Broken	66
34	Glass Breakup is a Local Phenomenon	69
35	Glass Breakup is a Mass/Volume/Area Phenomenon such that the Fraction of Glass Broken is Identical for the Two Cylinders	69
36	Particle Size Distributions for Large Specimens	70
37	Particle Size Distributions for Small Specimens (Controls and 117 fps Specimens Only)	71
38	Magnitude of Sub-20 $\mu$ Fraction for Both Large and Small Specimens	73
39	Prediction Curves for Sub-10 $\mu$ Fines Generation	76
40	Illustration of Sieving Approximation	78
41	Fractional Increase in Geometric Surface Area	81
42	Calculated Deposition of Particles in Nasopharyngeal (N-P), Tracheobronchial (T-B), and Pulmonary (P) Compartments, Relative to Number Inhaled	88
B.1	Photomicrographs of a Sample from the <5 $\mu$ Fraction of Large Test Specimen 2	B.2
B.2	Photomicrographs of a Sample from the <5 $\mu$ Fraction of Small Test Specimen 5	B.3

## LIST OF TABLES

1	Impact Test Velocities	13
2	Chemical Compositions of Simulated Calcine, Frit and Glass	16
3	Comparison of Test Canisters with Full-Size Reference Canister	21
4	Test Conditions for Large Canisters	28
5	Test Conditions for Small Canisters	30
6	Pre- and Post-Impact Measurements of Small Canisters	35
7	Breaches in Small Canisters	38
8	Large Canister Dimension Changes	42
9	Large Specimen Material Distribution	64
10	Small Specimen Material Distribution	65
11	Representative Values of Parameters in Considering Unaccounted-For Material	74
A.1	Particle Size Distribution Table	A.1
B.1	Data from Size Sampling with Microscope	B.1

## 1.0 SUMMARY

This work was performed in support of a risk analysis of a conceptual management system for high-level nuclear waste. Three basic driving forces are generally associated with accidental release of radioisotopes: mechanical and thermal forces and dissolution processes. These forces could not only breach the containment barriers, but also modify the form of the waste. For example, mechanical forces acting on a canister of solidified (e.g., vitrified) waste could not only fail the canister, but also break the glass into smaller, potentially respirable particles. The increased glass surface area would also hasten dissolution and volatilization if driving forces for these were present.

Because no data for impact breakup characteristics of encapsulated waste glass were located, this test program was begun. The objectives, in order of priority, were to estimate 1) the quantity of respirable glass fines produced; 2) the increase in glass surface area; 3) the impact resistance of the filled canisters. Even if all test canisters were to remain intact, the first two items are needed because it cannot be guaranteed that every production canister will be fabricated soundly and maintained properly.

Two series of tests were conducted using nonradioactive waste glass type 72-68 (simulated waste composition PW-4b-2) in cylindrical 304L stainless steel canisters. Six specimens of a 1/2 scale model of a 10-ft canister were impacted at room temperature and at velocities up to 10 CFR 71 requirements of 44 fps. Twenty-two smaller specimens were tested at room temperature and at elevated temperature (425°C), at velocities up to that of high-speed train impact (80 mph or 117 fps). Both series included specimens which were essentially glassy and those which had been partially devitrified by thermal treatment.

The canisters breached only at the two highest velocities (66 and 117 fps). The breaches were all very small cracks. Pre- and post-test weight checks indicated that very little, if any, glass escaped through the cracks.

The resulting fines were removed and sieved. Particle size distribution curves were plotted. The inventory fraction smaller than  $10 \mu$  typically ranged from  $10^{-8}$  for control specimens to  $10^{-4}$  for 80 mph impact. This compares with approximately  $10^{-2}$  for nonimpacted calcined waste (and probably for impacted calcine also).

Geometric calculations were made of the surface area created. The surface area typically increased by only a few percent of the initial surface area for control specimens, but by a factor of 40 for 80 mph impact.

Within the scatter of the limited data obtained, no consistent difference was observed between the essentially glassy and the partially devitrified specimens nor between small and large canisters when the results were compared on a fractional breakup basis. Testing of specimens which are more severely devitrified might lead to observable differences between glassy and devitrified waste. Testing at elevated temperature increased the quantity of large particles produced, but no significant effect was observed on the quantity of particles smaller than about 20 to 50  $\mu$ .

## 2.0 INTRODUCTION

### MANAGEMENT OF HIGH-LEVEL NUCLEAR WASTE

High-level waste originates in aqueous form as a result of solvent extraction in the reprocessing of spent nuclear fuel. Current regulations call for solidification of commercial waste within 5 years of its generation and shipment to a Federal repository within a total of 10 years. The product may be stored for up to 100 years in a Retrievable Surface Storage Facility (RSSF) before permanent disposal. One possible scheme for waste solidification and fixation by reprocessors involves producing a calcine followed by fixation in a glass/ceramic form.

Decisions regarding management of high-level waste depend heavily upon product comparisons of candidate waste forms. An ultimate framework for such comparisons is that of system safety studies.

### WASTE FIXATION PROGRAM

Battelle Pacific Northwest Laboratories is conducting the Waste Fixation Program (WFP) for the Energy Research and Development Administration (ERDA). Primary objectives are development of improved product forms and demonstration of practical production on an engineering scale. The program is expected to provide technological bases for early adoption and implementation, by industry or a Federal facility, of techniques to convert high-level waste to solid forms of superior performance and stability.

Silicate glasses presently appear the most promising in terms of low dispersibility, ease of processing, and insensitivity to changes in waste composition. However, other product forms are also being investigated. Of particular interest are comparisons between these forms and calcined waste.

### SAFETY AND SYSTEMS EVALUATION TASK OF THE WASTE FIXATION PROGRAM

The purpose of the safety and systems evaluation task is to define and evaluate parameters of waste management systems as related to

containment and risk. The results of the task will guide R&D efforts, formulation of waste product criteria, and comparisons of alternative waste management schemes.

The chief thrust of the task is to perform a risk analysis of a conceptual management scheme for high-level waste. A representative management scheme (Figure 1) involves storage of liquid waste followed by solidification, encapsulation, and canister storage, all at the reprocessing plant. The waste is then shipped to a RSSF for interim storage. This is followed by shipping to and emplacement in ultimate disposal facilities. As a first attempt, the total annual risk of system processes 1 through 9 for the year 2000 is being estimated.

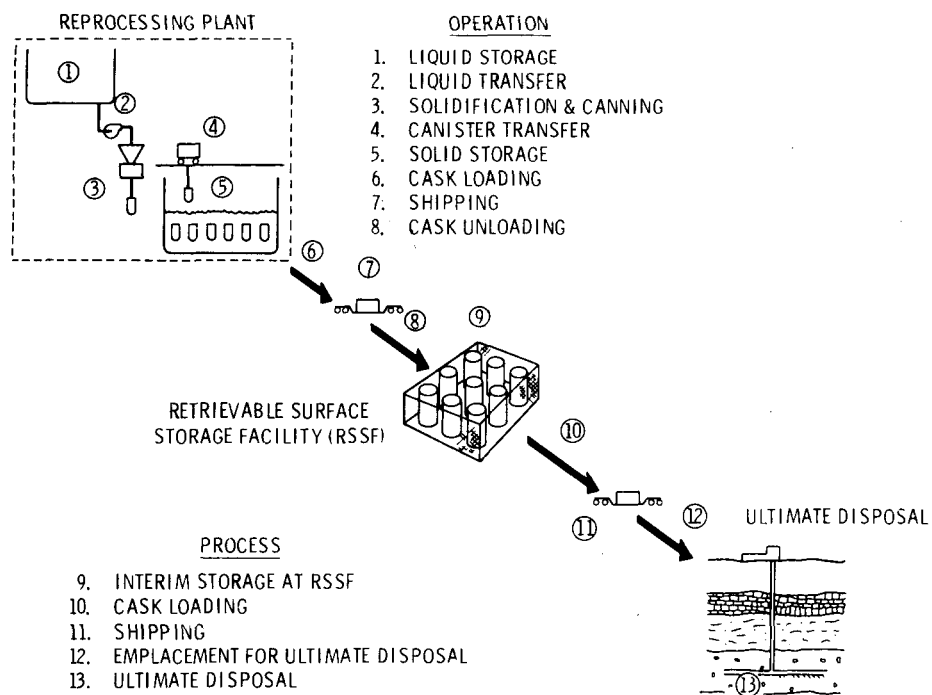


FIGURE 1. Representative Year-2000 Waste Management System

NEED FOR IMPACT DATA

In the risk analysis methodology, potential failure sequences are analyzed by relating release probability to release consequences. This relationship is expressed mathematically as the product of the expected frequency of release and the radiological consequences. The relationships among the various informational inputs are shown schematically in Figure 2.

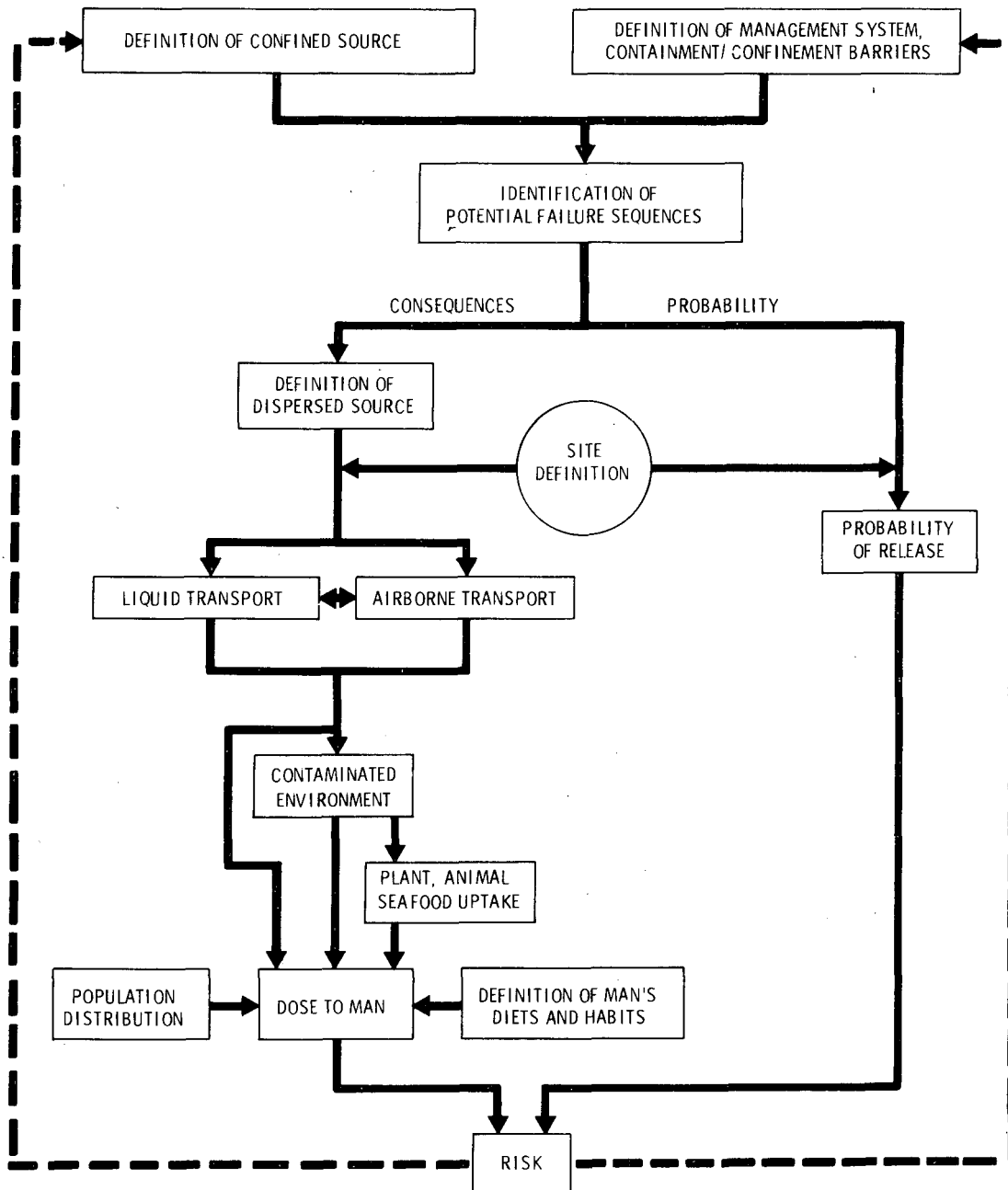


FIGURE 2. Risk Analysis Methodology

A key step in ascertaining release consequences is estimation of the quantity and characteristics of material released by a postulated failure sequence. This step, designated "Definition of Dispersed Source" in Figure 2, provides input to models describing radionuclide transport from one environmental component to another. Depending on the type of failure event, physical properties of the waste can be drastically altered during the release. For example, exposure of monolithic solids to high temperature can result in release of semivolatile constituents as submicron particles. Obviously, such transformations affect transport of radionuclides through the environment.

Three basic physical properties are prominent in dispersed source descriptions: volatility, leachability, and frangibility. These are pertinent to release sequences involving the following respective events: fires, contact with groundwater or surface water, and mechanical forces such as those in impact.

Studies of the leachability and volatility of waste solids had been conducted<sup>(1-4)</sup> before the risk analysis was under way. However, only preliminary percussion tests had been conducted<sup>(5)</sup> on phosphate ceramics and glasses in the predecessor to the WFP. The need was evident for definitive information on impact behavior of solid waste forms in terms of the size distribution of particles produced and the increase in surface area.

This need was the basis of the impact tests described here. The data have been related to potential failure modes involving impact events such as could be encountered in transportation, handling and storage. Knowledge of the quantity of extremely small particles ( $\sim 10 \mu$ ) produced is important for studies of airborne transport. Knowledge of the glass surface area produced is important, along with leachability, for analysis of release to groundwater or surface water.

### 3.0 REVIEW OF PREVIOUS WORK

Although the literature on impact is voluminous, publications closely related to this problem are scarce. Previous work which may aid in understanding impact of glass in metal canisters is briefly reviewed here.

#### CANISTER IMPACT BEHAVIOR

Although shell response has been studied at least since 1828, most studies have assumed linearly elastic systems, which are not representative of severe impact. Aerospace nuclear safety programs of the 1960s and early 1970s have provided data and the first useful simplified theories for plastic deformation and failure of shells in impact.<sup>(6)</sup> Much of that work built upon efforts of Stoneking et al.,<sup>(7,8,9)</sup> who tested hollow and partially-filled spheres and cylinders and formulated theories describing the impact behavior. Most studies since Stoneking's have concerned small hollow spheres.

Haskell<sup>(6)</sup> produced a simple failure criterion based on correlations of the Stoneking data. Morris used dimensional analysis along with the Stoneking data and more recent data to correlate deformation<sup>(10)</sup> and failure<sup>(11)</sup> of hollow spheres. Bodenschatz<sup>(12)</sup> correlated end-on failure velocities of filled cylinders and found only weak dependence of failure velocity on the L/D ratio of the cylinder, as long as  $L/D \geq 2$ . This result is more obvious from Haskell's tabulation of the Stoneking data, presented in Figure 3. Use of shortened cylinders, required in a portion of the present program, is therefore expected to have a small effect on cylinder deformation and failure. However, the effect on fines produced could not be predicted and is discussed in Section 10.0.

Impact tests of radioisotopic fuels and capsules were summarized by Dalby.<sup>(13)</sup> The above-mentioned theories were reviewed by Barsell<sup>(14)</sup> for spherical capsules, compared with new data, and modified for improved predictive capability. Barsell<sup>(15)</sup> also analyzed fueled spherical capsules

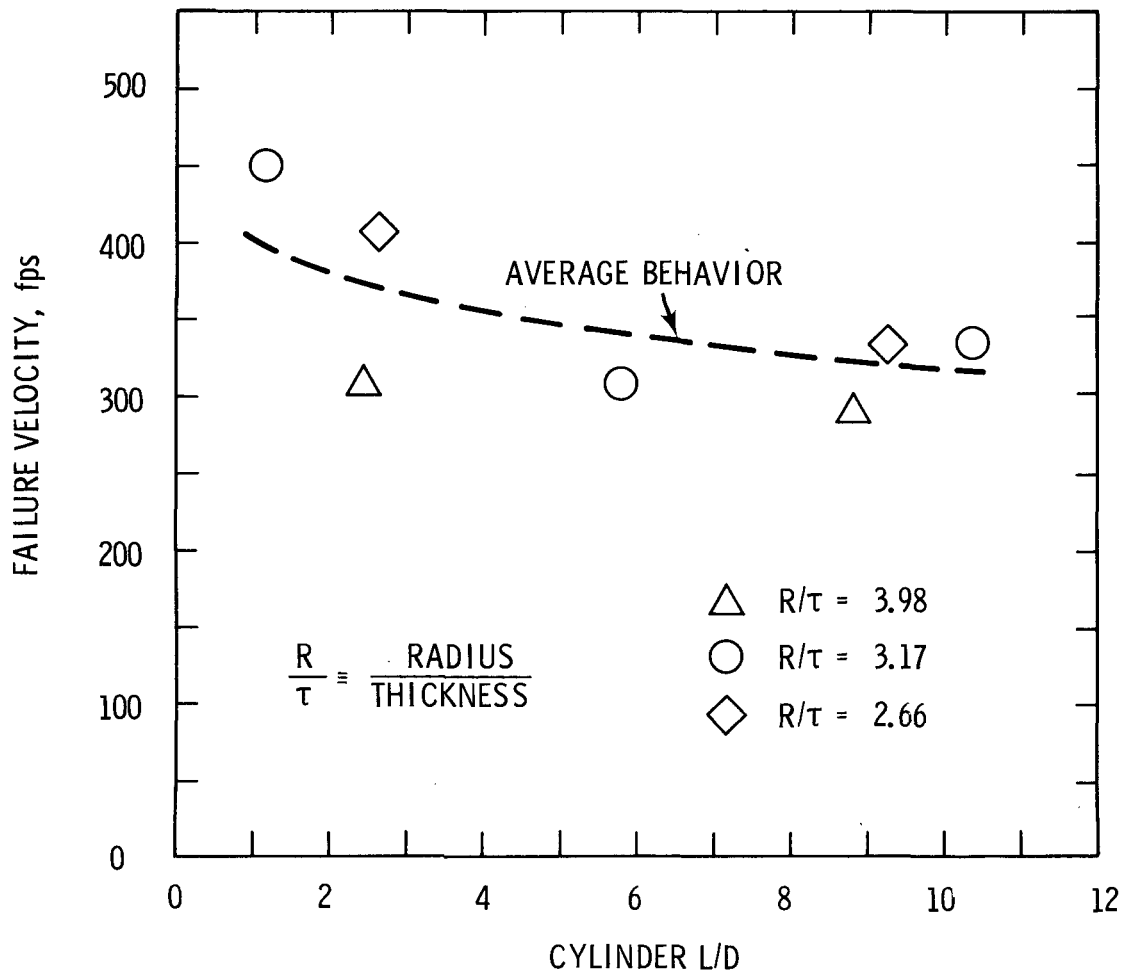


**FIGURE 3.** Dependence of Failure Velocity of Filled Cylinders on Length/Diameter Ratio (Adapted from Reference 6)

using a time-integrated energy approach. Adaptation of Barsell's method to cylindrical capsules seems the most promising theoretical approach for prediction of canister behavior.

Considerable testing and analysis of shipping casks have been performed at Oak Ridge National Laboratory (e.g., Ref. 16).

High strain-rate mechanical properties of Type 304 Stainless Steel, similar to that used in the present tests, have been published by Steichen and Paxton.<sup>(17)</sup>

DATA FOR POST-IMPACT PARTICLE SIZE DISTRIBUTION

Capsules containing <sup>238</sup>PuO<sub>2</sub> fuel as pressed oxide, PuO<sub>2</sub>-Mo cermet and microspheres were impacted under aerospace nuclear safety programs.<sup>(18-21)</sup>

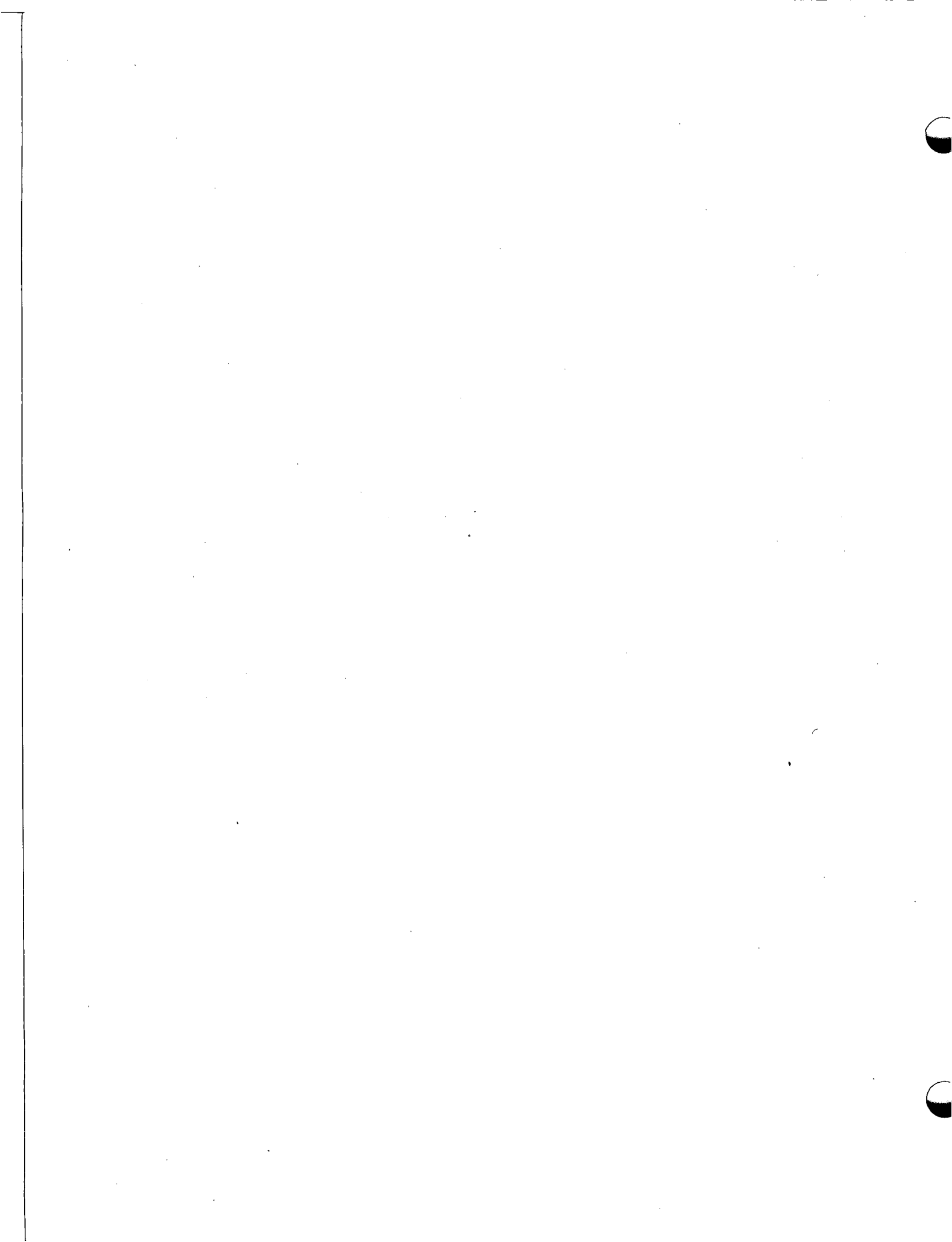
Particle size distributions resulting from these tests were reviewed in Reference 22 as part of the present impact program. The distributions of References 18-20 were matched poorly by log-normal and Rosin-Rammler distributions. Plots of size fraction versus velocity for Reference 19 and 20 data showed considerable scatter. Less scatter and a better log-normal fit in the 10 to 100  $\mu$  range were found for the data of Reference 21.

Preliminary percussion fines data were obtained in the Waste Solidification Program.<sup>(5)</sup> A weight was dropped on bare samples of radioactive waste or stand-ins of these forms: phosphate ceramic, phosphate glass, borosilicate glass. Particles were screened only down to the fraction <0.02 in.

A large body of literature (e.g., Ref. 23) concerns particle size distributions resulting from crushing and grinding. Many publications (e.g., Ref. 24) deal with fractures produced in bare glass by impact. However, none of these study areas directly applies to the requirements of this program.

#### SCALING LAWS

Scaling laws for impacted canisters have been formulated by Duffey<sup>(25)</sup> and by Tsai.<sup>(26)</sup>



## 4.0 TEST PROGRAM RATIONALE

### OBJECTIVES

The objectives of the program, in order of priority, were to estimate, on a preliminary basis, 1) the quantity of respirable fines produced from the borosilicate waste glass; 2) the increase in glass surface area; and 3) the impact resistance of the filled canisters. Supporting objectives included the following: determine the effects of several parameters upon the results; by means of correlations, facilitate prediction of results for impact environments not tested; facilitate comparisons of the impact behavior of borosilicate glass with that of calcine. All of these objectives were to be addressed within the context of accident environments identified in the WFP risk analysis.

### APPROACH

The need for timely input to the WFP risk analysis constrained the program to use locally available equipment. More elaborate impact facilities are available at ORNL and Sandia.<sup>(27,13)</sup> Two facilities in the Hanford area were utilized. The Donald W. Douglas Laboratories (DWDL) operates a rotating-arm impact facility capable of impact at high velocities and temperatures but limited in the specimen size it can accommodate. Operation of a large mobile crane is provided by the Atlantic Richfield Hanford Company (ARHCO), and large reinforced concrete slabs suitable for drop tests are located nearby. This equipment can accommodate rather large specimens but is not capable of testing at high velocities nor controlled elevated temperatures.

The approach combined the capabilities of both facilities so as to provide maximum information. The tests consisted of two series of simulated accident environments. The main series used the crane and concrete pad for testing of a limited number (6 including controls) of half-scale specimens. To supplement this series, a series of 22 (including controls) shortened one-sixth scale specimens was tested at the DWDL facility. The smaller

size permitted more test runs because of reduced costs of fabrication and of fines analysis. The DWDL facility's flexibility allowed ranges of parameter variations, such as impact velocity and temperature, not available at tower drop facilities. Results of the two series were to be correlated for estimates of impact behavior under a wide range of conditions.

It was recognized from the outset that 1) the difficulties and cost of precisely modeling impact conditions with a large number of full-size specimens were prohibitive; 2) compromises necessary to complete the program at reasonable cost would affect the results to some extent; 3) the program was essentially a pioneering effort in testing impact behavior of vitreous waste forms. Therefore the results were expected to provide order-of-magnitude estimates at best. Comparisons between values were expected to be more reliable than absolute results.

#### SELECTION OF TEST CONDITIONS

The basic considerations are what to test and under what conditions. Though such decisions are somewhat arbitrary, justification is given here for the decisions made.

The waste form (nonradioactive simulant) chosen was borosilicate glass, the prime WFP candidate. Two structural variations were studied: one glassy and the other purposely devitrified by time-temperature exposure. The latter was included because of possible post-fabrication devitrification in the waste management system of Figure 1. No variations in waste composition, other than local effects within a batch, were included.

A major decision concerned containment of the glass during the tests. Possible configurations were 1) bare glass, tested briefly in an earlier program; 2) glass formed inside the canisters anticipated for primary containment and use in handling and water basin storage; 3) glass/canisters placed inside heavy shipping casks or RSSF storage casks. Test conditions were chosen to correspond to accident sequences identified in fault tree analyses of the WFP safety task. Because bare nonmolten glass is not intended to exist in the waste management system, configuration 1 was eliminated. Transportation accidents (Steps 7 and 11, Figure 1) could

involve configuration 3, as could RSSF storage (Step 9). Accidents involving configuration 2 could occur in Steps 3, 4, 5, 6, 8, 10 and 12. Because this containment configuration is relevant for the greatest portion of the management system and because of reduced cost and complexity, the impact tests used simulated glass/canister systems (configuration 2). Detailed descriptions of the impact specimens are given in Section 5. It should be stressed that the impact behavior of the containment was not of prime interest except insofar as it influenced fracture of the waste simulant.

The impact velocities (25, 44, 66, and 117 fps) were selected to represent potential accident conditions (Table 1). The small specimens were tested at all four velocities, while the large specimens were tested only at 25 and 44 fps.

TABLE 1. Impact Test Velocities

<u>Velocity</u> <u>fps</u> <u>mph</u>	<u>Equivalent Drop</u> <u>Height, ft</u>	<u>Small</u> <u>Specimens</u>	<u>Large</u> <u>Specimens</u>
25    17	10	X	X
44    30	30	X	X
66    45	>68	X	
117   80	>213	X	

NOTE: A large specimen was dropped onto a penetrator from a height of 40 in. (15 fps).

The two lower velocities correspond to free drop distances of 10 and 30 ft, respectively. If a drop occurred within the facilities under consideration, a 10-ft distance would not be unusual, whereas a 30-ft distance would be near the upper limit. The 30-ft drop also matches the transportation packaging requirement of 10 CFR 71, Appendices B and D. The test targets were essentially unyielding, although no attempt was made to minimize yielding effects.

The 66 and 117 fps values (45 and 80 mph) represent velocities associated with severe train accidents. Approximately 90% and 99%,

respectively, of freight train accidents occur at velocities lower than these.<sup>(28)</sup> Only lower limit drop distances can be attached to the higher velocities because aerodynamic drag, a function of canister orientation, becomes significant.

There are two cautions in relating the higher velocity tests to railroad accidents. First, the canisters tested were not inside simulated shipping casks. Second, objects on board a train would generally experience much lower impact velocities than that of the train, because of cushioning provided by deformation of the cars and mountings. However, results of the present tests may be useful for limiting analyses. When data become available relating vehicle velocity to the effective impact velocity of cargo, the present results may furnish crude estimates of expected behavior.

The impact orientation selected was edge-on. This orientation was hypothesized to be the most severe. It could also be the most probable orientation. An accidentally released canister would generally experience some rotation-producing moment, either at release or during descent. One small specimen was tested end-on to check the effects of orientation.

Details of the test conditions are discussed in Section 6. This includes canister orientations, impact temperatures, glass forms, target descriptions, and uncertainties in test parameters.

## 5.0 SPECIMEN DESCRIPTION

### GLASS DESCRIPTION

The precise composition of high-level waste will depend on the reprocessing scheme as well as on the type of spent fuel and its reactor exposure. In addition, many glass compositions could result from a given waste composition.

The glass used for the impact tests was made to simulate the 72-68 glass composition<sup>(29)</sup> proposed for high-level waste fixation studies. It was prepared from 75 wt% frit (glass formers) and 25 wt% calcine (particulate simulated high-level waste) prepared in a continuous spray calciner.<sup>(30)</sup> The simulated waste composition, designated PW-4b-2, of the calcine is shown in Table 2. Substitutions made for reasons of cost and availability include Fe for Ru, Mo for Tc, K for Rb and Cs, Co for Rh, and Ni for Pd. A natural rare earth mix containing Y and Ce is used in place of the actual Y and rare earth distribution. Actinides are not included nor substituted.

The premelted and presized frit was added to the melter as particles sized between 6-mesh and 20-mesh. The composition of the frit, identified as 73-1, is given in Table 2.

The final glass composition is also listed in Table 2. The frit and calcine are fed semicontinuously into an Inconel 690 melter<sup>(30)</sup> which forms batches of 35-40 lb of glass. The melts are formed at 1150°C and are of low viscosity (~10 poise). The melting temperature is not sufficient to bring all materials into the glass solution. Thus the "glassy" specimens were not 100% glassy. Residue crystals of CeO<sub>2</sub>, Zircon, and a spinel composed of Fe, Cr, Ni, and Zn have been identified in similar melts.<sup>(1)</sup>

The glass has a strain point of 475°C, annealing point of 502°C, and average thermal expansion coefficients of  $7.9 \times 10^{-6}/^{\circ}\text{C}$  between room temperature and 330°C and  $10.0 \times 10^{-6}/^{\circ}\text{C}$  between 330°C and 500°C.

TABLE 2. Chemical Compositions of Simulated Calcine,  
Frit and Glass

<u>Oxide</u>	<u>Wt% in PW-4b-2 Calcine</u>	<u>Wt% in 73-1 Frit Glass Formers</u>	<u>Wt% in 72-68 Glass</u>
Fe <sub>2</sub> O <sub>3</sub>	9.50		2.38
Cr <sub>2</sub> O <sub>3</sub>	1.00		0.25
Ni O	3.01		0.75
P <sub>2</sub> O <sub>5</sub>	1.96		0.49
MoO <sub>3</sub>	18.44		4.61
SrO	3.05	2.0	2.26
BaO	4.52	2.0	2.63
K <sub>2</sub> O	3.30	5.5	4.95
RE <sub>2</sub> O <sub>3</sub> (a)	37.65		9.41
ZrO <sub>2</sub>	14.39		3.60
CoO	0.81		0.20
TeO <sub>2</sub>	2.09		0.52
Cd O	0.28		0.07
SiO <sub>2</sub>		37.0	27.75
B <sub>2</sub> O <sub>3</sub>		15.1	11.33
Na <sub>2</sub> O		5.5	4.13
ZnO		28.9	21.68
CaO		2.0	1.50
MgO		2.0	1.50

a. A natural rare earth mix containing CeO<sub>2</sub> + Y<sub>2</sub>O<sub>3</sub>

## CANISTER DESCRIPTION

### 1. Small Specimens

The canisters, shortened 1/6-scale models, were made from 304L stainless steel tubing machined to 0.040-in. wall thickness. The tubes were approximately 1.96 in. OD, with flat end caps of 0.0375 in. 304L stainless steel welded to form a closed cylinder approximately 4.04 in. long. Exact dimensions of each specimen before and after testing are given in Section 7.0.

Welds were checked by dye penetrant. Specimen weight, including glass, ranged from 540 to 610 g (1.2 to 1.35 lb). Exact weights are given in Section 10.0. Figure 4 illustrates typical pretest dimensions. The depth of glass fill, discussed in the next subsection, is also shown.

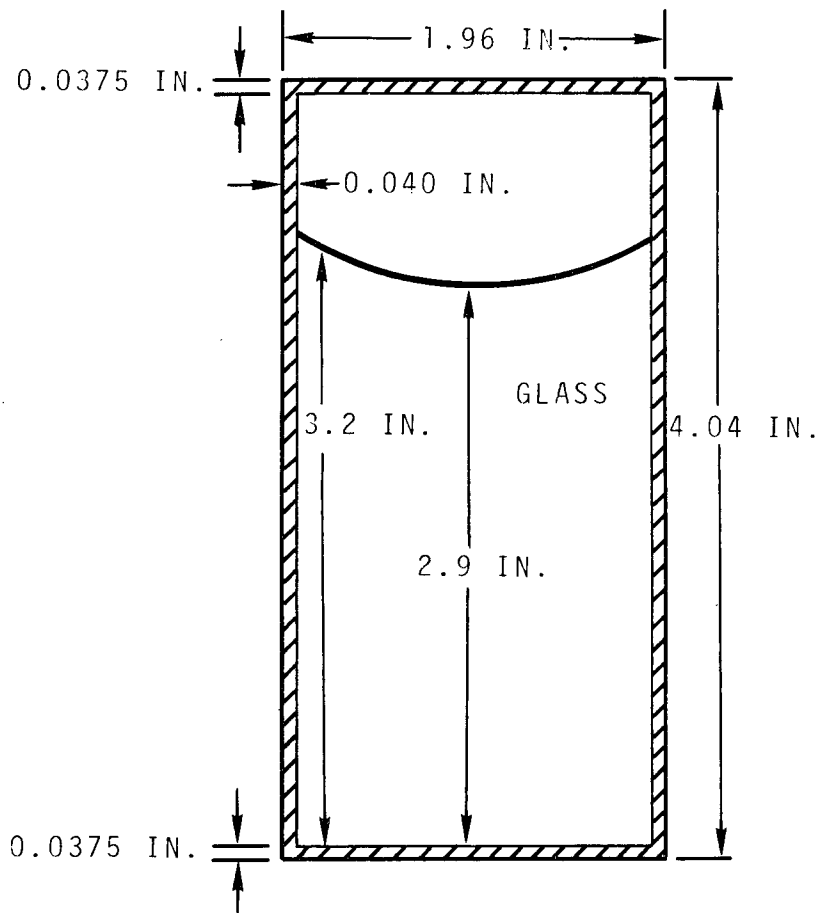


FIGURE 4. Typical Pre-Impact Dimensions of Small Specimens

## 2. Large Specimens

These cylindrical specimens, 1/2-scale models, were fabricated from 6-in. schedule 10 (6.625-in. OD, 0.134-in. wall) 304L stainless steel pipe. The pipe had been formed by rolling and had a continuous longitudinal weld. End plates were 0.134-in. 304L stainless, attached by V-type full-penetration welds. Outside length of the cylinders was approximately 62.2 in. Figure 5 illustrates typical pretest dimensions of the large specimens. Dimensional changes accompanying testing are given in Section 7. The depth of glass fill, discussed in the next subsection, is included. Specimen weight, including glass, ranged from 234 to 246 lb. Exact weights are given in Section 10.0.

Lifting eyes which protruded 1-1/2 in. from the outside wall were welded 2 in. below the top of the canisters. All welds were dye checked for cracks or pin holes.

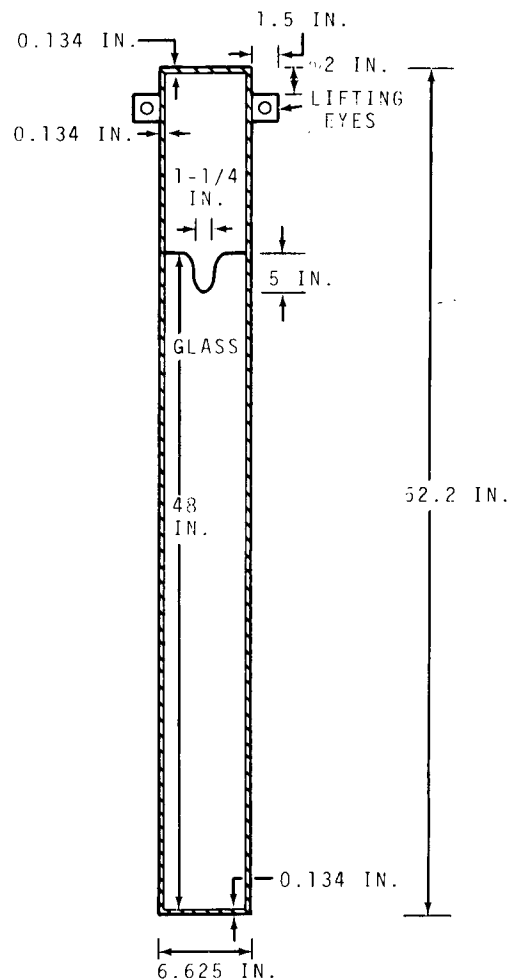


FIGURE 5. Typical Pre-Impact Dimensions of Large Specimens

### 3. Comparison of Test Canisters with Full-Size Canisters

The test canisters are simplified models of the primary containment canisters anticipated for the handling, shipping, and storing of high-level waste. There is presently no official canister design. Diameters from 6 to 24 in. and lengths from 2 to 15 ft are under consideration in RSSF studies. A reference design<sup>(31)</sup> for calcined waste is shown in Figure 6. The canister is 10 ft long and 12.75 in. OD with a 0.375-in. wall of 300 series stainless steel. The canister contains 6.28 ft<sup>3</sup> of waste, implying a fill depth of 8 ft. Filled weight would be on the order of 1700 lb. The canister has a neck section, which serves as a fill port, and a connector pin for lifting.

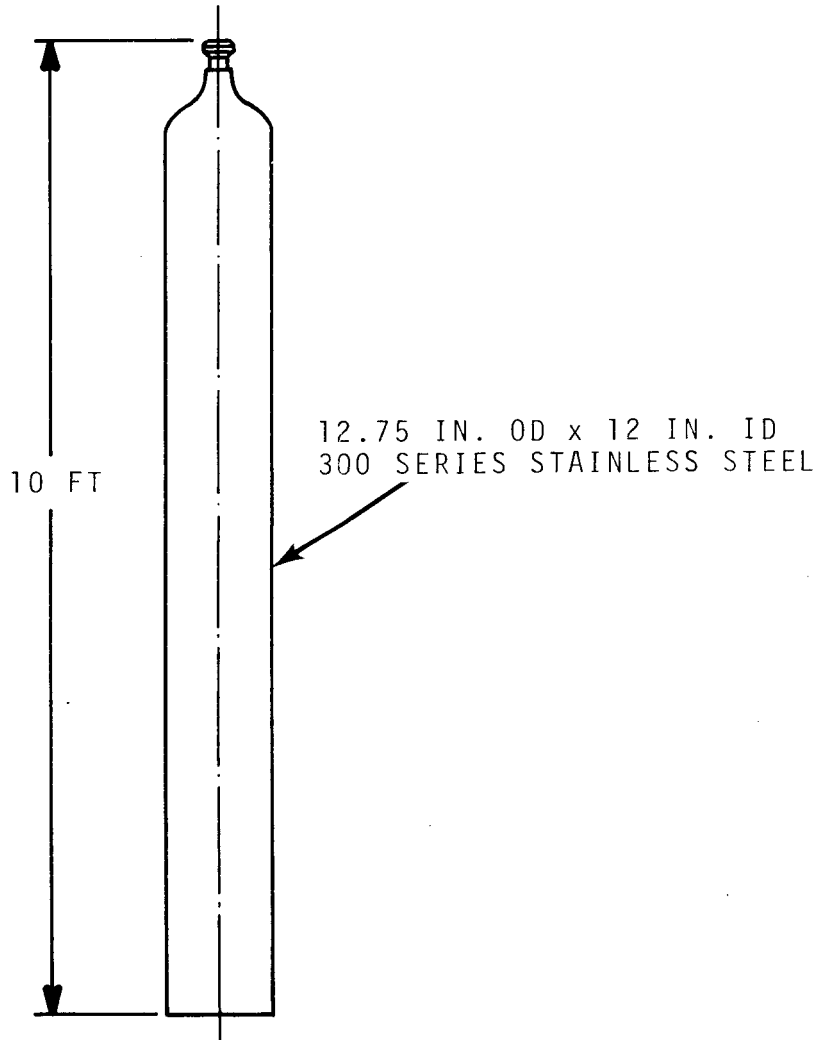


FIGURE 6. Reference Canister for Calcined Waste (Ref. 31)

The design of canisters containing glass is not established. The neck portion may be unchanged, larger, or even nonexistent. No attempt was made to model the neck portion in designing the test canisters. For any impact orientation except the unlikely impact on the upper end, this effect is expected to be negligible.

The dimensions and dimension ratios of the two test canister designs are compared with those of the full-size reference canister in Table 3. A few comments are in order regarding differences in the dimension ratios. To control costs, the test specimens were generally made from standard-dimension pipe tubing and plate. The ratio of head thickness to wall thickness is a close match. The ratio of radius to wall thickness for the test specimens reflects the 0.250-in. wall thickness of an earlier reference canister at the time of design of the specimens. The ratio of length to diameter for the large specimens closely matches that of the reference. The small specimens were shortened considerably to allow use of the DWDL rotating-arm facility, which has a specimen length limit of about 4 in. If the small specimens had been scaled precisely from the earlier reference, the wall thickness would have been 8 mils, which of course is unreasonable for fabrication. Therefore, the diameter and wall thickness were kept in the proper ratio, but the L/D ratio was reduced. For non-side-on impact, the effect of the L/D value on canister behavior is small for  $L/D \geq 2$ . The effect on fines production was not known at the time of design. Unfortunately, the required use of shortened small specimens resulted in the simultaneous variation of two parameters--size and L/D ratio. Thus, it is difficult to separate these two effects in the results of the tests.

#### CANISTER FILLING AND HEAT-TREATING PROCEDURES

##### 1. Small Specimens

The small specimens were divided into two lots for filling with glass, each lot being filled from one melter batch. The canisters were held under the melter and filled to 80 to 85% of the internal volume. However, the glass contracted about 6 vol% during cooling, reducing the effective fill depth to 75 to 80%. The upper surface became concave because of shrinkage.

TABLE 3. Comparison of Test Canisters with Full-Size Reference Canister

	Small Canister	Large Canister	Full-Size Reference Canister
Average <sup>(a)</sup> radius, $R_a$ , in.	0.96	3.245	6.1875
Wall thickness, $t_w$ , in.	0.040	0.134	0.375
Head thickness, $t_h$ , in.	0.0375	0.134	0.375
Average <sup>(a)</sup> length, $L_a$ , in.	4.00	62.1	119.6
$R_a/t_w$	24.0	24.2	16.5
$t_h/t_w$	0.94	1.0	1.0
$L_a/(2R_a) = L_a/D_a$	2.1	9.6	9.7

a. Average of inside and outside dimensions

The heat capacity and low thermal conductivity of the glass allowed several minutes for handling between filling and cooling of the outside surface to the annealing point. During this period, the samples were put into a furnace at 530°C and allowed to stabilize at that temperature. The furnace was then cooled by hourly adjustments of a set point controller. The cooling rate was 5°C/hr to 490°C, then 8°C/hr to 436°C, and finally 44°C/hr to room temperature. The above cycle was calculated from equations<sup>(32)</sup> for production of an annealed sample of glass.

## 2. Large Specimens

The large specimens, being 3-1/2 times the diameter and 15 times the length of the smaller specimens, required about 180 times as much glass per specimen. This involved six batches of glass per canister. Each 35 to 40 lb batch filled about 8 in. of the canister. To prevent thermal shock to the glass as each batch was added, the canisters were held in a 565°C furnace during filling. Four canisters were held in the furnace at one time to

duplicate cooling rates and allow higher production rates. The glass in the first canister filled, therefore, had a residence time of about 3 days at 565°C while subsequent canisters were being filled. When the four canisters were filled to the desired 4-ft depth, the furnace was cooled at 5°C/hr to 530°C and the temperature then maintained for 3 hr to allow the glass to approach equilibrium.

The annealing was started at 0.5°C/hr with temperature adjustments of 4°C every 8 hr until the temperature reached 490°C. The 4°C adjustments were then made every 4 hr until the furnace temperature was 440°C, after which 5°C adjustments were made hourly until the samples reached room temperature. The complete cooling required 9 days.

The cooled castings appear monolithic. However, acoustic monitors coupled to the canisters indicated that some cracking may have occurred during cooldown below 440°C. This may represent metal-glass interactions due to differential thermal expansion. The glass contracted significantly during cooling, leaving a void in the top surface about 1-1/4 in. in diam and 5 in. deep.

## IMPOSED DEVITRIFICATION

### 1. Background

The metastable glassy or vitreous state exists only because its high viscosity retards the diffusion of ionic species necessary for crystal nucleation and growth. At elevated temperatures, generally above 500°C., the lowered viscosity permits crystallization, or devitrification, to begin.

This process is complex in relatively simple glasses and even more so in the waste glass system. It depends on composition and on time-temperature history. A number of crystalline species can form, each of which leads to a change in composition of the residual glass phase.

Since canisters of waste glass will be self-heating, centerline temperatures during handling, shipping, and storage may reach 700°C., sufficient for some devitrification to occur. Centerline temperatures may be constrained to lower levels by finning or other means.

Although the waste glass is relatively resistant to devitrification, purposely devitrified samples were included in this study to assess the effect on impact behavior. Effects of devitrification on other glass properties, such as leach rate, are under study separately.

The thermal histories of the devitrified specimens are described in the following sections. Basically, the time-at-temperature was 3 to 4 days at 700°C. It should be stressed that although the devitrification was probably sufficient to approach a steady state at that temperature, it was not 100% complete. X-ray diffraction analysis of a glass sample held at 700°C for 24 hr indicated that the primary crystals present were  $\text{SrMoO}_4$  and a  $\text{CeO}_2\text{-ZrO}_2$  solid solution. Minor phases may also be present but were not detected.

Structural changes resulting from devitrification are expected to be more significant than those resulting, either directly or indirectly, from radiation. The major damage is expected to occur from alpha decay of the actinides.<sup>(29)</sup> One form of this damage may be from helium buildup within the glass, which has been postulated to result in significant stress levels over long time periods.<sup>(30)</sup> Experiments are under way involving simulated waste glass doped with  $^{244}\text{Cm}$  to accelerate possible effects of alpha damage.

## 2. Treatment of Small Specimens

The first lot of samples was subjected to a devitrification process after filling and cooling. The process involved a 25°C/hr heating rate to 700°C, with 72 hr at temperature for crystal growth. The specimens were cooled to 530°C at 25°C/hr then annealed in the previously described cycle. To limit oxidation of the stainless steel, the specimens were covered with an atmosphere of flowing argon while the temperature was above 500°C. To prevent glass vaporization, the canisters were welded before devitrification. During welding of the upper end cap, the samples were held in water to avoid thermal shock of the glass.

A group of the small specimens immediately prior to impact testing is shown in Figure 7.

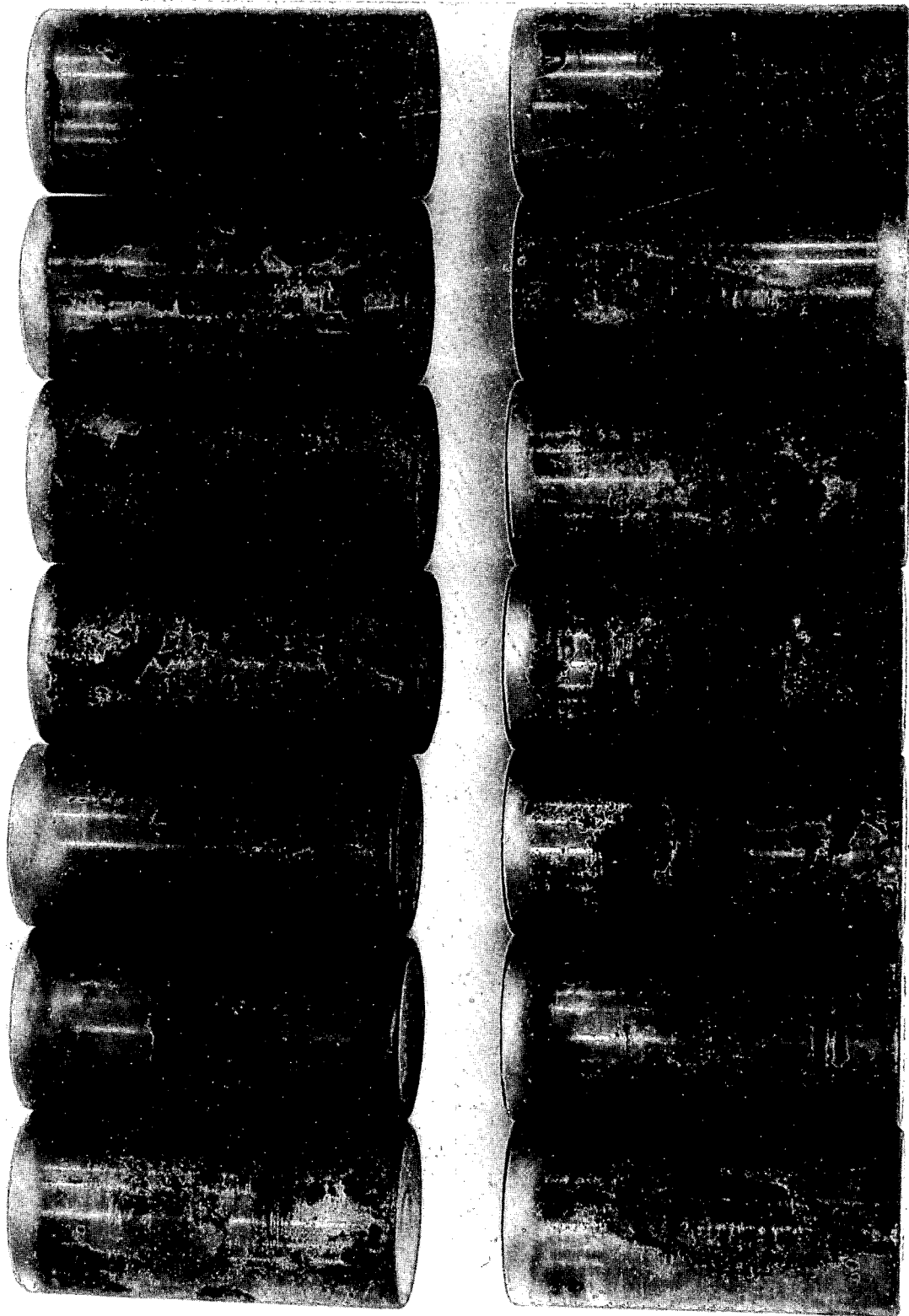


FIGURE 7. Small Canisters Before Impact Testing

### 3. Treatment of Large Specimens

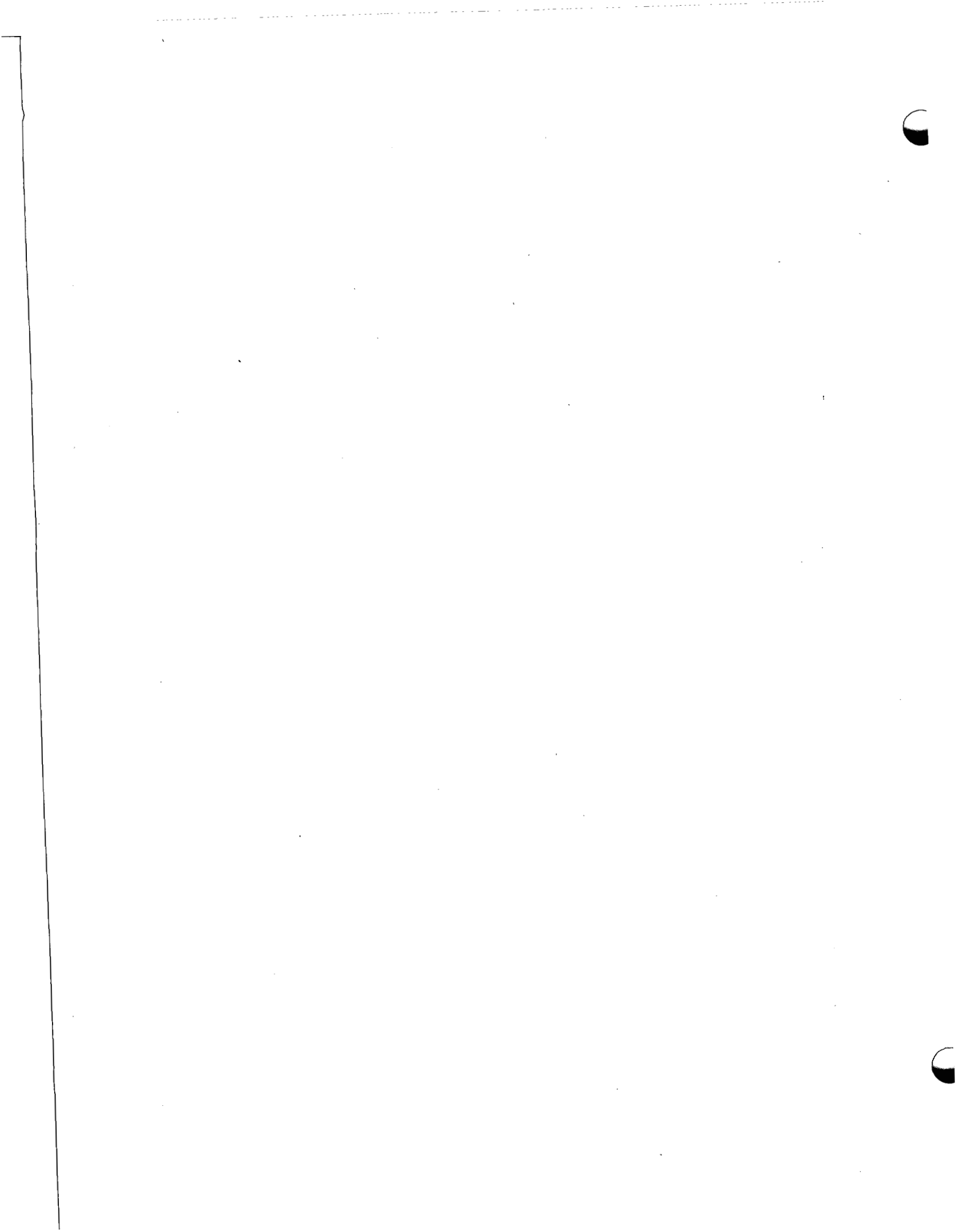
Two additional large canisters were filled similarly to those described above. After filling, however, the furnace temperature was increased to 700°C and held for 88 hr to initiate devitrification. The canisters were cooled at 25°C/hr to 565°C, then 10°C/hr to 530°C. Slow annealing was started with 5°C adjustments twice daily to 490°C. The 5°C adjustments were made three times daily down to 440°C. Then 5°C adjustments were made hourly nine times a day until the canisters reached room temperature. The total cooling cycle for these canisters covered 3 weeks.

After cooling, the canisters to be impacted were welded closed with the upper section kept wet to avoid thermal shock to the glass.

#### COMPARISON OF GLASS PROCESSING OF SPECIMENS WITH PROPOSED LARGE-SCALE PROCESSING

The currently proposed process for large-scale glassification of calcined waste is in-can melting with a maximum temperature of about 1000°C. (The melt temperature for this impact program glass was 1150°C.) This lower processing temperature would increase the amount of crystalline material not soluble in the glass phase. The effect on the glass properties is not completely characterized, but the behavior probably lies between the present glassy and devitrified samples.

A second difference which could have more effect is the faster cooling rates being considered for full-scale canisters. These cooling rates would lead to some fracturing of the glass by thermal stress. The impact behavior of such material is expected to be inferior to that of the fully annealed samples used in these impact tests.



## 6.0 TESTING PROCEDURES AND CONDITIONS

### LARGE SPECIMENS

Six large specimens were fabricated and subjected to the heat treatments described in Section 5.0. Two of these serving as controls were subjected to the same handling sequence except for impact and the transportation to and from the impact site.

The four test specimens were impacted at ambient temperature by dropping from a large mobile crane. A special harness and release system minimized changes in orientation caused by the release process. Visual observation and detailed analysis of high-speed films revealed no significant effect of release on the impact angle. A lightweight rope, marked at the 10- and 30-ft points, was taped to the bottom of the canister to gage the drop height. Drop height uncertainty is estimated to be ~1%.

The canisters were dropped onto a reinforced concrete block atop and part of a large, 6-in. thick pad. The block dimensions are about 7 ft by 5 ft by 18 in. in thickness. The weight of the block alone is approximately 35 times that of a large canister. No visible damage to the block resulted from the testing.

Two canisters were dropped 10 ft and one dropped 30 ft, each onto the bottom edge, with the center of gravity directly above the impact point. A 40-in. side-on drop (canister horizontal) onto a 3-in. diam steel penetrator was also conducted. This was a 1/2-scale simulation of a full-size canister undergoing the puncture test of 10 CFR 71 Appendix B.

Impact conditions are summarized in Table 4. After impact the canisters were dye checked, photographed, and characterized dimensionally.

### SMALL SPECIMENS

Twenty-four small specimens were fabricated and subjected to the heat treatments described in Section 5.0. Three of these specimens serving as controls were subjected to the same fabrication, handling, and transportation sequence as the test specimens. Two specimens were incorrectly impact tested due to failure of the injection device.

TABLE 4. Test Conditions for Large Canisters

<u>Canister Number</u>	<u>Glass Condition</u>	<u>Drop Height</u>	<u>Impact Velocity</u>	<u>Impact Orientation</u>
1	G	C 0	N T R 0 L	
2	G	30 ft	44 fps	bottom edge
3	G	40 in.	15 fps	side-on <sup>(a)</sup>
4	G	10 ft	25 fps	bottom edge
5	DV	C 0	N T R 0 L	
6	DV	10 ft	25 fps	bottom edge

a. Onto 3-in. diam steel penetrator  
 G ≡ Glassy  
 DV ≡ Devitrified

Early in the program two of the controls were taken through the same pre-impact heatup and post-impact cooldown as the test specimens, but without impact. This was done because of the possibility of thermal stresses inducing sufficient glass breakage to obscure results from the impact. Such concern proved to be unwarranted.

The DWDL impact facility<sup>(21)</sup> has a 75-lb granite block mounted on a counterbalanced rotating arm. Specimens up to about 3 lb can be tested. The specimen is held at precisely controlled temperatures (up to 1500°F) in an argon-purged furnace above the plane of rotation. The impact angle is precisely controlled by mounting the specimen in a thin quartz holder attached to an injection mechanism. The specimen is injected into the path of the rotating block between revolutions by means of a pneumatic cylinder timed by the position of the rotating arm shaft. Impact velocity is known to within 1 fps. The specimen rebounds from the granite block and is caught in a ceramic fiber receiver to dissipate the kinetic energy without secondary damage to the specimen. (Tests of the large specimens involved repeated secondary impact from multiple bounces. This is the more realistic accident situation and is a small point of difference between test procedures for small and large specimens.)

The arm, furnace, and receiver are in a reinforced concrete pit below ground level. The test area is covered with plywood to preclude release of debris. Motor control, injection actuation and furnace operation are accomplished remotely with recording capability for temperatures and velocity. High-speed photographic coverage is available, but was not included in the current test series.

The nineteen noncontrol specimens were impacted according to the conditions in Table 5.<sup>(33)</sup> Approximately half were tested at room temperature and the other half at 800°F (425°C) in order to study effects of temperature on glass behavior. The 800°F value is the approximate bulk temperature of the waste in full-size 10-ft canisters in typical shipping, handling, and storage configurations. (The centerline temperature is 1000 to 1100°F; peripheral temperature, 400°F.) Heatup prior to testing was performed slowly ( $\sim 1^\circ\text{F}/\text{min}$ ) to minimize thermal stresses. The calculated temperature change during the period between removal from the furnace and impact is negligible.

Impact velocities were 25, 44, 66, and 117 fps. All specimens were impacted edge-on (through the center of gravity, an angle of about 23°), except for one end-on specimen to check for orientation effects.

The test matrix (Table 5) was designed to measure the reproducibility of the test results: specimens 24, 23, and 4 were tested under ostensibly identical conditions. The matrix also provides simple checks on the effects of variables. Pairs of glassy and devitrified specimens are evident throughout, as are pairs of room temperature and elevated temperature tests.

Specimens were weighed, measured, photographed and leak-checked after impact.

TABLE 5. Test Conditions for Small Canisters<sup>(33)</sup>

<u>Specimen</u>	<u>Waste</u>	<u>Velocity, (a)</u> <u>fps</u>	<u>Orientation</u>	<u>Temperature,</u> <u>°F (b)</u>
1	G	No Impact	-	802
24	G	117	Edge-on	800
23	G	117	Edge-on	800
4	G	117	Edge-on	800
5	DV	117	Edge-on	796
6	G	117	End-on	802
7	G	66	Edge-on	802
8	DV	66	Edge-on	798
9	G	44	Edge-on	800
10	DV	44	Edge-on	798
11	G	25	Edge-on	800
12	DV	25	Edge-on	796
13	DV	No Impact	-	798
14	G	114	Edge-on	RT
15	DV	117	Edge-on	RT
16	G	66	Edge-on	RT
17	DV	66	Edge-on	RT
18	G	44	Edge-on	RT
19	DV	44	Edge-on	RT
20	G	25	Edge-on	RT
21	DV	25	Edge-on	RT
22	G	No Impact	-	RT

G ≡ Glassy

DV ≡ Devitrified

RT ≡ Room Temperature

- a. Velocity of the impact block was checked with a stop watch at low speed and a strobe light at higher speeds. Indicated velocities above were approximately 1% higher than actual test velocities. This difference was neglected.
- b. Temperatures were controlled by a Research Incorporated Data-Trak Programmer set up to heat the specimen from room temperature to approximately 800°F in a smooth ramp over a 10-hr period. Temperatures were sensed by a thermocouple in contact with the specimen until the specimen was ejected from the furnace. Maximum temperatures prior to injection ranged between 796° and 812°F.

## 7.0 IMPACT EFFECTS ON THE CANISTERS

Because this report is organized by procedural steps, this section reviews the effects of impact on the canisters (deformation and breach of containment), effects of secondary interest in this study. The subject of primary interest, impact effects on the glass within the canisters (particle size distribution and surface area increase), is covered in Section 10.0.

### SMALL CANISTERS

#### 1. Deformation

As shown in Figures 8-13, impact at 25 or 44 fps produced little deformation. Impact at 66 or 117 fps resulted in greater deformation, but the effects were still localized.

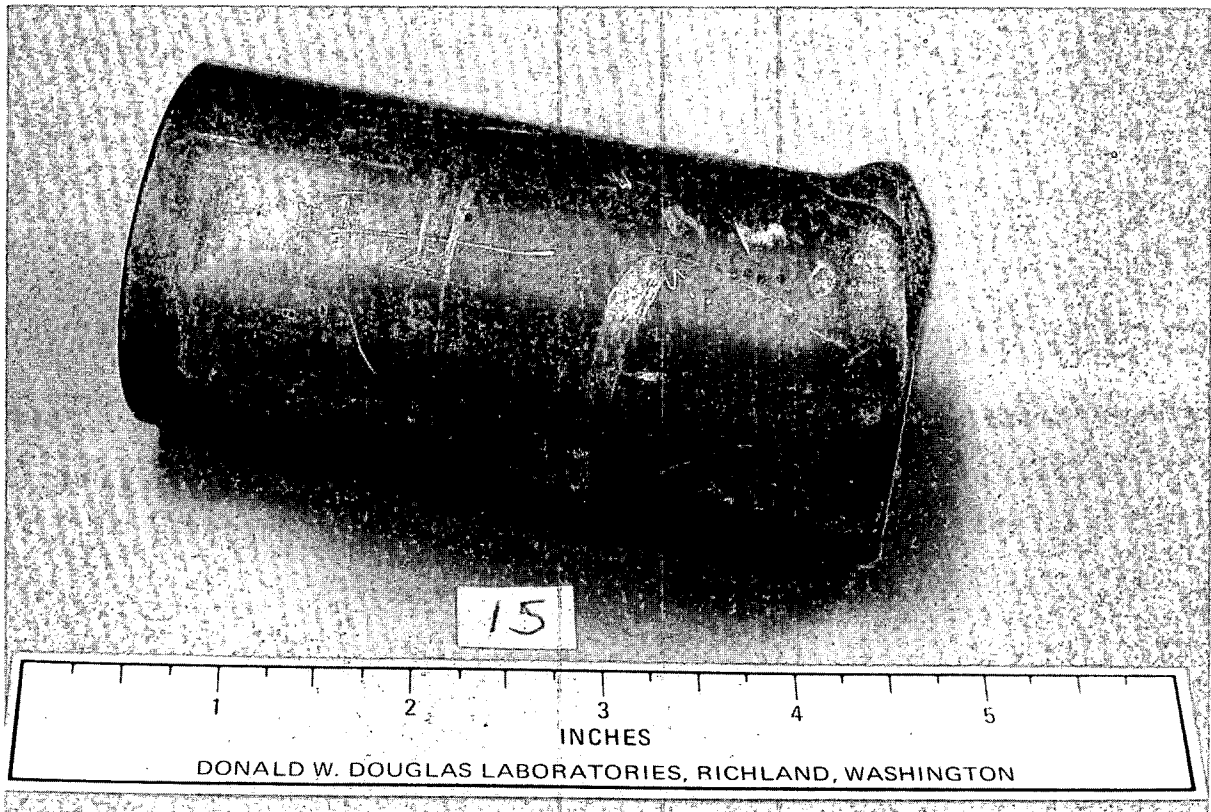


FIGURE 8. Specimen 15 After Edge-On Impact at 117 fps



FIGURE 9. Specimens 23 and 14 After Edge-On Impact at 117 and 114 fps, Respectively

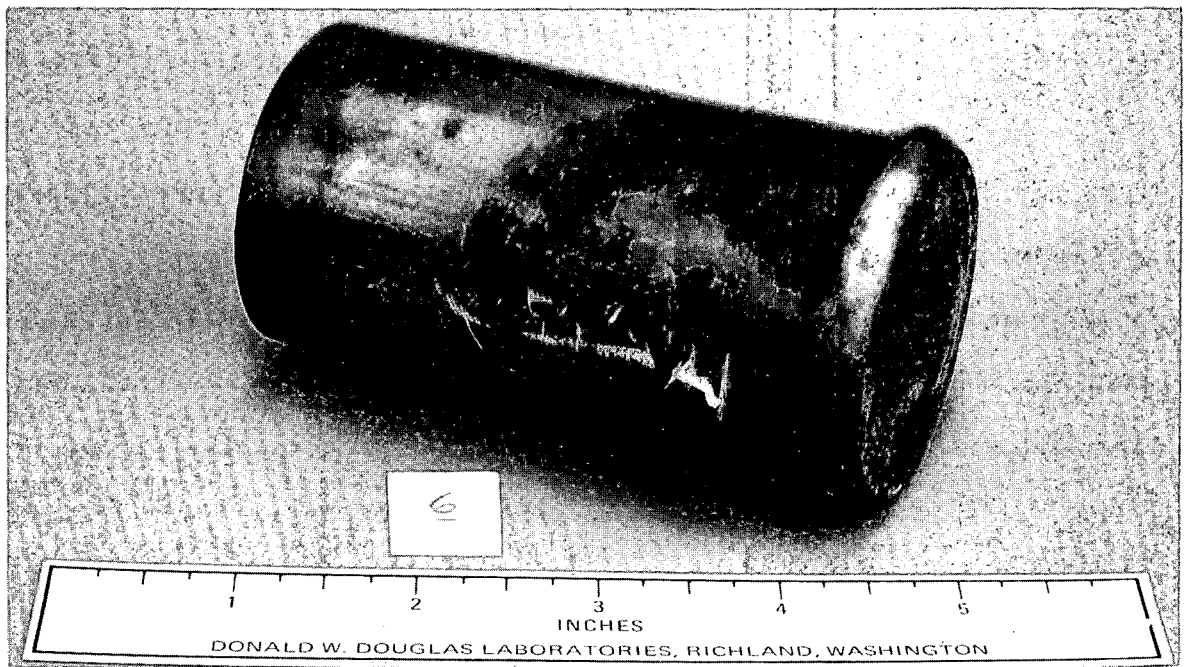


FIGURE 10. Specimen 6 After End-On Impact at 117 fps

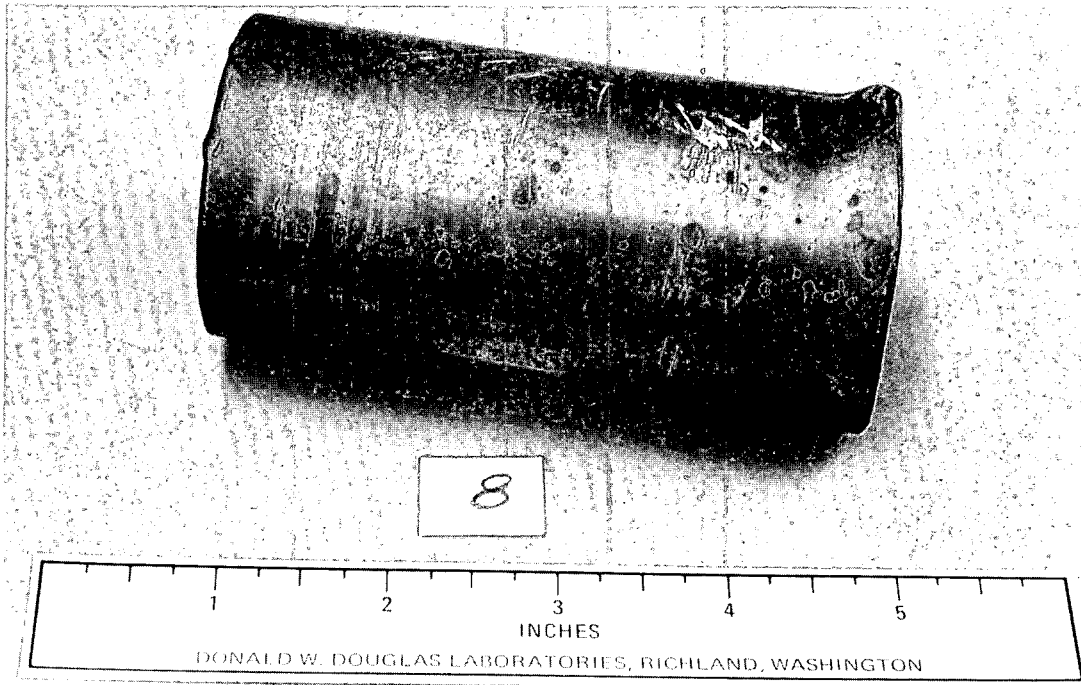


FIGURE 11. Specimen 8 After Edge-On Impact at 66 fps

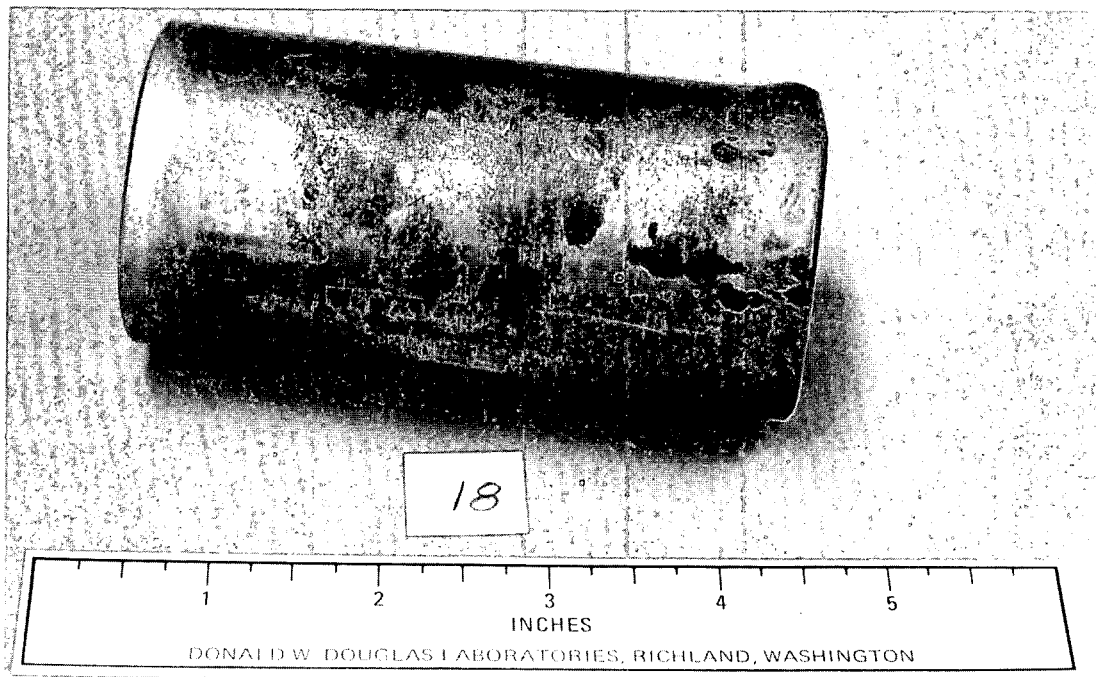
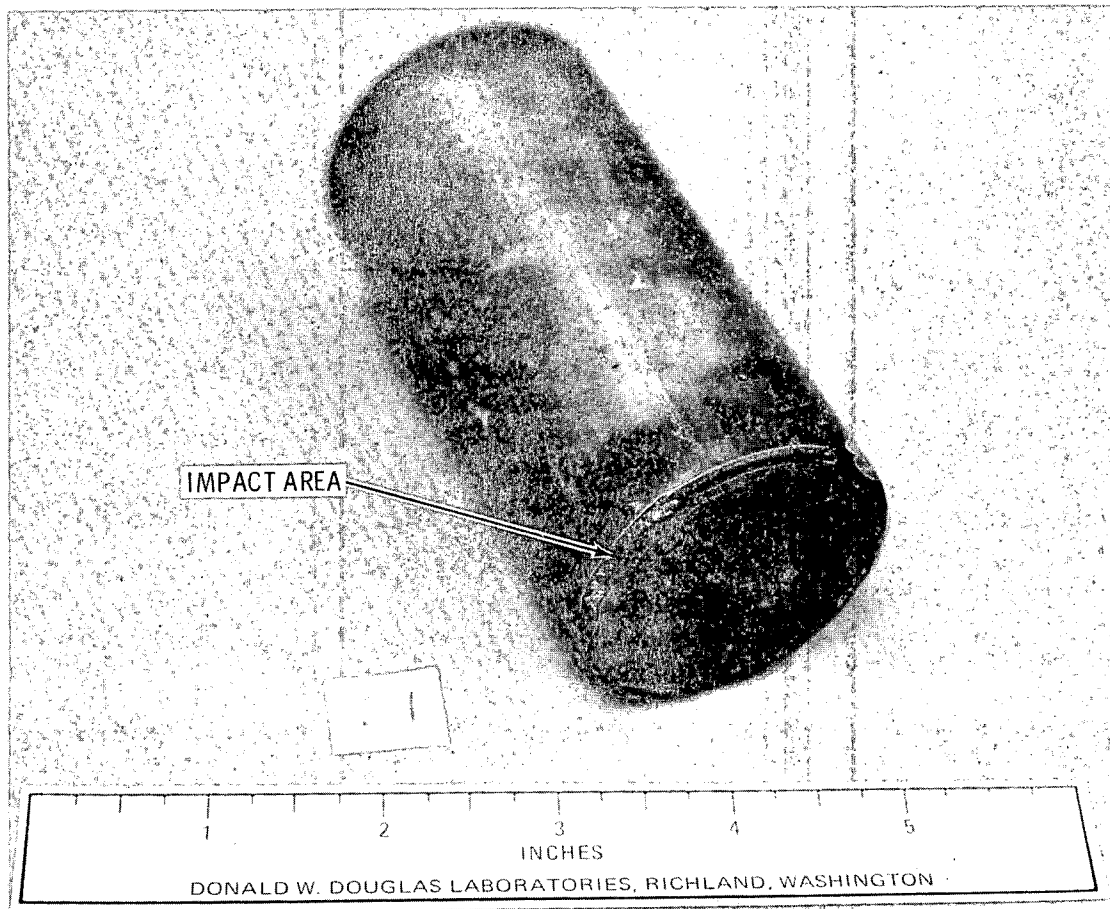


FIGURE 12. Specimen 18 After Edge-On Impact at 44 fps

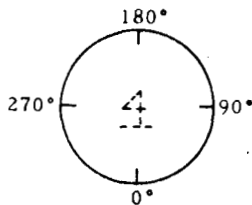


**FIGURE 13.** Specimen 21 After Edge-On Impact at 25 fps

Pre- and post-impact measurements are presented in Table 6 (Ref. 33). Three problems make exact comparisons between canisters impossible:

- 1) Because the edge-on impact was not at the same circumferential point (with reference to the 360° coordinate system in Table 6) for every canister, it was difficult to determine the maximum decrease in length,  $\Delta L_{\max}$  for a given canister.
- 2) Measurement reference markings were obliterated by impact, especially at the higher velocities. The missing length measurements are generally those which would have shown the greatest  $\Delta L$  values.
- 3) The postimpact end bulge of the specimens made it difficult to define a minimum canister length. However, representative  $\Delta L_{\max}$  values derived from posttest photographs are 0.4 in. for 117 fps, 0.2 in. for 66 fps, 0.1 in. for 44 fps, and 0.05 in. for 25 fps.

TABLE 6. Pre- and Post-Impact Measurements of Small Canisters (33)



Diameters taken 1/4 in. from each end (from 0° to 180°) and at mid-length (from 0° to 180° and from 90° to 270°).

Upper end is where void space remains.

Minor differences in lengths are not significant because measurements were made over weld beads and vary somewhat with small changes of position of the vernier calipers.

Specimen	Length (in.)				Diameter (in.)				Weight (gm)
	0°	90°	180°	270°	Upper 0°-180°	Lower 0°-180°	Midpoint 0°-180° 90°-270°		
Pre-1	4.037	4.037	4.042	4.037	1.956	1.960	1.959	1.960	593.5
Post-1	No Measurements				No Measurements				593.5
Δ	No Measurements				No Measurements				0
Pre-24	4.037	4.038	4.036	4.028	1.961	1.960	1.959	1.961	602.9
Post-24	4.036	4.000	-(2)	4.022	1.961	2.184	1.996	1.975	602.9
Δ	-0.001	-0.038	-	-0.006	0	0.224	0.037	0.014	0
Pre-23	4.038	4.036	4.045	4.046	1.962	1.965	1.962	1.964	589.9
Post-23	-	4.025	4.041	-	1.963	2.042	1.976	1.976	589.9
Δ	-	-0.011	-0.004	-	0.001	0.077	0.014	0.012	0
Pre-4	4.041	4.042	4.040	4.040	1.951	1.960	1.957	1.959	603.4
Post-4	4.041	-	-	4.042	1.951	2.068	1.976	1.980	603.4
Δ	0	-	-	0.002	0	0.108	0.109	0.021	0
Pre-5	4.052	4.048	4.049	4.041	1.956	1.961	1.947	1.956	591.4
Post-5	4.052	4.045	-	-	1.959	2.047	1.960	1.969	591.4
Δ	0	-0.003	-	-	0.003	0.086	0.013	0.013	0
Pre-6	4.049	4.046	4.031	4.031	1.959	1.963	1.963	1.961	595.9
Post-6	3.914	3.926	3.918	3.906	1.960	2.105	1.976	1.964	595.9
Δ	-0.135	-0.120	-0.113	-0.125	0.001	0.142	0.013	0.003	0
Pre-7	4.040	4.037	4.043	4.046	1.950	1.959	1.957	1.955	594.9
Post-7	-	4.032	4.045	4.045	1.949	2.025	1.966	1.960	594.9
Δ	-	-0.005	0.002	-0.001	-0.001	0.066	0.009	0.005	0
Pre-8	4.055	4.060	4.052	4.044	1.952	1.961	1.961	1.948	584.1
Post-8	4.051	-	4.051	4.043	1.953	1.961	1.961	1.945	584.1
Δ	-0.004	-	-0.001	-0.001	0.001	0	0	-0.003	0
Pre-9	4.037	4.035	4.026	4.040	1.960	1.962	1.962	1.963	609.5
Post-9	-	4.039	4.027	4.040	1.959	2.006	1.965	1.966	609.5
Δ	-	0.004	0.001	0	-0.001	0.044	0.003	0.003	0
Pre-10	4.042	4.045	4.037	4.042	1.955	1.955	1.951	1.955	578.2
Post-10	4.043	4.044	-	4.042	1.956	2.001	1.952	1.955	578.2
Δ	0.001	-0.001	-	0	0.001	0.046	0.001	0	0

TABLE 6. (contd)

Specimen	Length (in.)				Diameter (in.)				Weight (gm)
	0°	90°	180°	270°	Upper 0°-180°	Lower 0°-180°	Midpoint 0°-180°	90°-270°	
11 Pre-	4.039	4.035	4.034	4.031	1.954	1.958	1.958	1.955	589.7
11 Post-	4.038	4.036	4.024	4.033	1.953	1.986	1.959	1.966	589.7
11 Δ	-0.001	0.001	-0.010	0.002	-0.001	0.028	0.001	0.011	0
12 Pre-	4.046	4.044	4.050	4.047	1.957	1.966	1.962	1.957	582.9
12 Post-	4.048	4.046	4.048	4.042	1.956	1.968	1.964	1.958	582.9
12 Δ	0.002	0.002	-0.002	-0.005	-0.001	0.002	0.002	0.001	0
13 Pre-	4.031	4.032	4.040	4.040	1.952	1.963	1.960	1.960	543.5
13 Post-	4.031	4.031	4.038	4.042	1.952	1.963	1.960	1.961	543.5
13 Δ	0	-0.001	-0.002	0.002	0	0	0	0.001	0
14 Pre-	4.041	4.035	4.037	4.045	1.959	1.960	1.960	1.961	615.0
14 Post-	4.045	4.036	4.037	-	1.959	1.960	1.961	1.960	615.0
14 Δ	0.004	0.001	0	-	0	0	0.001	-0.001	0
15 Pre-	4.050	4.048	4.053	4.052	1.951	1.965	1.962	1.965	589.9
15 Post-	-	4.049	4.050	4.052	1.951	2.040	1.962	1.964	589.9
15 Δ	-	-0.001	-0.003	0	0	0.075	0	-0.001	0
16 Pre-	4.042	4.039	4.036	4.041	1.954	1.958	1.957	1.959	598.2
16 Post-	4.042	4.041	4.035	-	1.953	1.959	1.956	1.959	598.2
16 Δ	0	0.002	-0.001	-	-0.001	0.001	-0.001	0	0
17 Pre-	4.063	4.050	4.047	4.060	1.950	1.961	1.955	1.958	580.0
17 Post-	-	4.050	4.047	4.060	1.951	1.990	1.956	1.956	580.0
17 Δ	-	0	0	0	0.001	0.029	0.001	-0.002	0
18 Pre-	4.028	4.022	4.033	4.037	1.957	1.964	1.960	1.959	613.7
18 Post-	4.027	-	4.033	4.035	1.957	1.963	1.960	1.960	613.7
18 Δ	-0.001	-	0	-0.002	0	-0.001	0	0.001	0
19 Pre-	4.050	4.046	4.042	4.046	1.958	1.966	1.964	1.966	571.0
19 Post-	4.050	4.045	4.048	4.048	1.958	1.976	1.966	1.966	571.0
19 Δ	0	-0.001	0.006	0.002	0	0.010	0.002	0	0
20 Pre-	4.040	4.043	4.046	4.045	1.947	1.956	1.952	1.948	605.2
20 Post-	4.039	4.042	4.046	4.043	1.948	1.956	1.951	1.948	605.2
20 Δ	-0.001	-0.001	0	-0.002	0.001	0	0.001	0	0
21 Pre-	4.046	4.055	4.057	4.060	1.953	1.965	1.957	1.951	598.1
21 Post-	4.044	4.053	4.055	4.061	1.953	1.974	1.953	1.952	598.1
21 Δ	-0.002	-0.002	-0.002	0.001	0	0.009	-0.004	0.001	0
22	No Measurements				No Measurements				

Hypens indicate that posttest length measurements were omitted because impact deformation destroyed the measurement reference point.

Comparisons of canister ductility with glassy versus devitrified waste are inconclusive based on  $\Delta L_{\max}$  values. The same is true for comparisons of test results for room temperature and elevated temperature.

Of interest are the similar  $\Delta L$  values at all measurement points for end-on impact (Specimen 6). This similarity indicates a nearly perfect end-on orientation at impact.

Upper-end diameter changes were less than the measurement uncertainty. Except for canister 4, mid-length diameter changes were very small. Lower diameter changes are uncertain because of the rotational orientation of the canister at impact. Estimated maximum diameter increases are 0.3, 0.1, 0.06, and 0.04 in. for impact velocities of 117, 66, 44, and 25 fps, respectively.

## 2. Canister Integrity

Posttest canister integrity was evaluated by visual observation and dye penetrant checks. The former technique can detect holes of dimensions greater than about 8 mils. The latter technique is good down to about 0.04 mils. A smaller breach could not release significant quantities of a low-leachability glass within a reasonable time.

No breaches were detected after impact at 25 or 44 fps. Impact surfaces of higher velocity canisters were obscured by debris (fragments of granite and paint from the impact block) ground into the point of impact. It was very difficult to distinguish between adherent debris and cracks in the canisters. But after most of the debris was removed, the breaches listed in Table 7 were apparent.

There seems to be no correlation of breach frequency with waste form or impact temperature. The only observed correlation is with velocity: no canisters breached at 25 or 44 fps, half breached at 66 fps, and nearly all breached at 117 fps.

Specimen 6, the end-on unit, was damaged much less than its edge-on counterparts. This result supports the hypothesis that the edge-on impact orientation is the most severe, at least for the canister.

TABLE 7. Breaches in Small Canisters

<u>Specimen</u>	<u>Impact Velocity, fps</u>	<u>Impact Temperature, °F</u>	<u>Waste Form</u>	<u>Equivalent Total<sup>(a)</sup> Crack Dimensions, in.</u>
7	66	802	G	0.01 x 0.3
17	66	RT	DV	0.01 x 0.2
4	117	800	G	0.05 x 0.7
5	117	796	DV	0.1 x 0.8
14	114	RT	G	0.01 x 0.5
23	117	800	G	0.03 x 0.6
24	117	800	G	0.1 x 0.5

RT ≡ Room temperature

G ≡ Glassy

DV ≡ Devitrified

a. In a few instances, there was more than one crack.

Pre- and post-test weights were recorded to estimate the quantity, if any, of glass lost during impact. In no case was there any measurable weight change. The weights were uncertain to about  $\pm 0.1$  g and were further obscured by the adherent debris. Although a small amount of glass could have exited during impact, the consistent lack of any measurable weight change indicates that this quantity must have been extremely small.

## LARGE CANISTERS

### 1. High-Speed Photographic Coverage

Impact of the large canisters was recorded by a Fastex high-speed ( $\sim 4000$  frames per second) 16 mm camera. Ektachrome E.F. Daylight film was used. Figure 14 and 15 show every tenth frame near the time of impact for two canisters. The film coverage provided a record of the sequence of primary and secondary impacts for each canister. It facilitated measurement of actual impact angle (as opposed to drop angle) to within 1 to 2° and actual impact velocity (as a check on drop height) to within 5 to 10%. It also facilitated estimation of the impact duration.

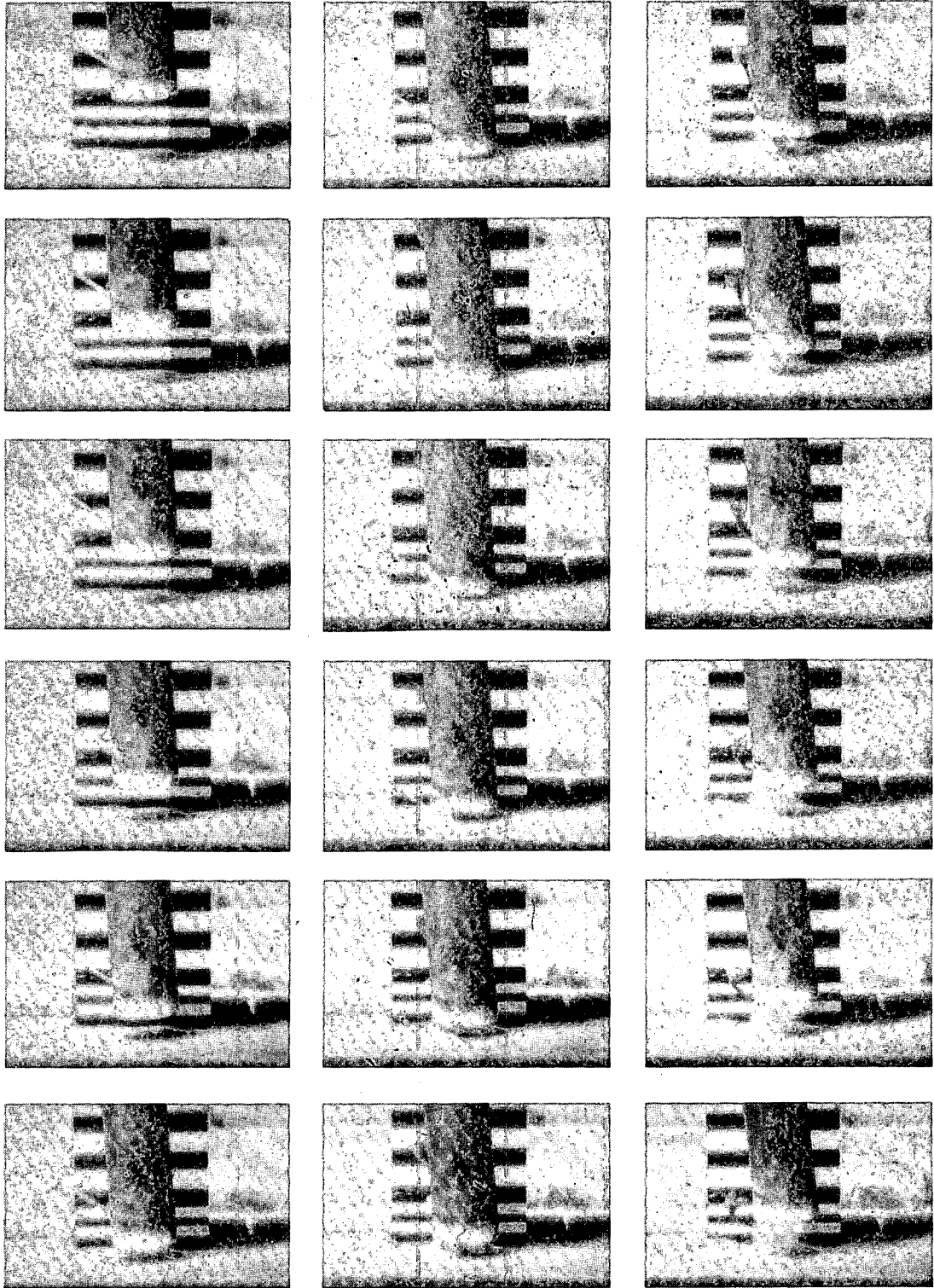
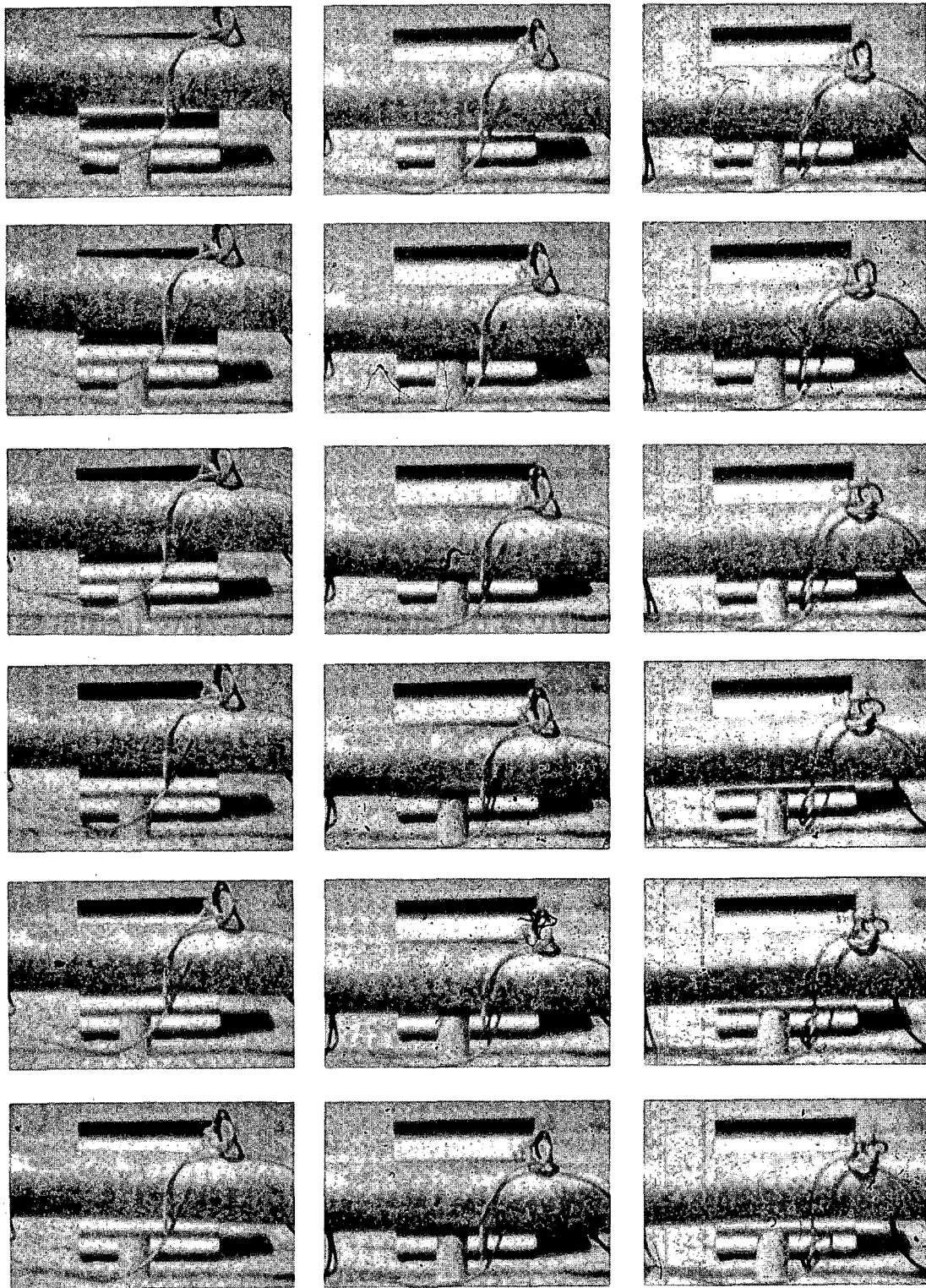


FIGURE 14. High-Speed Photographic Coverage of 30-ft Drop Impact. Every tenth frame is shown. Camera speed is 4680 frames/second.



**FIGURE 15.** High-Speed Photographic Coverage of Side-On Penetration Test. Every tenth frame is shown. Camera speed is 3480 frames/second.

The impact velocity of canister 2 was seen to be about 44 fps, matching the intended value. Impact angle was 4 to 5°. (The intended angle, with the center of gravity above impact point is 5°, for a canister with no lifting eye. Adding the lifting eye increases the equilibrium angle of suspension to about 6°. Thus there was little apparent tendency of the canister to change orientation during release and descent.) The duration of impact was 1 to 2 1/2 msec. Shadows and parallax effects precluded a more accurate measurement. Rebound velocity was approximately 15 fps, giving a coefficient of restitution of about 0.3. The canister bounced about 5 ft high while canting over. The second impact was on the top edge of the canister and on the lifting eye.

The impact velocity of canister 4 was estimated at 24 fps, just below the intended 25 fps. Impact angle was 7 to 8° and impact duration was 2 to 4 1/2 msec. Rebound velocity was about 6 fps, for a coefficient of restitution of 0.2 to 0.3. The rebound height was about 9 in. The second impact was on the bottom but at a greatly changed angle. The third impact was on the top and the fourth on the bottom. Numerous small seesaw bounces followed.

The impact velocity of canister 6 was not checked. The impact angle was 6 to 7° and the duration was 2 to 3 msec. Rebound velocity was about 10 fps and rebound height was 24 to 30 in. The sequence of secondary impacts was the same as that of canister 4, which was dropped from the same height.

Canister 3 impacted the penetrator at an angle of 3°, compared with the intended 0°. Impact duration was 10 to 15 msec. Symmetric elastic bending of the canister about the point of impact was readily observable on the film. The canister bounced almost directly upward about 5 in. Succeeding contacts with the penetrator were at increasingly greater angles.

## 2. Deformation

Close visual observation was required to detect impact areas of most large canisters. The point of greatest deformation on the edge-on canisters

was near the lifting eye. This resulted from secondary impact on a small area of contact with no glass support. Table 8 lists several dimensional changes accompanying impact. Figure 16 shows specimen 2 following a 30-ft edge-on drop.

TABLE 8. Large Canister Dimension Changes

Specimen Number	Impact Velocity, fps	Maximum Diameter Increase at Bottom, in.	Maximum Decrease in Length, in.	Radial Indentation at Mid-length, in.	Radial Indentation Near Lifting Eye, in.
2	44	0.37	0.34	--(c)	--
3	15 <sup>(a)</sup>	--	--	~0.005	--
4	25	0.22	0.16	--	0.62
6	25	0.04	0.13 <sup>(b)</sup>	--	0.54

a. Side-on onto penetrator

b. The bottom face was also bulged outward in the axial direction, with the net decrease in length being only 0.03 in.

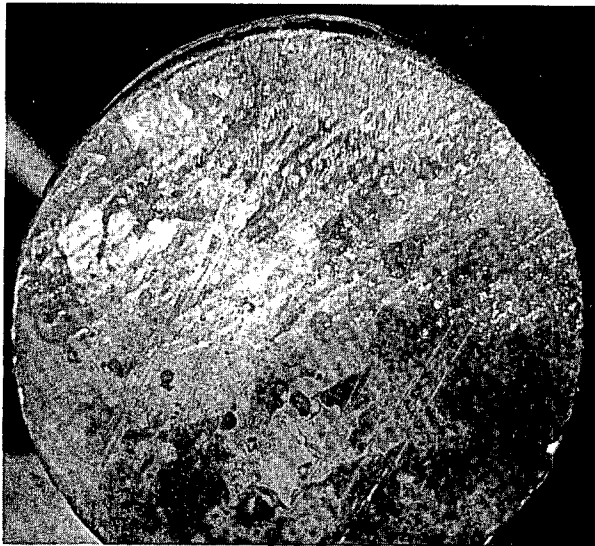
c. Blanks denote no measurement recorded.

### 3. Canister Integrity

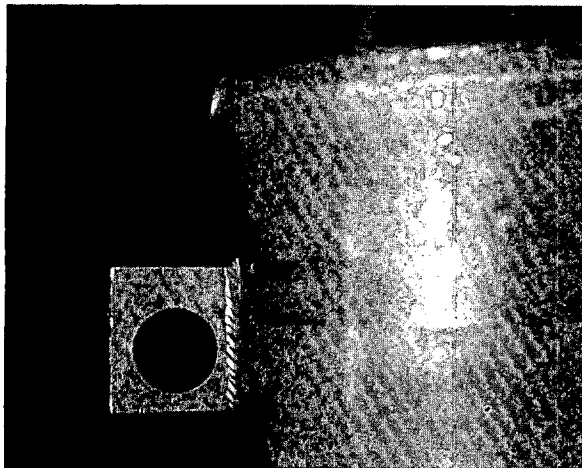
Visual observation and dye penetrant checks revealed no penetrations of canister walls.



Bottom Edge

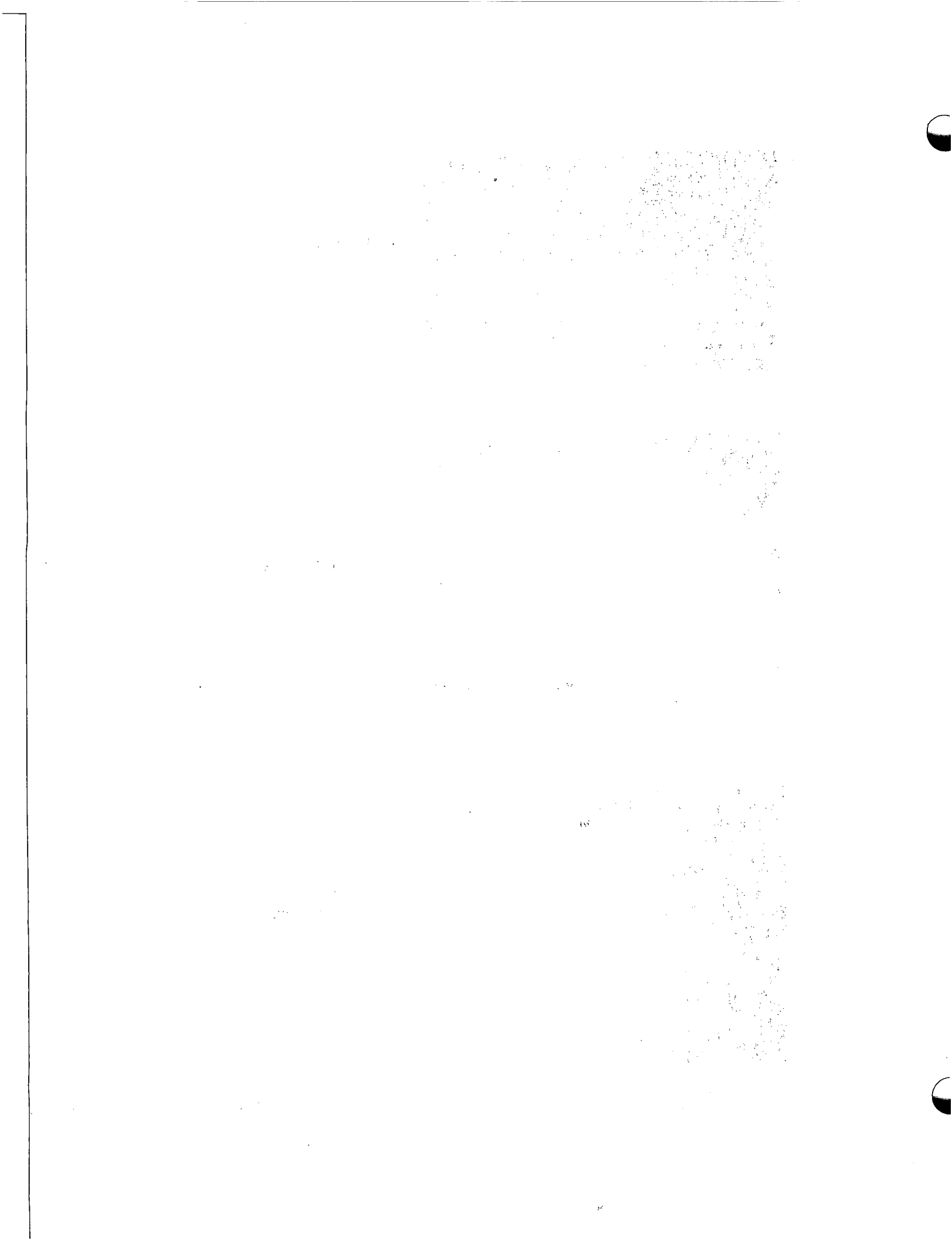


Bottom Surface



Top End Near  
Lifting Eye

FIGURE 16. Large Canister 2 After 44 fps Edge-On Impact



## 8.0 CANISTER OPENING AND PARTICLE REMOVAL PROCEDURES

### LARGE CANISTERS

Because of their size and weight as well as the shell thickness, the large canisters were delivered to the J. A. Jones Company machine shop for initial opening in a large milling machine.

#### 1. Top Opening and Particle Removal

The top end was cut off just below the canister top, about 12 in. above the glass surface. Loose material was brushed into quart cartons.

#### 2. Impact Area Opening

Impact areas were opened in two stages to minimize loss of material. The bottom end was scored across a diameter almost to the glass surface, leaving a thin sheath of steel to be penetrated by hand cutting. A groove approximately the depth of the wall was milled through the canister wall, up each side about 8 in. and then around half the circumference (Figure 17). The section of canister wall thus isolated included the impact area. In a few places the milling cutter did cut through to the glass.

On the side impact canister, the side was milled to produce two longitudinal 8-in. scores 180° apart. The score ends were connected by milling halfway around the canister (Figure 18). One control canister was scored both on the bottom and on the side about midway up but 180° opposite.

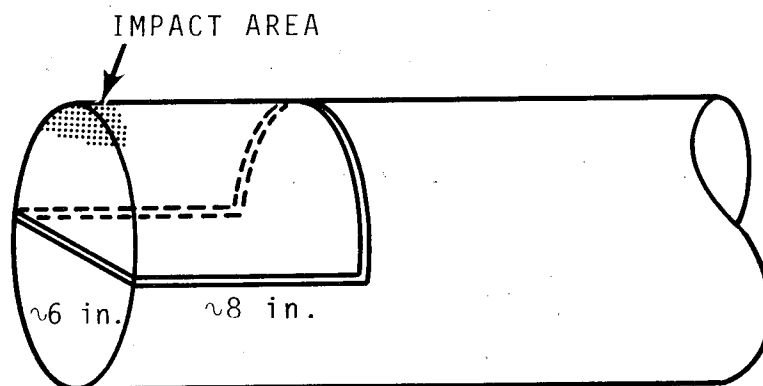


FIGURE 17. Wall Removal Scheme for Large Canisters in Edge-On Impact

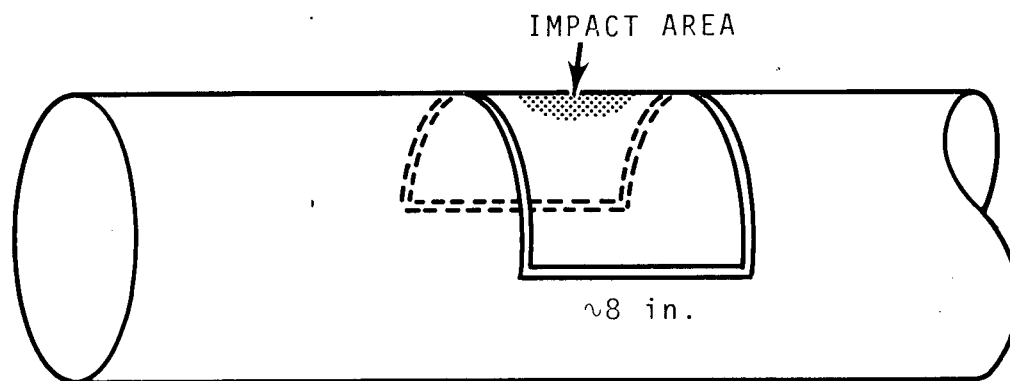


FIGURE 18. Wall Removal Scheme for Large Canister in Side-On Impact

The canisters were then brought to the PNL Atmospheric Sciences Department Laboratory to complete the opening and to remove the fragmented material for particle sizing. Final cutting of the shell was done with a Dremel Moto-Tool, a hand-held, high-speed motor equipped with an abrasive cutting wheel. After the remaining thin steel shell was cut through, it was tapped lightly with a hammer and cold chisel until the cut metal was loose and could be removed. Aluminum foil was placed under the canister to catch particles that fell during opening.

On canister 1 a small amount of glass adhered to the metal shell as it was removed. Breakage apparently occurred during opening. The same occurred with canister 5. In the other cases the metal came away cleanly. On canister 2, as the cutting tool cut almost through the canister, a cracking noise was heard and the cut began to open of itself as if the material were under compression. Nothing unusual was noticed in opening of the other canisters.

Photographs of the area exposed by removing the metal appear in Figures 19-25.

### 3. Impact Area Particle Removal

Forceps were used to pick out larger pieces. This facilitated removal of smaller pieces which began falling out when the shell was tapped. By means of brushing and tapping, all fragmented material that could be removed was collected.

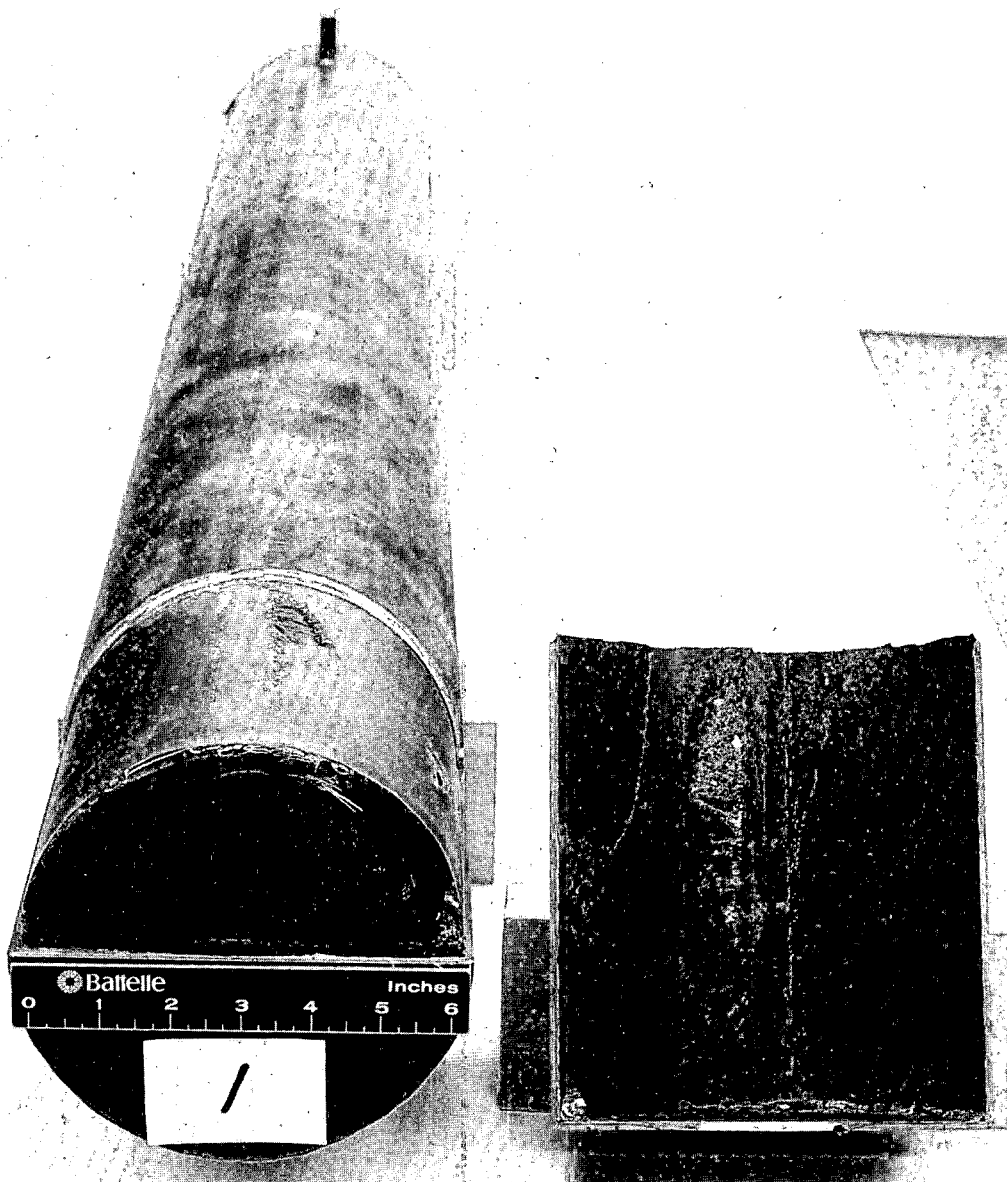


FIGURE 19. Large Canister 1 After Opening

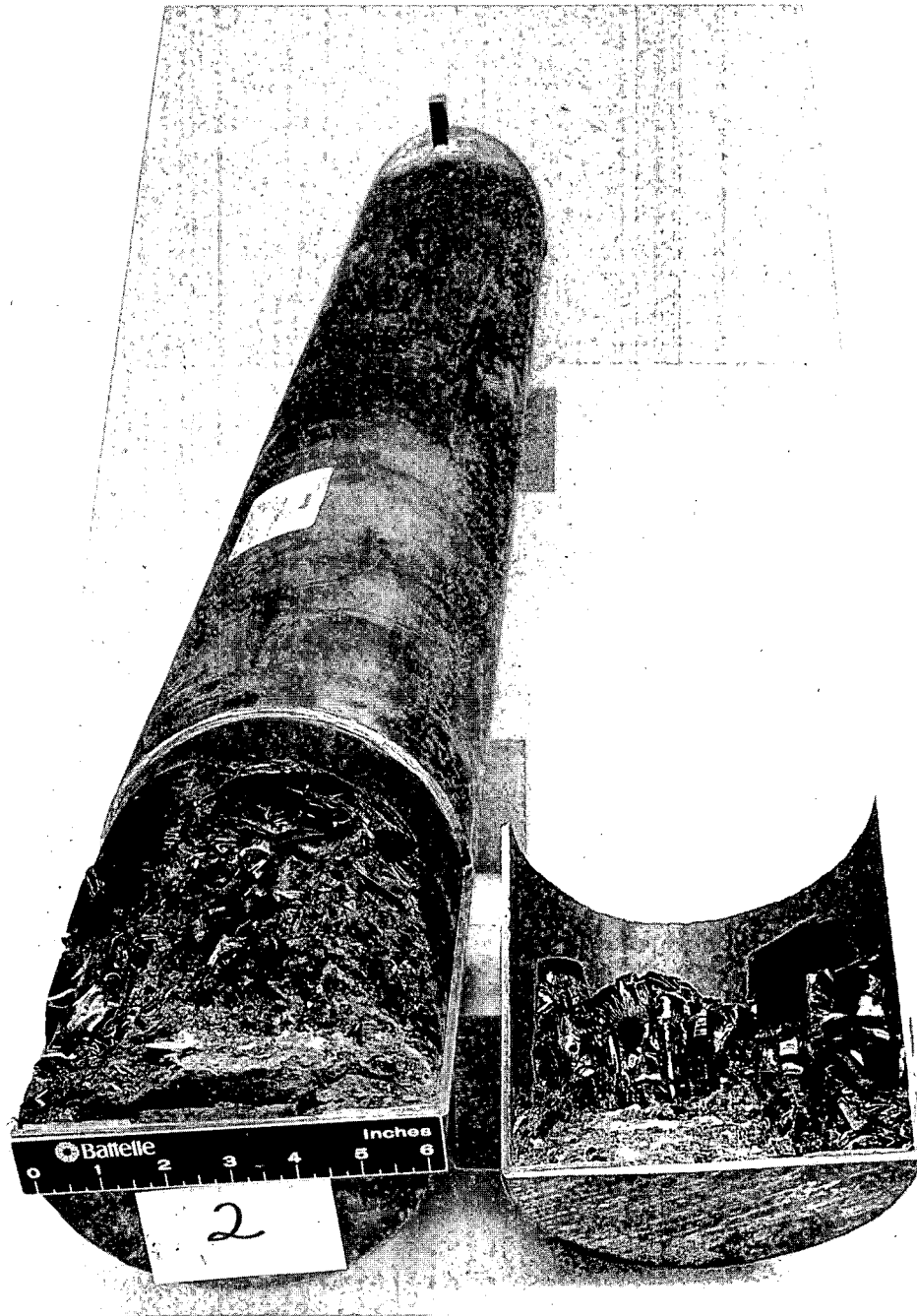


FIGURE 20. Large Canister 2 After Opening

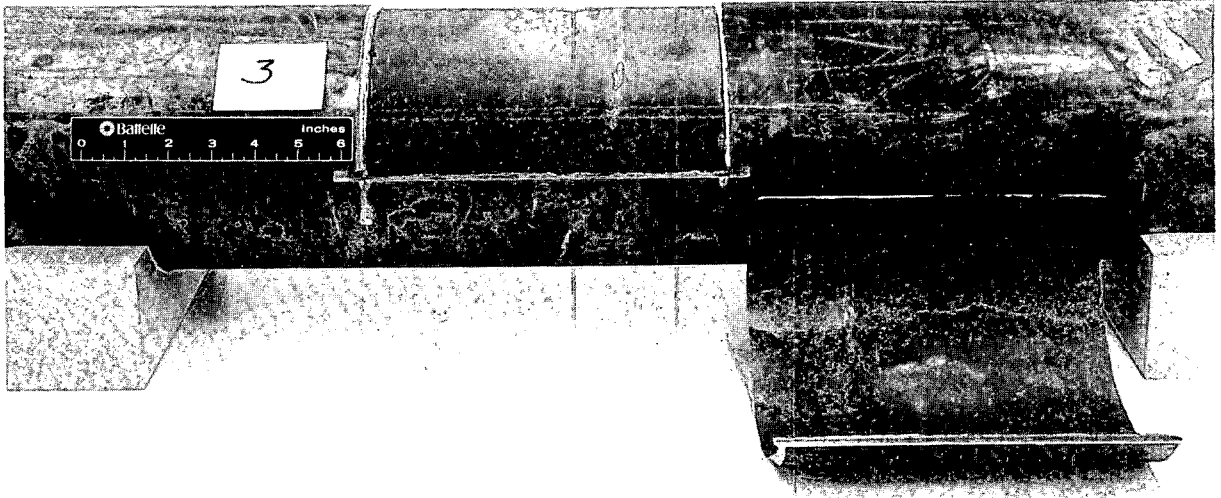


FIGURE 21. Large Canister 3 After Opening

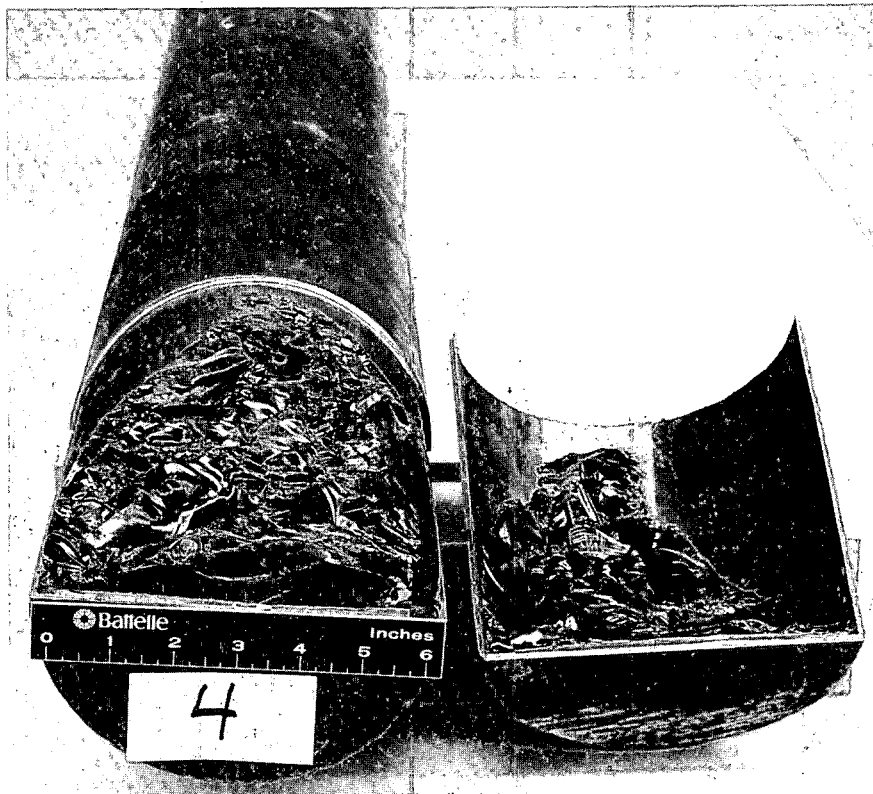


FIGURE 22. Large Canister 4 After Opening

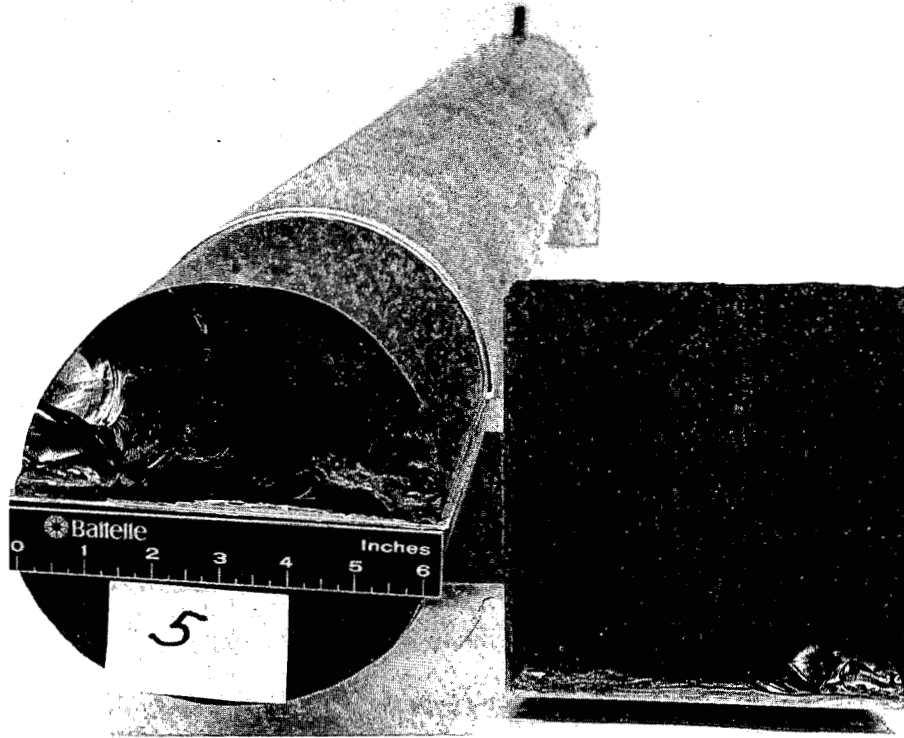


FIGURE 23. Large Canister 5, Edge Area, After Opening

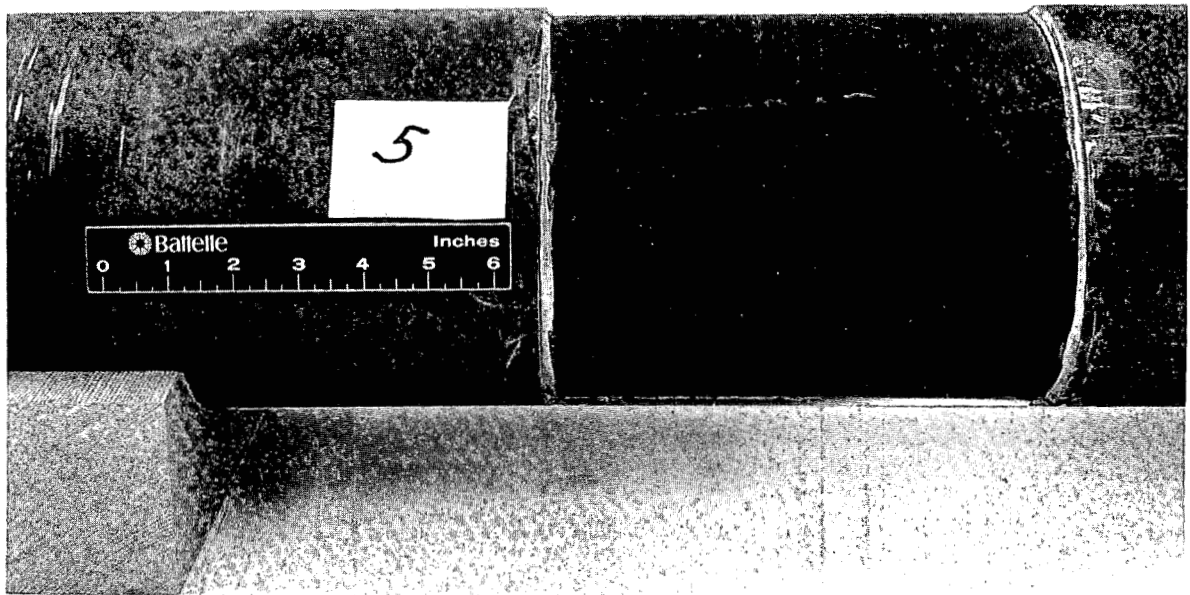


FIGURE 24. Large Canister 5, Mid-Region, After Opening

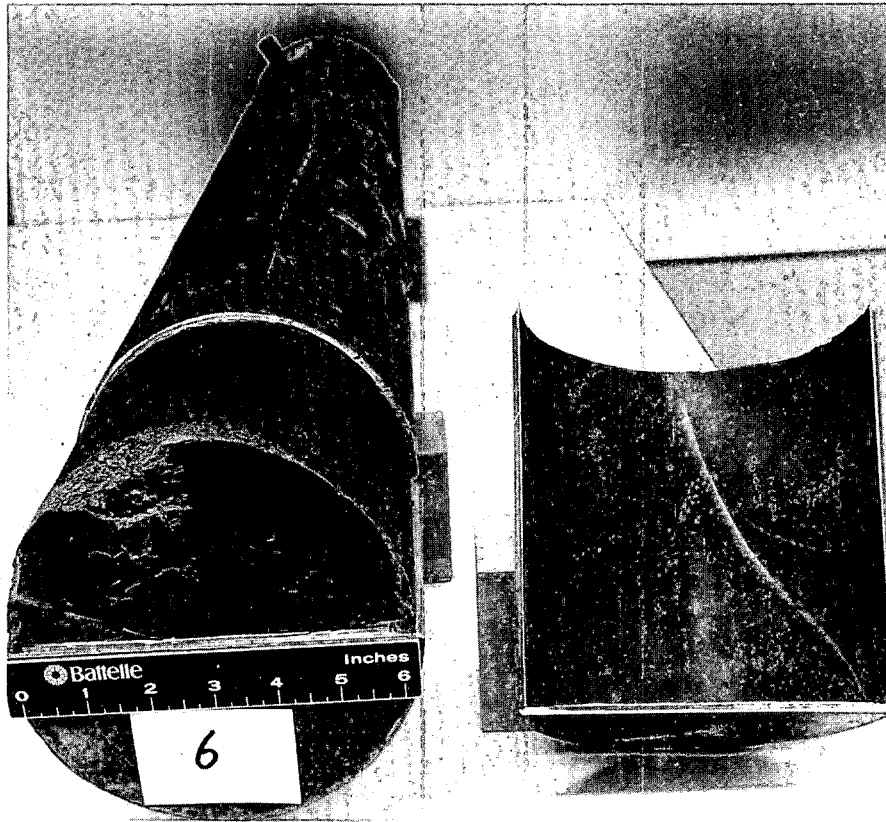


FIGURE 25. Large Canister 6 After Opening

### SMALL CANISTERS

After impact testing, the small canisters were sent to the PNL Atmospheric Sciences Department Laboratory for opening, particle removal and sieving.

#### 1. Top Opening and Particle Removal

The canisters were opened in the head space above the glass, just below the canister top. The canister was held in a padded vise to avoid further fracturing of material during opening. The canister was cut with a sharp pipe cutter by slowly rotating the cutter several times, avoiding deformation arising from the contact pressure of the operation.

All glass fragments were then removed from the top area by rolling and by brushing with a camel's hair brush. No attempt was made to force material out, but some that was loose and entrapped was picked out with forceps.

## 2. Bottom Opening and Particle Removal

Because of the severe impact conditions, it had been expected that the glass would be severely broken up and could be poured out the opened top. However, in all but one canister, after removal of the small amount of broken material from the top, a glass monolith remained between the top and the impact area. The stepwise scheme for opening the bottom of the canisters is explained below.

By means of a milling machine a 5/8-in. hole was cut in the bottom near the impact area. The rotodie cuts through the steel to a predetermined depth and avoids cutting the glass. The glass was removed first by rolling the canister then by tapping it and picking and removing all loose material. A few of these two fractions were sized individually, but later this separation was considered unnecessary and discontinued.

Because a further opening step was needed on some canisters, a 1-3/4-in. hole was cut in the canister bottom, extending the opening to encompass almost the complete bottom area. For canisters yielding no material this was the final step. Other canisters had broken material exposed by this step. This fractured material was removed by tapping the canister and picking out glass fragments where necessary. By brushing, tapping, shaking and inverting the canisters, all material that could be removed was collected.

Certain canisters (10, 11, 12, 19, 20, 21) required still more opening to expose the impact area for particle removal. They were cut by hand around the impact area using a Dremel Moto-Tool.

Figures 26-31 show several small canisters after opening.

Canisters 19 and 20 were cut lengthwise from top to bottom with a glass saw to reveal the interior of the glass monolith (Figure 32). This result and other observations suggested that the fraction of particles recovered was close to unity.

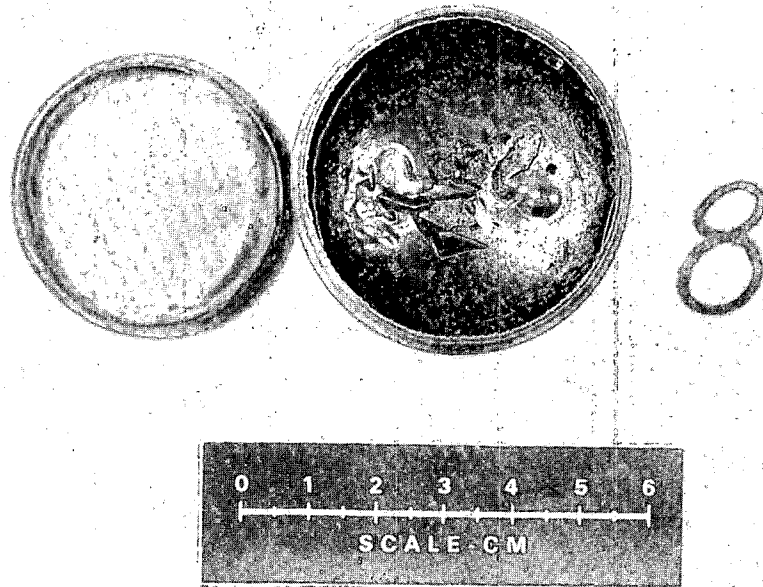


FIGURE 26. Small Canister 8 After Opening, Top View



FIGURE 27. Small Canister 8 After Opening, Inverted

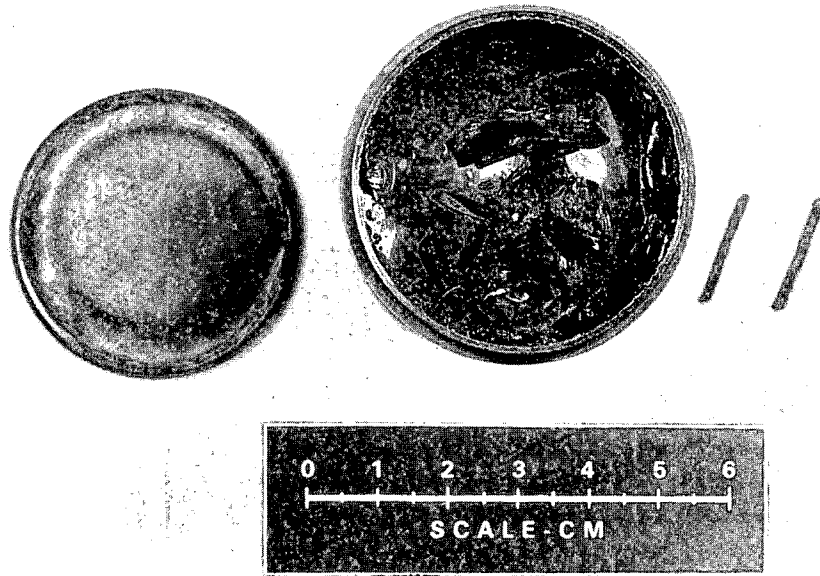


FIGURE 28. Small Canister 11 After Opening, Top View

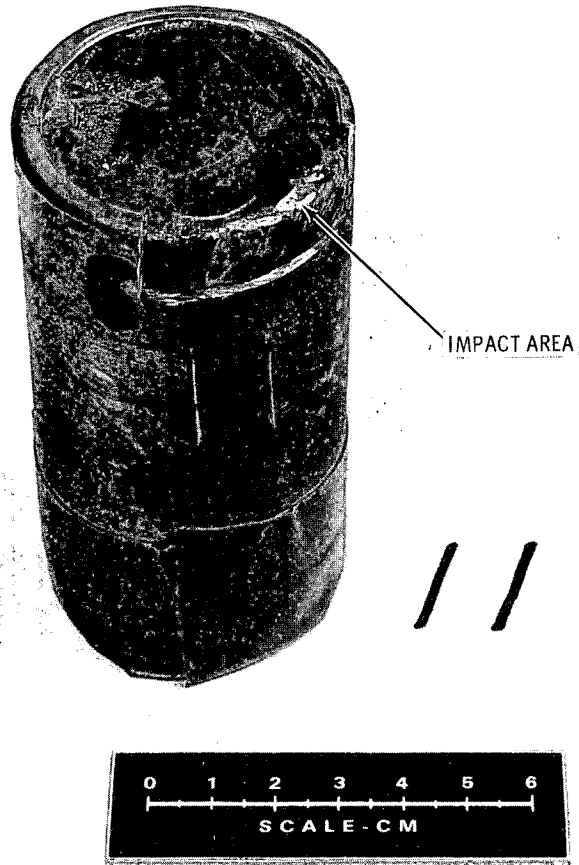


FIGURE 29. Small Canister 11 After Opening, Inverted

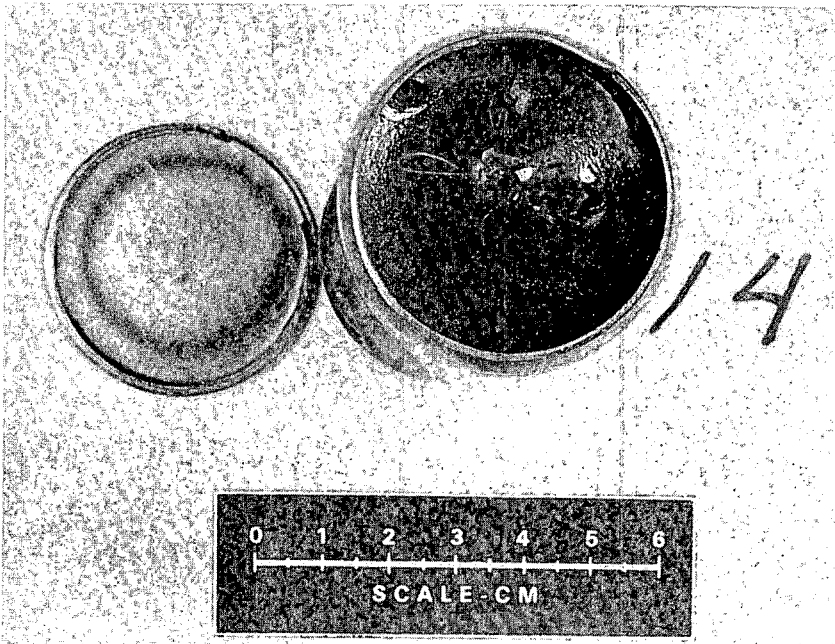


FIGURE 30. Small Canister 14 After Opening, Top View



FIGURE 31. Small Canister 14 After Opening, Inverted

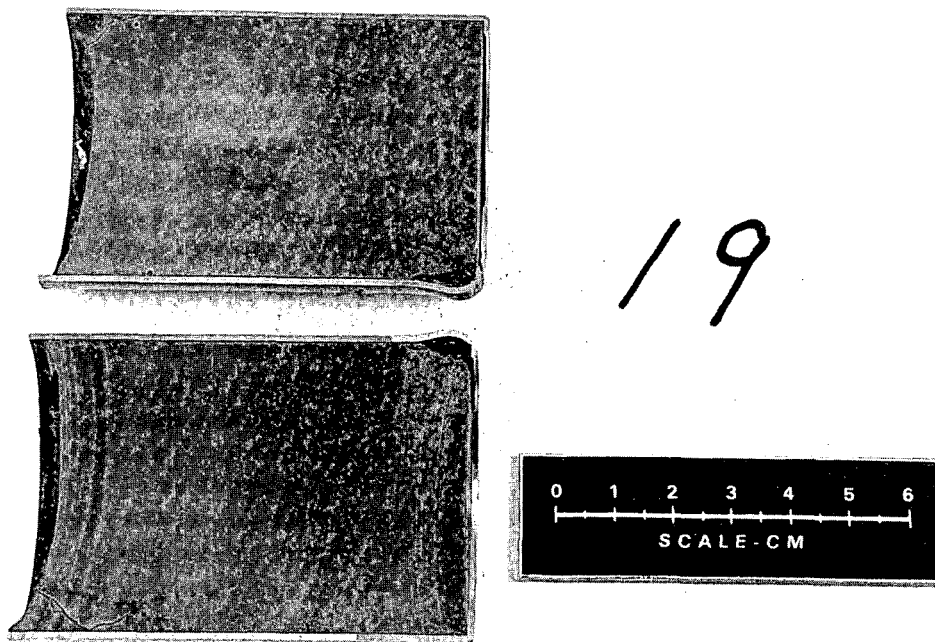


FIGURE 32. Small Canister 19 After Opening and Longitudinal Sectioning

#### ERRORS INTRODUCED BY THE PARTICLE REMOVAL PROCEDURES

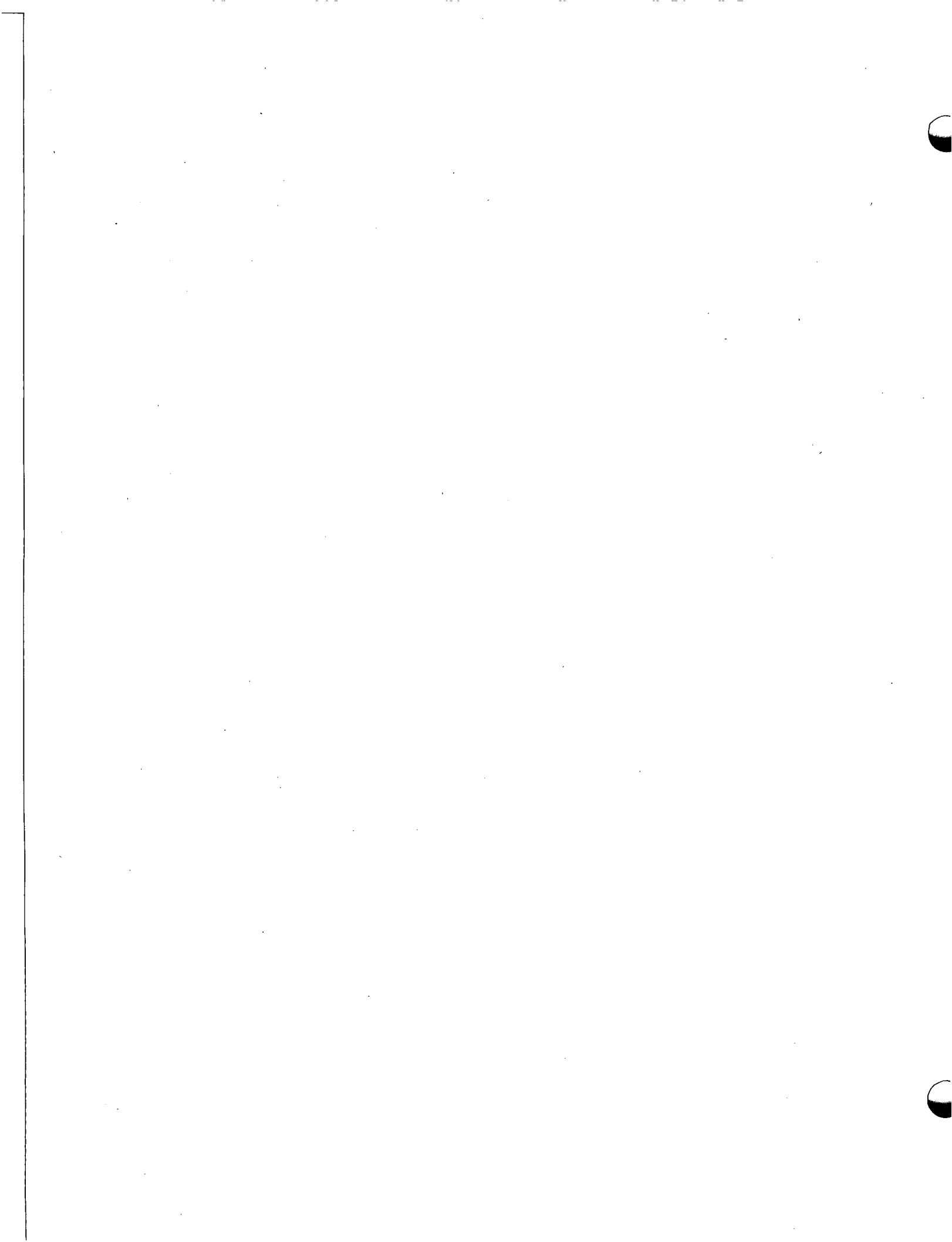
Ideally, the metal canisters could be made to disappear to allow removal of the glass particles. Nonidealities of the canister opening and particle removal procedures are discussed here.

During opening and removal care was taken to avoid generation of new fragments. Handling was held to a minimum since the bare glass is subject to breakage. Despite these precautions, the procedures had a potential for introducing errors into the results in several ways. Cutting and opening operations can introduce new particles by 1) cutting too deeply through the steel and grinding the glass; 2) introducing pieces of ground steel shell into the sample; 3) mechanically stressing the glass.

Though the milling machines used are precise, some material was still generated on a few canisters. If the material was obviously not from impact (as metal shavings), it was not included in the material collection. Little error is expected here.

The milling machine is equipped with a holder to minimize canister deformation. While cutting the canister with the Dremel tool, the operator wiped the area clean frequently to remove generated particles. The small canisters were held by a padded vise while the top was opened by a pipe cutter, thus minimizing deformation of the steel shell. This process is not expected to be a significant source of error.

Loss of material was minimized in the small canisters by taping the top back in place after opening. Bottom areas were placed in a plastic bag after opening. The small canisters were opened above a clean glossy paper. Final opening of the large canisters was done with aluminum foil suspended beneath the canister to catch material. For both large and small canisters, the material was immediately removed to a tared container, which was reweighed and covered.



## 9.0 PARTICLE SIZING PROCEDURES

### LARGE CANISTERS

Broken material, top and bottom, was removed from the canisters and weighed. Lots weighing more than 100 g were sieved on standard Tyler sieves with the following size numbers: 12 (1,700  $\mu$ ), 20 (841  $\mu$ ), 70 (210  $\mu$ ), 100 (149  $\mu$ ), and 200 (74  $\mu$ ). A Tyler portable sieve shaker was used. Lots of less than 100 g were sieved by means of an Allen-Bradley sonic sifter, with 210  $\mu$ , 149  $\mu$ , 74  $\mu$ , 37  $\mu$ , 20  $\mu$ , 10  $\mu$ , and 5  $\mu$  sieves.

Sieving of the bottom material from canister 2 was initially done through the set of large sieves from No. 12 to No. 200. Since there was a large quantity of fractured material (2493.5 g), this lot was sieved in 4 aliquots and the numerical results combined. After the large material had been removed, the material <74  $\mu$  remained to be sized. Two aliquots of this fraction were sieved through fine mesh screens using the Bradley sonic sifter. Since the limit on sample size for sonic sieving is 3 g, it was decided that sieving the entire 72.3 g of material <74  $\mu$  would be too time consuming. Another separation was made using the large screens, and this fraction was divided into fractions >44  $\mu$  and <44  $\mu$ . Aliquots of the <44  $\mu$  fraction were then sieved through the sonic sieves: 37  $\mu$ , 20  $\mu$ , 10  $\mu$ , and 5  $\mu$ . About 1 g was the optimum quantity of material for this sonic sieve analysis. Bottom fractions from the other canisters presented no unusual problems.

Top material removed at J. A. Jones was found to have metal pieces inextricably incorporated with the sample. Top material from canister 2 was so contaminated with metal pieces that the sizing results were inaccurate. As there were no glass particles <37  $\mu$  in any of the top fractions, the omission is not serious.

### SMALL CANISTERS

Where there was sufficient sample, the fragments were separated into  $>74 \mu$  and  $<74 \mu$  fractions, using a standard No. 200 sieve and shaking for half an hour. On later samples, this procedure was modified because the abrasive glass destroyed the sieve.

The  $>74 \mu$  size fraction was sieved on Tyler sieves with the following size numbers: 12 (1651  $\mu$ ), 20 (841  $\mu$ ), 40 (420  $\mu$ ), 70 (210  $\mu$ ), 100 (149  $\mu$ ), and 200 (74  $\mu$ ). The samples were shaken on a Tyler mechanical sieve shaker for 1 hr. Sieves were weighed before and after shaking, which gave the quantity collected in each size fraction. After shaking, there was a small amount of material in the solid brass pan below the 74  $\mu$  screen. Since the sample had first been divided into  $>74 \mu$  and  $<74 \mu$  fractions and the  $<74 \mu$  material removed for separate sizing, the material in the solid pan was not considered a valid sample. It was considered to consist of newly generated particles. When the procedure was later modified to eliminate the initial split at 74  $\mu$ , the shaking time was shortened to 15 min to avoid generation of new material.

The  $<74 \mu$  size fraction was sized by sonic sieving in an Allen-Bradley sonic sifter, with sieves weighed before and after sifting. This procedure separated the 37  $\mu$ , 20  $\mu$ , 10  $\mu$ , and 5  $\mu$  fractions. Since the canisters had experienced different impact velocities and contained different quantities of fines, each canister required individual sizing consideration.

### SIZE SAMPLING WITH MICROSCOPE

Two  $<5 \mu$  fractions (small canister 5 and large canister 2) were sized further using a Bausch and Lomb Microscope with overhead projector. A representative field was selected. Images of all particles within an area along a path were scanned and measured (equivalent circular dimension) until 200 particles had been sized. The results were grouped in the following distribution:  $>5 \mu$ , 3-5  $\mu$ , 1-3  $\mu$ , and  $<1 \mu$ . See Appendix B.

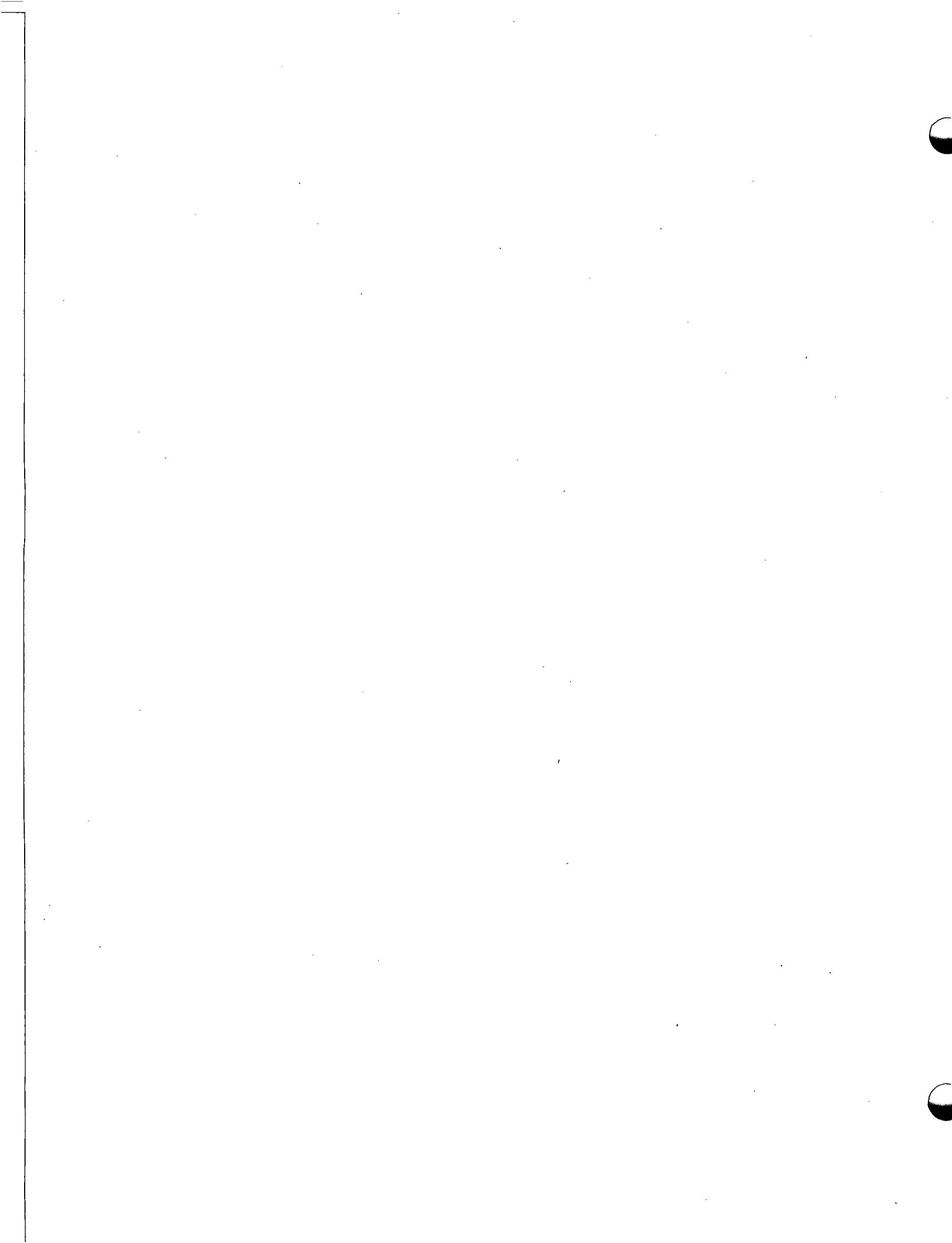
## SIEVING ACCURACY

Sizing by means of sieves is rapid and relatively straightforward. However, a sieve cannot make a perfectly sharp separation, especially of irregular particles. Results can be distorted because elongated particles can pass through a sieve opening if the particles are oriented end-on. Also small particles may not pass through a larger opening because they never get immediately next to it. The fraction of particles passing through depends on mesh size and manner of shaking, quantity of sample, moisture content, percentage of particles closely similar in size to the sieve openings, electrostatic attraction and other factors. However, if sieving procedures are standardized, reproducible results with a series of samples can be obtained.

The sieves used for sizing the  $>74 \mu$  fraction were the sieve size designations proposed by the ASTM International Standards. A mechanical shaker was used to standardize the shaking action. The shaker frame holds up to 13 sieves at a time and imparts both a circular and a tapping motion to the sieves. Recommended sieving times range from 20 to 45 min depending on the material. Because excessive shaking with this material seemed to generate new particles, a 15-min shaking was used as a compromise between new particle generation and complete separation. As the sieves fit well, dust loss was minimal.

If the sample size is too large, agglomeration can occur, particularly on the sonic sieves. In one case of an aliquot from large canister 2,  $>44 \mu$ , the material seemed to ball up, so smaller aliquots were chosen. The sonic sieving time is inversely proportional to the fraction of open sieve area. Forty-five minutes shaking was found optimum. To avoid weighing errors, the screens were equilibrated to room temperature before and after sieving.

There is some loss during material transfer related to sieving. The significance of this uncertainty is addressed in Section 10.0.



## 10.0 GLASS IMPACT RESULTS

### FRACTION OF INVENTORY BROKEN

#### 1. Large Specimens

Table 9 presents material balances for the large specimens. The pre-impact weight of the nearly-monolithic glass is given, along with the quantities of broken glass collected from various locations on the canister. Broken material retrieved from all locations was conservatively totaled for calculation of the maximum potential release fraction as a direct result of impact. This approach ignores post-impact containment by the canister. The tests showed that, even if a canister failed, generally only a small part of the broken waste glass could move because the remainder of the canister and unbroken glass would provide barriers.

Table 9 indicates that, for edge-on impact specimens 2, 4 and 6, most of the broken glass came from the (bottom) impact end. A small fraction (very small for higher velocity specimen 2) came from the top, caused by spallation or by secondary impact on the top. Side-on impact of specimen 3 against the penetrator resulted in surprisingly little glass breakup near the impact area. Control specimens 1 and 5 indicate the amount of glass breakup during fabrication, handling and opening.

#### 2. Small Specimens

Table 10 summarizes material balances for the small specimens. Section 8.0 described how the bottoms of these canisters were opened in stages--first a 5/8-in. hole, then a 1-3/4-in. hole, then (if necessary) removal of the entire bottom and lower edge. The objective was to estimate how much broken glass would migrate through various-sized holes. As the results were not definitive, the procedure was changed to combine all material gathered from the bottom of the canister. However, in all cases but one the amount of broken material which passed through a 5/8-in. hole was 1/2 to 2 orders of magnitude less than the total quantity of broken bottom material. Inhibition of flow is attributed to compression of the broken

TABLE 9. Large Specimen Material Distribution

Canister	Original Glass Weight, lb <sub>m</sub>	Top Material, lb <sub>m</sub>	Bottom Material, lb <sub>m</sub>	Total Fraction Broken
1	189	~0	0.0169	0.000089
2	191	~0.01 <sup>(e)</sup>	5.50	0.029
3	193	0.0514 <sup>(a)</sup>	0.0011 <sup>(b)</sup>	0.00027 <sup>(c)</sup>
4	193	0.105	0.216	0.0017
5	190	0.0394 <sup>(d)</sup>	0.0676	0.00056
6	182	0.122	0.740	0.0047

- a. At the canister end containing the void space. The other end was not opened. Less broken material is expected there than that at the void end.
- b. At impact area (on side of canister) for side-on drop onto penetrator.
- c. This number is less than the total fraction broken. See notes a and b.
- d. Plus an additional 0.046 lb<sub>m</sub> in one very large chunk (characteristic dimension of 2.4 cm = 24,000 μ).
- e. Exact quantity not known because of contamination of the sample by metal shavings.

glass by the canister. Once the canister was opened past the edge, this compression was much reduced and the broken glass easily removed.

Table 10 shows that for only four of the impacted specimens was the top portion of broken glass greater than 10% of the bottom portion. This pattern could be correlated neither with impact velocity nor glass condition. The small canisters did not experience secondary impact.

### 3. Comparisons

#### General

Figure 33 plots the "Total Fraction Broken" columns of Tables 9 and 10 versus impact velocity. Points at zero velocity represent control specimens. The general dependence on velocity is evident. If data scatter and the different types of specimens are considered, a linear fit is seen to be a creditable approximation.

TABLE 10. Small Specimen Material Distribution

<u>Specimen</u>	<u>Original Glass Weight, g<sup>(a)</sup></u>	<u>Top Material, g</u>	<u>Bottom Material, g</u>	<u>Total Fraction Broken</u>
1	442.5	0.203	-	0.00046
24	451.9	6.384	321.1	0.72
23	439.1	196.9 <sup>(b)</sup>	236.8	0.99
4	452.5	3.097	297.1	0.66
5	440.3	3.877	351.2	0.81
6	444.8	10.083	271.3	0.63
7	443.9	1.437	66.8	0.15
8	433.4	0.387	11.577	0.028
9	458.6	1.772 <sup>(b)</sup>	3.550	0.012
10	427.3	0.358	5.236	0.013
11	439.0	1.967 <sup>(b)</sup>	1.454	0.0078
12	432.0	0.18	4.61	0.011
13	392.4	0.025	-	0.00006
14	463.8	0.096	14.95	0.032
15	439.0	0.036	14.1	0.032
16	447.4	0.043	7.51	0.017
17	429.0	0.051	5.52	0.013
18	462.4	0.017	0.246	0.00057
19	419.9	0.118	1.78	0.0045
20	454.4	0.055	5.337	0.012
21	447.3	0.34 <sup>(b)</sup>	0.208	0.0012
22	445.0	0.026	-	0.00006

- a. Obtained by subtracting the average canister weight from the specimen weight and assuming 0.0 g of glass exited during impact.
- b. Top portion  $\geq 10\%$  of bottom portion, excepting control specimens 1, 13, 22.

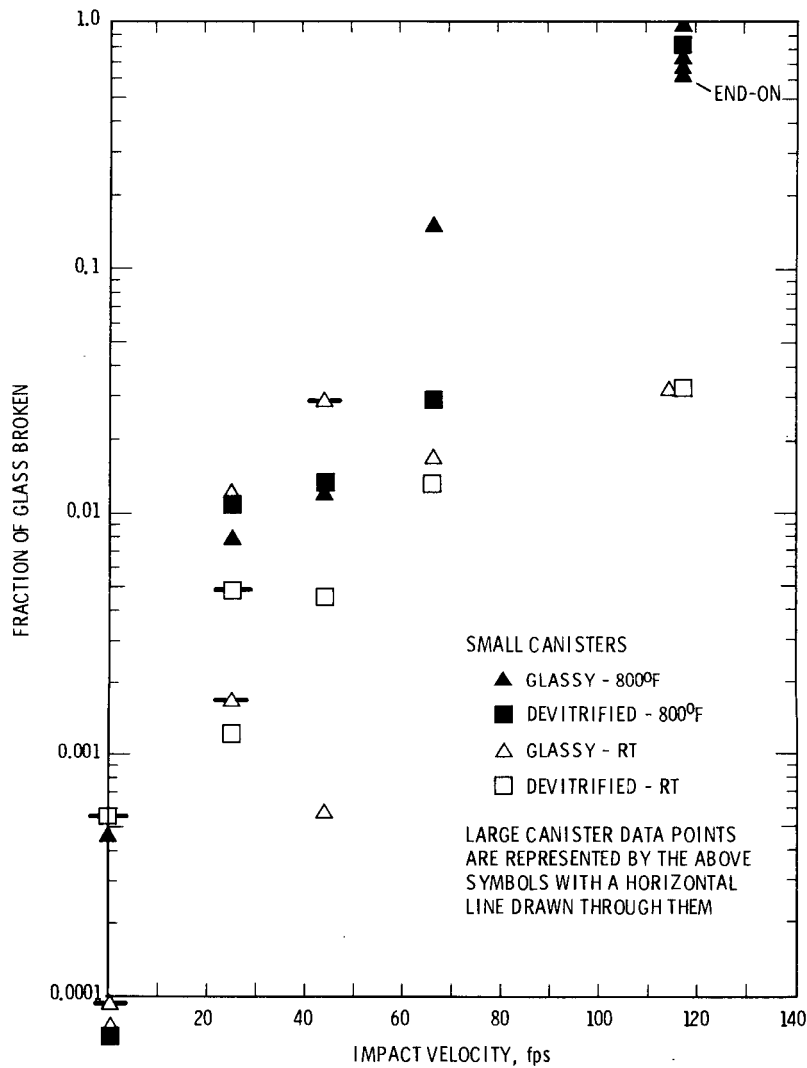


FIGURE 33. Fraction of Glass Broken

Effects of Glass Condition and Test Temperature

For the small specimens, nine pairs of points were compared on the basis of glassy versus devitrified breakup under identical conditions. In four pairs, the glass broke up more; in two pairs, the devitrified; in three pairs, essentially no difference. In no case was the difference more than one order of magnitude. Thus no significant effect of glass condition was apparent. The conclusion holds at both room temperature and elevated temperature.

Two pairs of points for the large specimens indicated greater breakup for the devitrified waste, but the sample size was too small to draw conclusions.

Comparison of small canister data at low and at elevated temperatures leads to a rather surprising conclusion. One might expect less waste breakup at elevated temperature because of increased ductility. However, greater breakup (by up to 1-1/2 orders of magnitude) was observed at elevated temperature in eight of the nine pairs of points compared. (In the ninth case, the difference was very small.) This effect, whose magnitude was generally a factor from 3 to 10, was independent of impact velocity and of glass condition.

It might be suspected that thermal treatment in the impact injection furnace or thermal shock upon ejection and cooldown was responsible for this greater breakup. The evidence is against this explanation. If time at temperature were responsible, devitrified specimens, which experienced a more severe treatment than the specimens impacted at elevated temperature (700°C for 4 days versus 425°C for a few hours), would exhibit greater breakup than glassy specimens. As noted previously, there was no consistent difference between glassy and devitrified specimens. If the ejection and cooldown transient were responsible, one would expect considerable breakup in the elevated-temperature control specimens. However, specimens 1 and 13 exhibited very low breakup fractions. The control specimens fall about where one would expect to find them by extrapolating back to zero velocity.

Another possible explanation is that the glass strength may be significantly less at elevated temperature. However, the modulus of elasticity at 425°C is within 5% of its room temperature value.<sup>(34)</sup> The failure strain for high-speed loading is expected to be only slightly changed. This waste glass retains its brittle nature, especially at high loading rates, from room temperature to above 425°C, the maximum temperature of the impact tests. The "ductile-brittle" transition is about 500°C.<sup>(35)</sup>

Another explanation, supported by calculations, can be postulated from review of the glass processing steps. Viscous molten glass is poured into canisters which are held at (or soon increase their temperature to) at least 550°C. On cooling after glass solidification (the glass becomes fairly rigid at 500°C), the stainless steel contracts more than the glass, placing the glass in compression and the steel in tension. Average thermal expansion coefficients of the glass and stainless steel between 500°C and room temperature are approximately  $9 \times 10^{-6}/^{\circ}\text{C}$  and  $17 \times 10^{-6}/^{\circ}\text{C}$ , respectively. The precompressed room-temperature glass is more resistant to tensile stresses which might cause fracture on impact. On heating back to 425°C for elevated temperature tests, the preexisting compressive stresses are greatly reduced, if not eliminated, with a corresponding reduction in impact resistance.

The mismatch in glass and steel radii upon cooling is 3.6 mils for small specimens and 12 mils for large specimens. The calculated<sup>(36)</sup> contact pressure at room temperature is sufficient to yield the canisters and is expected to be limited to approximately 1700 psi because of the yielding. Thus the glass is stressed to 1700 psi compressive and the canister is slightly into yield with a hoop stress of about 42,000 psi. Upon reheating to 425°C, the contact pressure and glass precompression are eliminated because of the yielding which occurred during the initial cool-down. (With no intervening cooldown to room temperature the contact pressure at 425°C is calculated to be about 600 psi.)

Thus room-temperature precompression is of such magnitude that a significant effect on impact behavior would be expected. The tensile strength of borosilicate glass is typically 9,000-10,000 psi. The observed effect was in the predicted direction and, qualitatively, of the expected magnitude.

#### Large Versus Small Specimens

The small canisters are not scaled reductions of the large canisters. Because of specimen size limitations on the DWDL impact equipment, the small specimens were shortened from the large specimen L/D value of 9.6 to a value of 2.1, a factor of 4.6.

Canister behavior has been shown to be almost independent of L/D, but the L/D effect on glass behavior was expected to lie between two extremes (temporarily disregarding effects of specimen size). Figures 34 and 35 show two extreme models of breakup for cylinders of different L/D ratios. In one extreme, if glass breakup were a completely localized phenomenon (Figure 34), the amount of glass broken would be expected to be independent of specimen length. The fraction of glass broken would be inversely proportional to specimen length, and the shortened specimen breakup fraction would be 4.6 times that of the full-length specimen. In the other extreme (Figure 35), the L/D value would not be relevant, and shortened and full-length specimens would exhibit identical fractional breakup of the glass.

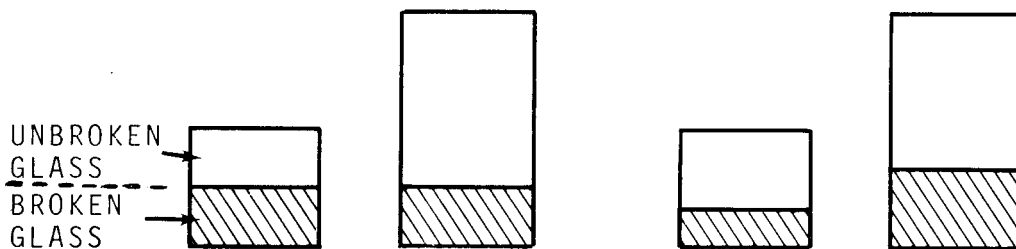


FIGURE 34. Glass Breakup is a Local Phenomenon. Quantity of glass broken is identical for the two equal-radius cylinders.

FIGURE 35. Glass Breakup is a Mass/Volume/Area Phenomenon such that the Fraction of Glass Broken is Identical for the Two Cylinders

In the various parts of Section 10, small and large specimen results are compared on the bases of the fractional breakup, the fraction  $<10 \mu$ , and the surface area produced. The comparison in this subsection is on the basis of fractional breakup.

At 25 and 44 fps, Figure 33 shows greater fractional breakup of the large specimens in two instances and of the small specimens in one instance. Control results show little difference. In these very limited comparisons, the model of Figure 35 appears to be the more representative for fractional breakup.

## PARTICLE SIZE DISTRIBUTION

### 1. Results

Tables of the size distribution of particles recovered from each specimen appear in Appendix A. The data are given in terms of sieve size. For order of magnitude estimates, the data are representative of particle size. More precise estimates require knowledge of particle shape and of sieving effectiveness, which are discussed in detail in the next subsection.

The data for the large specimens are plotted in Figure 36. Small specimen data for 117 fps impact and for controls appear in Figure 37. Intermediate velocity data show similar behavior but are not plotted because the large number of intertwined curves makes visual correlation difficult.

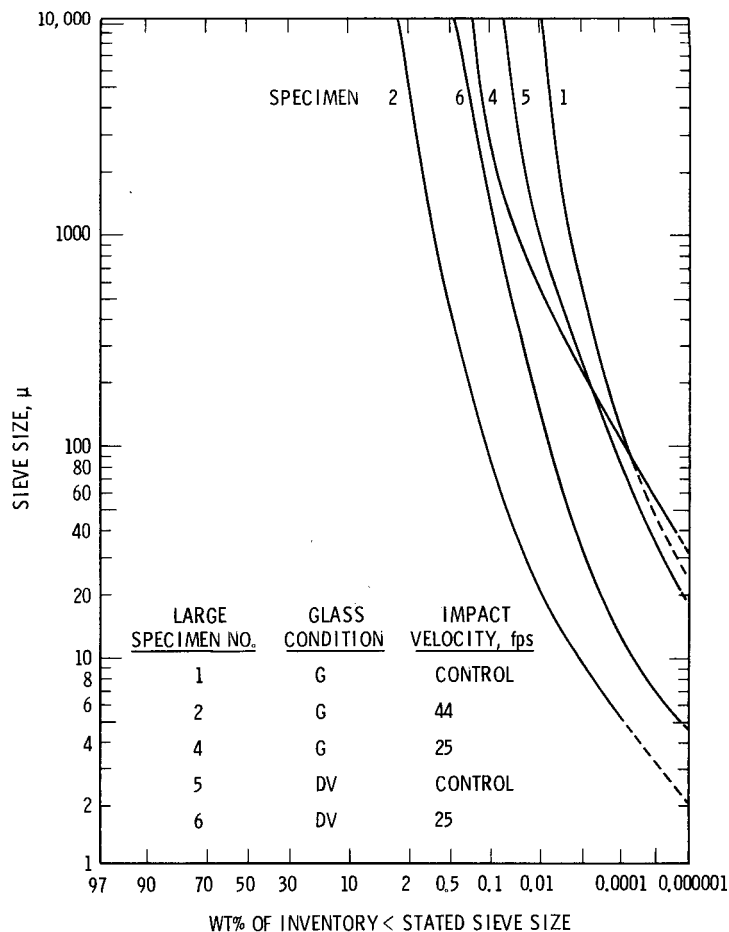


**FIGURE 36.** Particle Size Distributions for Large Specimens

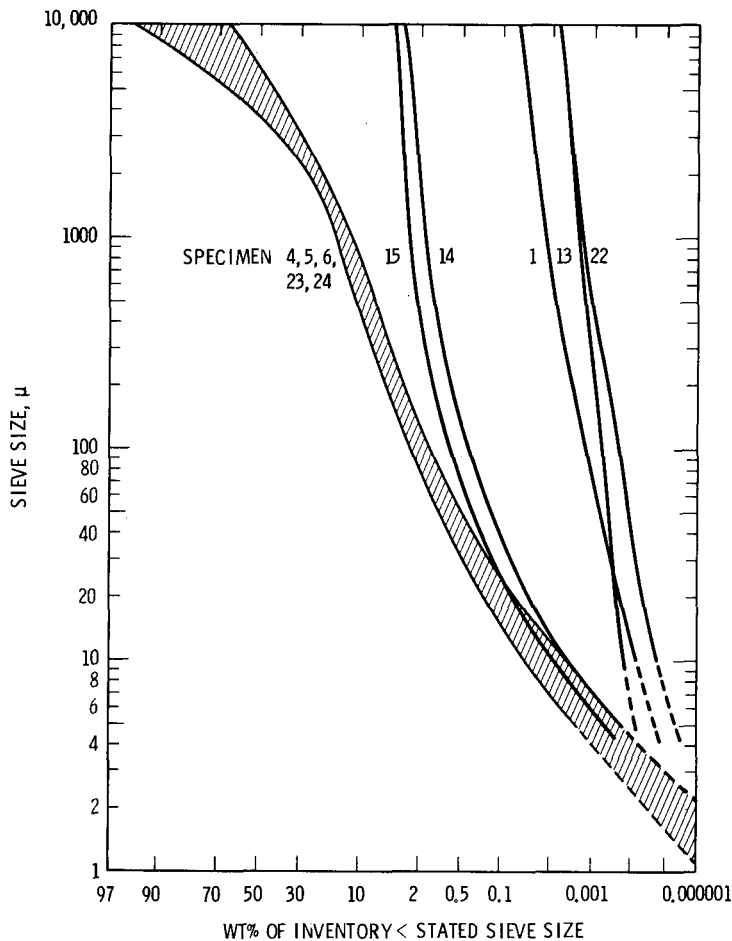


**FIGURE 37.** Particle Size Distributions for Small Specimens (Controls and 117 fps Specimens Only)

For completeness, the curves were extended beyond the data (generally  $>1700 \mu$  and  $<5 \mu$ ) of Appendix A. Crude extrapolation to larger sieves was made assuming the total breakup fractions of Table 9 represent the sum of all particles less than some size,  $L_{max}$ . The size,  $L_{max}$ , of the largest fragment lies between the largest sieve size ( $1700 \mu$ ) and, say, the canister radius ( $\sim 80,000 \mu$ ). For the small specimens, very few particles were larger than 1 cm ( $10,000 \mu$ ). This was the value chosen for  $L_{max}$  although a number of particles in the 1-in. range were found in the large specimens. The uncertainty in the value of  $L_{max}$  is approximately a factor of 3. Extension to particles  $<5 \mu$  was performed using the data of the two microscopic sizing samples (Appendix B) tempered with graphical extrapolation. This extension is highly uncertain because it is based on only small samples of material from only two specimens.

## 2. Comparisons

Detailed comparisons of specimens are difficult with the complete size distribution curves. Because particles  $>20 \mu$  are not generally of interest in airborne transport, comparisons were made only for the  $<20 \mu$  fraction. These can be drawn from Figure 38 although the data scatter often obscures the effects of parameter variations. Because few of the size distribution curves cross between  $10 \mu$  and  $20 \mu$ , the qualitative conclusions drawn from Figure 38 are generally true for the  $<10 \mu$  fraction also.

Three pairs of points (plus a pair of controls) in Figure 38 facilitate limited comparison of small and large specimen results. As in the preceding subsection, no consistent difference was observed between the two series, scatter between specimens masking any effects of L/D ratio and specimen size.

Comparisons of glassy versus devitrified for 11 pairs of points in Figure 38 indicate no consistent differences either at room temperature or at elevated temperature. The only trend is for a larger sub- $20 \mu$  fraction from the devitrified form than from glass in the large specimens. However, this trend is based on comparison of only two pairs of data points.

Nine pairs of data points in Figure 38 were compared on the basis of room temperature versus elevated temperature results. For both glassy and devitrified specimens the result at low impact velocities was for greater breakup at elevated temperature than at room temperature. At higher impact velocities there was no consistent temperature effect.

The greater total breakup at elevated temperature, discussed earlier, results from greater quantities of large ( $\approx 100 \mu$ ) particles. This is evident from Figure 37 if the results for specimens 14 and 15 are compared with the band for specimens 4, 5, 6, 23, and 24. The same effect is seen for impact at 66 and 44 fps.

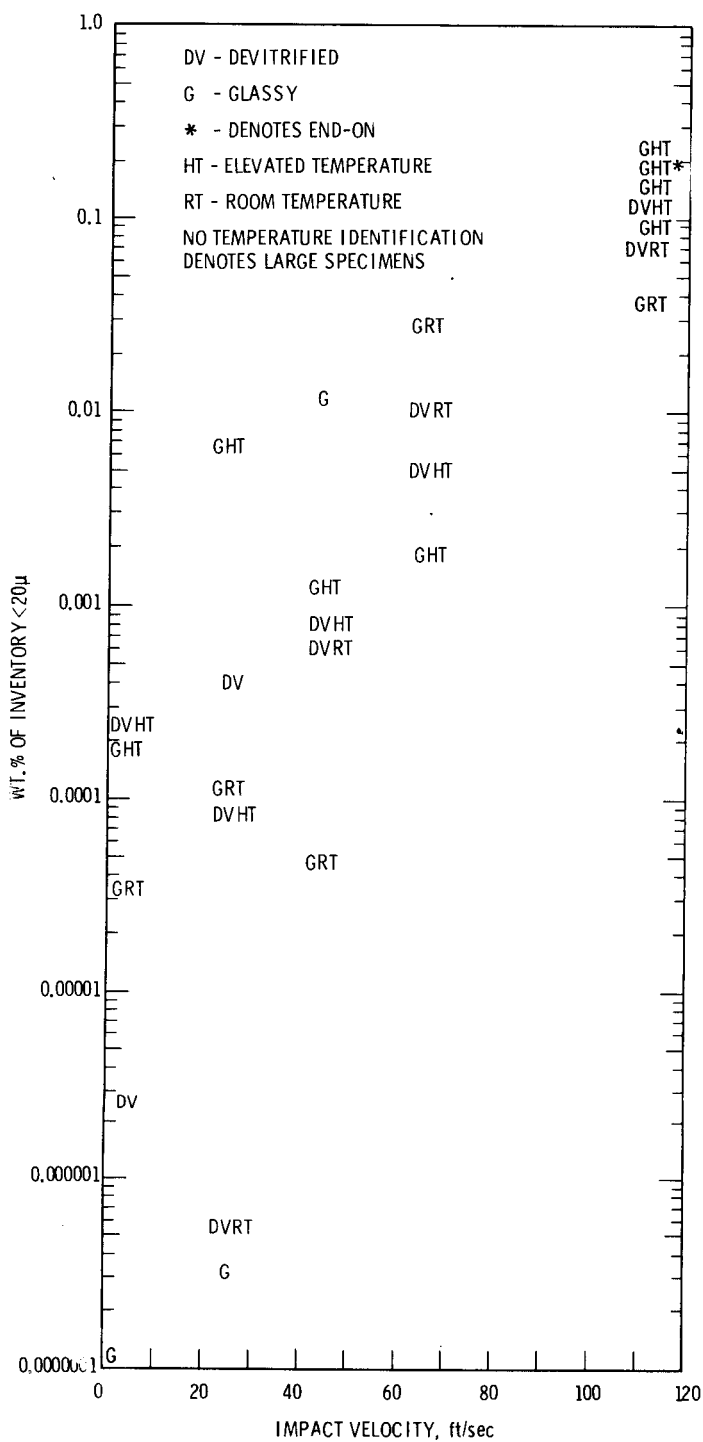


**FIGURE 38.** Magnitude of Sub-20 μ Fraction for Both Large and Small Specimens

### 3. A Consideration Regarding Uncertainty

If the sub-5  $\mu$  area of the curves of Figure 37 is observed, an uncertainty potentially much more important than that of extrapolation is evident. As mentioned in Section 9.0, if the weight of material recovered from a canister is compared with the total weight of material collected on the sieves, generally a small quantity of material is unaccounted for. It results from material not transferred from containers and from particle dust lost during agitated sieving. The quantity of unaccounted-for material (UFM) is usually greater than the weighing uncertainties.

Representative values of parameters related to UFM are given in Table 11. Considered by themselves, the values of UFM and of the fraction of material unaccounted for (UFM/QW) are well within the limits of acceptable laboratory procedures. However, Figure 37 shows that for particles <5  $\mu$  the sieving results are not highly reliable. The control specimens are pictured as having nearly the same <5  $\mu$  fraction as the high-velocity impact specimens. This uncertainty may be put into perspective by comparing the last column of Table 11 (UFM/Inventory) with the bottom scale of Figure 37.

TABLE 11. Representative Values of Parameters in Considering Unaccounted-For Material (UFM)

<u>Specimen No.</u>	<u>Description</u>	<u>Estimated <math>\Sigma</math> Weighing Uncertainties, g</u>	<u>Unaccounted-for Material UFM, g</u>	<u>Quantity Weighed QW, g</u>	<u>UFM/QW %</u>	<u>UFM/Inventory %</u>
<u>Large Canisters</u>						
2	Moderate Velocity	1.2	4.7	2500	0.2	0.005
1	Control	0.003	0.044	8	0.6	0.00005
<u>Small Canisters</u>						
4	High Velocity	1.2	2.5	300	0.8	0.6
22	Control	0.001	0.002	0.026	8	0.0005

The size distribution of the UFM is unknown. If it were identical to that of the remaining material, the uncertainty from this factor would be negligible. If the UFM were all  $<10 \mu$ , a highly unreasonable situation, the effect on the measured  $<10 \mu$  fraction would be great. A reasonable limiting case can be proposed. If the UFM is all  $<60 \mu$  and distributed similarly to the sub- $60 \mu$  fraction of the remaining material, the effect on the results is not substantial. If  $60 \mu$  is replaced by larger dimensions, the uncertainty in particle sizing becomes smaller, and vice versa.

Although variable from one specimen to another, the UFM effect is generally not considered important for particle sizes  $>10 \mu$ . The effect is thought to be of some importance at  $5 \mu$  and possibly of major importance at sizes  $<5 \mu$ .

#### 4. Recommended Assumptions for Sub- $10 \mu$ Fraction and Its Size Distribution

In the absence of additional data, recommended assumptions for the sub- $10 \mu$  fraction as a function of impact velocity are given in Figure 39. Optimistic and pessimistic bounds are shown, corresponding to the data scatter limits. Estimated magnitudes of possible UFM effects are included. It is recalled that the stated impact velocities represent impact onto an essentially unyielding target. For cases in which other bodies deform significantly, such as impact into soil or impact in a protective package, the force-time histories may be greatly changed. Glass breakup may be accordingly reduced to that resulting from granite impact at a much lower equivalent velocity.

In the absence of additional data, the size distribution of the sub- $10 \mu$  fraction may be taken from Figure 36 or Figure 37. The curves are seen to be nearly linear on logarithmic probability coordinates in this size range.

Particle shape factors and sieve size to particle size conversion factors for use in connection with Figure 39 are discussed in the next section.

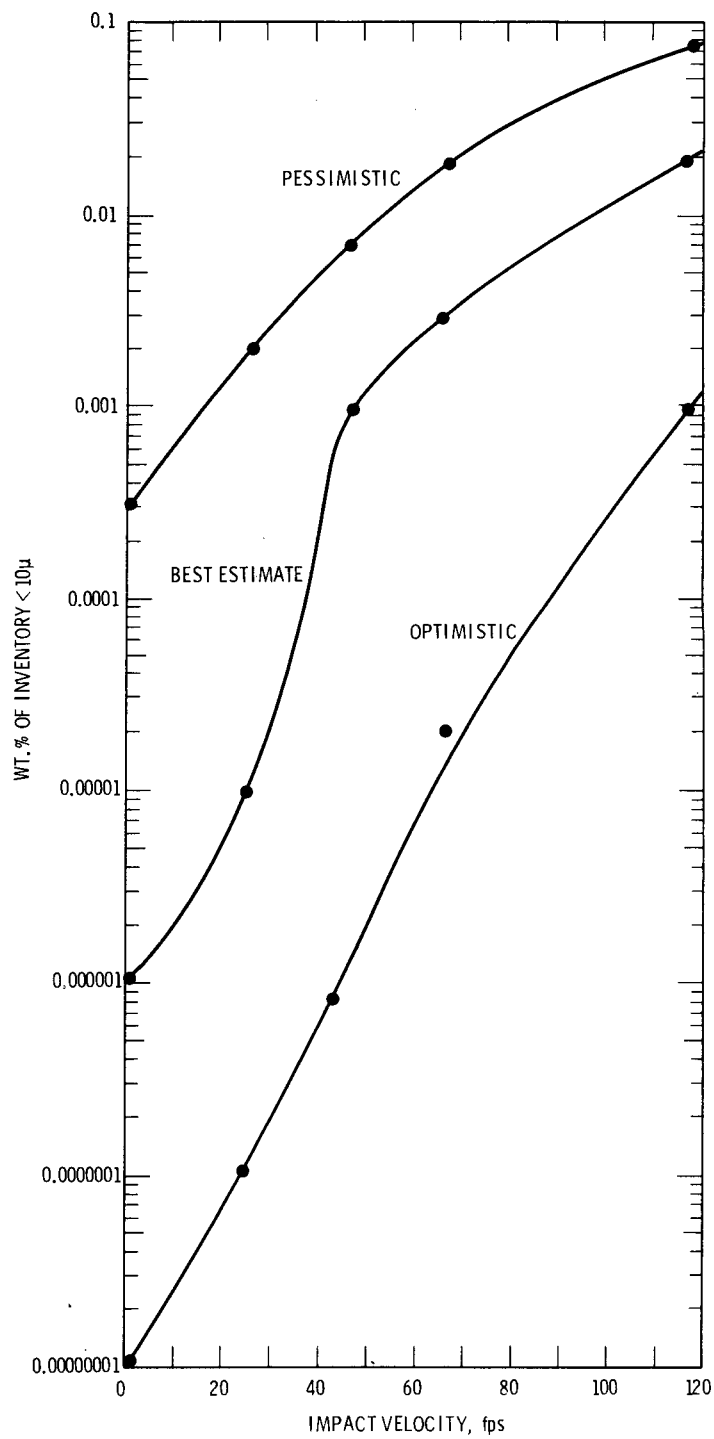


**FIGURE 39.** Prediction Curves for Sub-10  $\mu$  Fines Generation

## REPRESENTATIVE PARTICLE SHAPE; SURFACE AREA INCREASE

### 1. Representative Particle Shape

Precise interpretation of the foregoing size distribution curves requires an assumption of particle shape. The shape also enters into surface area calculations.

The glass particles produced by impact varied in shape from nearly spheric or cubic to plate-like. A representative shape was formulated based on visual and photomicrographic observation. Photomicrographs of samples from two sub-5  $\mu$  fractions appear in Appendix B. From these two-dimensional representations, the ratio  $L_1/L_2$ , (longest dimension/intermediate dimension) was determined for 64 particles in the 2 to 30  $\mu$  range of dimensions. The average ratio was 1.7:1. The third dimension (into the photograph),  $L_3$ , was assumed to be the smallest (particles assumed to be lying flat). The average value of the ratio  $L_3/L_2$  was estimated from visual examination of small particles to be 0.5. This average could conceivably range from 0.3 to 0.7. For purposes of modeling the particles as a group, all particles will subsequently be treated as smooth, rectangular parallelepipeds having dimensions in the ratio of 1.7:1:0.5.

Surface areas calculated by means of this assumption of shape will be termed herein "geometric surface areas." This is in distinction to the actual surface areas, which include contributions of surface irregularities, roughness, and porosity. Actual surface areas of common materials, as measured by means of gas adsorption techniques, may be orders of magnitude higher than geometric surface areas. However, because the glass particles are relatively smooth and nonporous, cognizant personnel project a ratio of from 2 to 10, with the lower value more probable.

### 2. Relation of Particle Size to Sieve Size

The essentially continuous distribution of particle size (not a log-normal distribution) will be approximated by a discrete distribution in which all the material which passes one sieve and is retained on the next smaller sieve is considered to be uniform in size. The size representing

this group of particles is taken to be the arithmetic mean,  $L$ , of these two (square) sieve openings. <sup>(37,39)</sup> Figure 40 illustrates the assumption, which is not expected to introduce significant error. [The dimensions of most consecutive sieve openings are in the ratio of 2:1, giving an arithmetic mean of 1.5. The geometric mean (based on the arithmetic mean of the logarithms) is 1.41.]

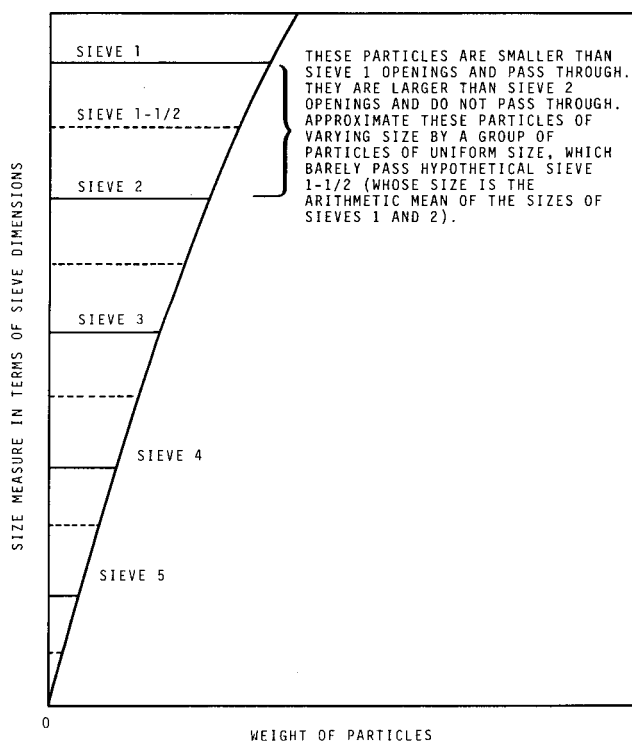


FIGURE 40. Illustration of Sieving Approximation

Related to the above discussion is the fact that a sieve cannot make a perfectly sharp separation. The fraction of particles passing through depends, among other factors, on the duration and manner of shaking. <sup>(38)</sup> Two simplified extreme cases will be examined to relate particle size to the size of the square holes in the sieve. One extreme involves the highest possible sieving and shaking effectiveness. This case assumes that all of the rectangular parallelepiped particles eventually become oriented so that they can pass end-on through the (arithmetic mean)

sieve opening of size  $L \times L$ . This case is designated RPEO. The sieve will thus barely pass an RPEO particle of dimensions  $1.7L \times L \times 0.5L$ . The particle surface area is  $6.1L^2$ ; the mass is  $0.85 \rho L^3$ ; and the ratio of these is  $7.2/(\rho L)$ .

The other case involves an extremely low sieving and shaking effectiveness. In this case, none of the particles becomes oriented end-on. Instead, all particles are assumed to pass through the  $L \times L$  sieve opening sideways. For this case, designated RPSW, the sieve will just barely pass an RPSW particle of dimensions  $L \times 0.59L \times 0.29L$ . The particle surface area is  $2.1L^2$ ; the mass is  $0.17\rho L^3$ ; and the ratio is  $12.4/(\rho L)$ .

Because the sieving was accompanied by mechanical shaking for periods on the order of an hour, the actual mode of particle passage through the sieves was much closer to the RPEO case than to the RPSW case. Both cases will be carried through the analysis, however, to provide perspective on possible effects of incomplete separation in sieving.

### 3. Procedure for Calculating Geometric Surface Area

Approximate calculations of geometric surface area were made, based on the preceding approximations and on the concept of specific surface, the surface area per unit mass ( $A/M$ ). For any number,  $n$ , of RPEO particles, all of size  $1.7L \times L \times 0.5L$ ,

$$\frac{A}{M} = \frac{n \cdot 6.1 L^2}{n \cdot 0.85 \rho L^3} = \frac{7.2}{\rho L}$$

as shown earlier. The value of  $L$  is the arithmetic mean of the two sieve dimensions bounding the group of particles. Similarly, for any number of RPSW particles of size  $L \times 0.59L \times 0.29L$ ,  $A/M = 12.4/(\rho L)$ . If there are several sieving fractions  $i$ , the total area of all particles is

$$A_p = \sum_i \left( \frac{A}{M} \right)_i M_i.$$

Each fraction  $i$  would have a different value of  $A/M$ ; and for a given fraction, the values of  $A/M$  differ for RPEO and RPSW particles.

For specimens exhibiting relatively little breakup, the surface area of the remaining unbroken monolith must be included in assessing postimpact surface area. This quantity is approximated geometrically by

$$A_{UB} = 2\left(\frac{\pi D_I^2}{4}\right) + \pi D_I L_I \frac{M_{UB}}{M_I}$$

where  $D_I$  is the preimpact diameter of the glass cylinder,  $L_I$  and  $M_I$  are its initial length and weight, and  $M_{UB}$  is the weight of unbroken glass. The ratio of surface areas after and before impact is

$$\frac{A_{new}}{A_I} = \frac{A_p}{A_I} + \frac{A_{UB}}{A_I}$$

where

$$A_I = 2\left(\frac{\pi D_I^2}{4}\right) + \pi D_I L_I$$

#### 4. Geometric Surface Area Results and Discussion

Fractional increases in surface area,  $(A_{new} - A_I)/A_I$ , were calculated for all large specimens except No. 3. Small specimens whose particle size distribution curves indicated either the greatest or the least breakup among specimens tested at a given velocity were also included. Results are presented in Figure 41. Each vertical data line represents one specimen. The upper limit of each line represents the area found with the RPSW model, while the RPEO model is represented by the lower limit. The latter model more closely represents actual sieving effectiveness.

Curves representing pessimistic and optimistic predictions bound the wide spread of data. A best-estimate curve was plotted through points about which the data appeared to cluster. Geometric area increases are strongly affected by velocity, ranging from a few percent for the controls to factors of 10 to 100 at 117 fps.

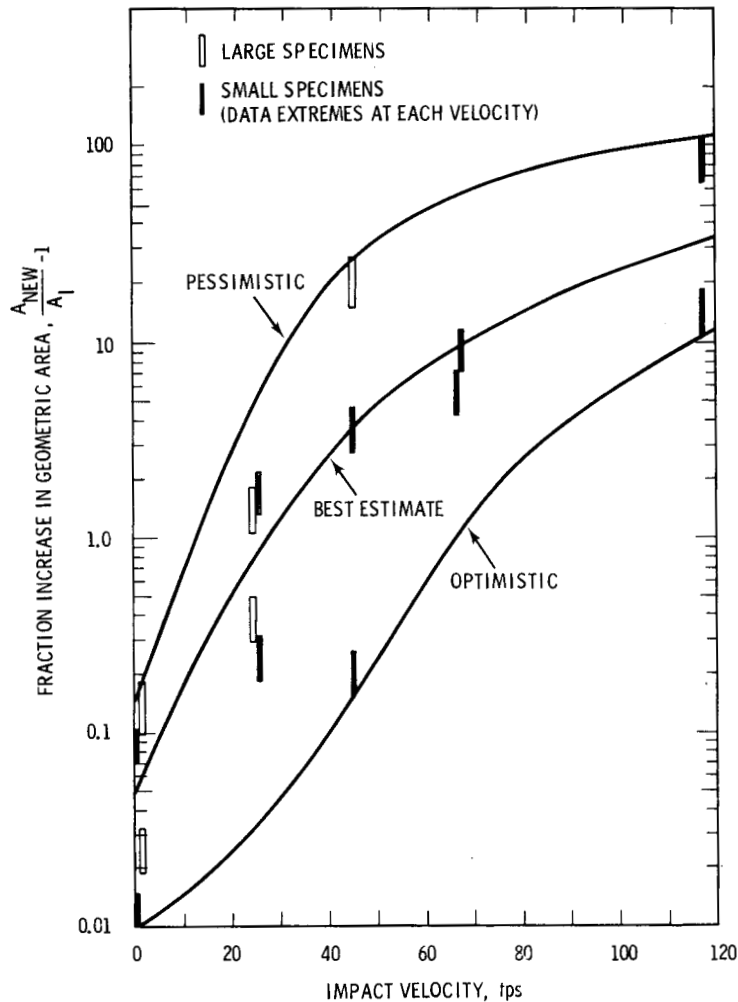


FIGURE 41. Fractional Increase in Geometric Surface Area

Comparisons on the bases of test temperature, waste form and canister size lead to the same conclusions reached for particle size distribution. No consistent effect of waste form was observed for the small specimens. Devitrified waste produced slightly more surface than did glassy waste in the large specimens. Elevated-temperature testing led to consistently higher surface areas. This resulted from the increased quantity of particles  $\gtrsim 100 \mu$ ; the quantity of particles  $\lesssim 100 \mu$  was not markedly affected by test temperature. Finally, no consistent effect of specimen size was apparent when the data were plotted on a fraction-of-inventory basis.

## 5. Scaling

Extensive theoretical derivations or predictions of impact behavior are beyond the scope of this report. The objective is only to report the test results. Theoretical models, especially those not incorporating empirically determined constants, have generally had limited success in predicting complex impact phenomena. Available theories differ considerably in their predictions. Furthermore, data presented herein indicate that specimens fabricated and tested under supposedly identical conditions can give results which vary significantly. However, dimensional analysis incorporating empirical determination of the constants which arise has had some success in predicting impact behavior.<sup>(10,11,14,15)</sup> For this reason scaling is briefly discussed in terms of this analytical tool.

Duffey<sup>(25)</sup> performed a dimensional analysis for multilayered fuel capsules subjected to impact and other mechanical loadings, as well as thermal loading. A set of 19 dimensionless  $\Pi$ -numbers was derived to express the requirements for scaling test conditions and results from small models to full-size specimens. The situation in which specimens differ in size but are constructed of identical materials matches the present tests. Under such conditions, it appears possible to satisfy all of the  $\Pi$ -number requirements except the one involving strain rate effects, which results in contradictory requirements unless the specimens are identical in size. The strength of 304L stainless is not highly sensitive to strain rate at the temperatures of interest for this study.<sup>(17)</sup> The strain-rate dependence of the glass behavior is unknown.

In certain respects, the two impact test models differed from the representative full-size canister after which they were designed. In these respects the  $\Pi$ -numbers for the two test models would not match the corresponding values for full-size specimens. The difficulty of elevated-temperature, high-speed testing of small specimens of the proper L/D ratio has been mentioned. The small specimens were impacted at a somewhat different angle than that for the large specimens. Targets were not precisely scaled. Neither small nor large specimens duplicated either the filling port or the temperature profile of a self-heating, full-size canister.

However, the results of the control tests and of comparisons between small and large canister data imply that these deficiencies were probably not serious within the context of the present tests. The scatter evident in the reproducibility tests supports this inference (compare small specimens 4, 23 and 24 in Appendix A).

Additional difficulties arise if the dimensional analysis is extended to focus on the glass breakup. Tsai<sup>(26)</sup> has noted a  $\Pi$ -number involving the glass surface energy which apparently cannot be satisfied unless both models are the same size. However, the overlap of surface area data of the large and small test specimens (Figure 41) indicates again that this deficiency was probably not serious compared with the data scatter.

Tsai's hypothesis illustrates the difficulties of scaling particle results. There are two basic theories of comminution, or pulverization,<sup>(39)</sup> and they are mutually contradictory.<sup>(23)</sup> The older and more widely accepted is the Rittinger theory, which states that the work consumed for reduction of particle size in homogeneous materials is directly proportional to the new surface produced. (The divitrified glass could be characterized as having few significant heterogeneities  $\sim 1 \mu$  in size. In the glassy state the scale of significant heterogeneity would be smaller.) The Kick theory states that the work required for crushing a given quantity of homogeneous material is constant for the same size reduction ratio, regardless of the original size. A unifying third theory, intermediate between these, has been proposed<sup>(23)</sup> more recently.

It can be shown that the theories of Kick and of Rittinger have quite different implications for scaling particle size results from small test specimens to larger full-size specimens of identical geometry under identical test conditions. For illustrating this, it is assumed that the impact is severe and that all particles produced from breakup of a given specimen are identical in size and shape. The scale ratio of the large and small specimens is taken to be  $\lambda \equiv L_{fs}/L_t$ , where  $L_{fs}$  and  $L_t$  are dimensional measures of the full-size and test specimens, respectively. Under these conditions Rittinger's Law predicts that the particles from the test specimen will be the same size as those from the full-size specimen, but that the

latter specimen will have  $\lambda^3$  times as many particles. Kick's Law predicts essentially the opposite scaling effect: equal numbers of particles will result, but each particle from the full-size specimen will be  $\lambda$  times the size of the particles from the test specimen.

Particle size distributions from the small and large specimens of the present tests have been plotted together on a weight fraction basis. Within the uncertainty of the data, there was no apparent effect of specimen size on the results. This conclusion would tend to support the validity of Rittinger's Law for these test conditions and materials. (As mentioned previously, the large and small specimens were identical in radius/thickness ratio, but not in length/diameter ratio.) On this basis, the results for full-scale specimens would not be expected to show significant effects of specimen size. This is especially true because there was a much greater size difference between small and large test specimens than between large test specimens and full-size specimens.

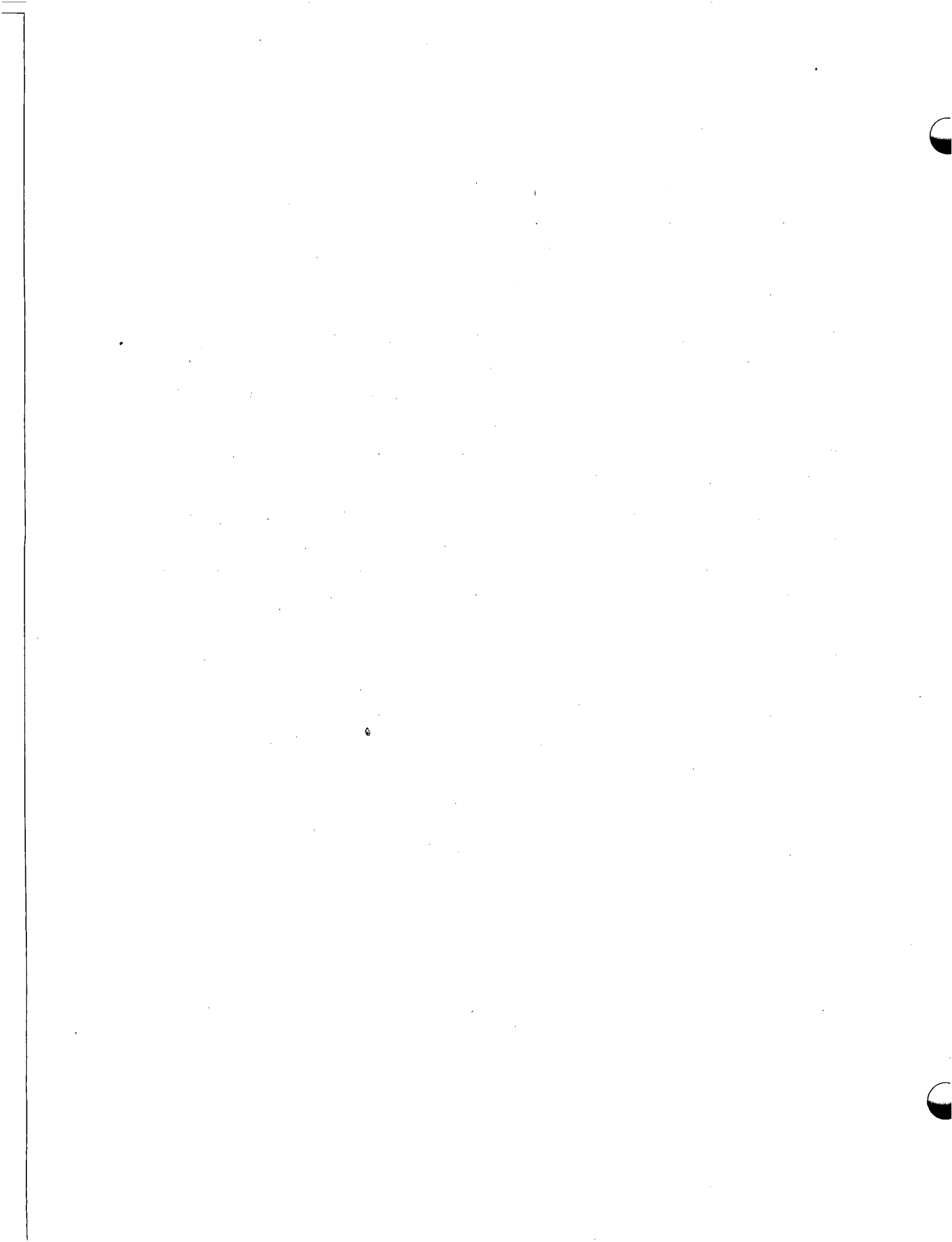
It can also be shown that Kick and Rittinger predict different scaling laws for particle surface areas. Kick predicts that the surface area ratio,  $(A_{fs}/A_{fs_0})/(A_t/A_{t_0})$  is unity. Here the subscripts fs, t, and o denote, respectively, full-size specimen, test specimen, and preimpact conditions. Rittinger predicts a value of  $\lambda$  for this ratio. Again, common plotting of the limited comparable data from large and small test specimens shows no consistent difference within the data scatter. This conclusion tends to support the validity of the Kick theory.

The fact that conflicting behavior is implied in the two comparisons above leads one to believe that conclusions regarding scaling laws are not justified on the basis of the limited and scattered data available. (It is unlikely that the effects of differences in geometry and size of the two test models would just counteract each other, both in particle size distribution and in surface area increase.) However, it seems safe to say that any error in scaling the results up to full-size specimens will be small compared with the scatter among specimens of the same size.

## 6. Shape Conversion Factors for Use with the Particle Size Distribution Curves

The results of subsections 1 and 2 immediately preceding can be used to interpret more precisely the particle size distribution curves. All particles are taken to be  $1.7 \times 1.0 \times 0.5$  rectangular parallelepipeds. The fines fraction retained between two consecutive sieve sizes (e.g.,  $20 \mu$  and  $10 \mu$ ) is based on the arithmetic mean,  $L$ , of the two sieve dimensions (e.g.,  $15 \mu$ ). See Figure 40. The RPEO model of particles passing end-on through the sieves is the better of the extreme cases and gives particles of dimensions  $1.7L \times L \times 0.5L$ . The RPSW sideways passage model leads to particles of dimensions  $L \times 0.59L \times 0.29L$ .

In the case of the fines fraction smaller than the smallest sieve size, say  $10 \mu$ , the above procedure for calculating  $L$  fails. A possible modification is this procedure: 1) examine the slope and curvature of the distribution curve in the small particle region, then extrapolate the curve; 2) imagine the imposition of successive sieves of smaller and smaller size (e.g.,  $5 \mu$ ,  $2.5 \mu$ ,  $1.25 \mu$ , . . .); 3) apply the previous rule for calculating  $L$ ; 4) read off the curve the weight fraction between the two hypothetical sieve sizes; 5) continue the process until the desired lower limit of dimensions or weight of particles is satisfied. See also Reference 39. This procedure requires no assumption of particle size distribution. Instead, extrapolations of the actual particle data (which within the experimental accuracy, do not appear to follow closely any common mathematical formulation) are used.



## 11.0 USE OF THE RESULTS IN ANALYSIS OF RADIOLOGICAL HAZARDS

The ultimate objective of the impact study was to provide information for estimating radiological hazards of potential accident sequences. However, the data from this study are not immediately usable for direct calculation of radiological hazards. Many important processes must occur following a hypothetical impact, involving canister failure and glass fracture, before radiological exposure of man can result. This section enumerates these intermediate processes, briefly describes analytical techniques for modeling them and discusses post-impact glass characteristics which influence the resulting exposure. Pathways involving airborne transport and groundwater transport are included.

### CONSIDERATIONS IN ANALYSIS OF THE AIRBORNE PATHWAY

#### 1. Relationships Between the Properties of Airborne Particles and the Physiological Attributes of Man

Although radiation damage can result from highly radioactive airborne particles which settle onto the skin, this potential is generally secondary in importance to inhalation. From the lung, the particles or a fluid containing the dissolved particles can move to other body sites.

Man's respiratory system has a complex structure which tends to trap particles of certain sizes. The system is basically composed of nasopharyngeal (N-P), tracheobronchial (T-B), and pulmonary (P) compartments. The N-P includes nose, mouth, and air passageways to the tracheal entrance; the T-B includes trachea and bronchi; and P includes bronchioles, alveolar ducts and alveolar sacs. Because the dimensions, air flow rates, and functions are different in each compartment, the fate and effects of a particle entering the respiratory system depend on its size, mass, solubility and other chemical properties, and the isotopes present. These properties affect deposition, retention and transfer to critical body organs. The half-life of the radionuclides in the particle, energy per disintegration, and radiation type are important in determining biological significance. The significance of particle size only is addressed here.

Figure 42 shows the lung deposition site and the estimated fraction of various size particles deposited.<sup>(40)</sup> Aerodynamic equivalent diameter (diameter of a unit density sphere with the same settling velocity and other aerodynamic properties as the particle in question) is the abscissa. Particles of the same geometric diameter may differ greatly in aerodynamic behavior due to differences in density. Figure 42 shows that particles larger than 7  $\mu$  are trapped in the N-P region, whereas most of the submicron particles are retained in the two lung compartments. Thus it is important in the hazard evaluation to know the size distribution, density, and shape of airborne particles which are susceptible to inhalation.

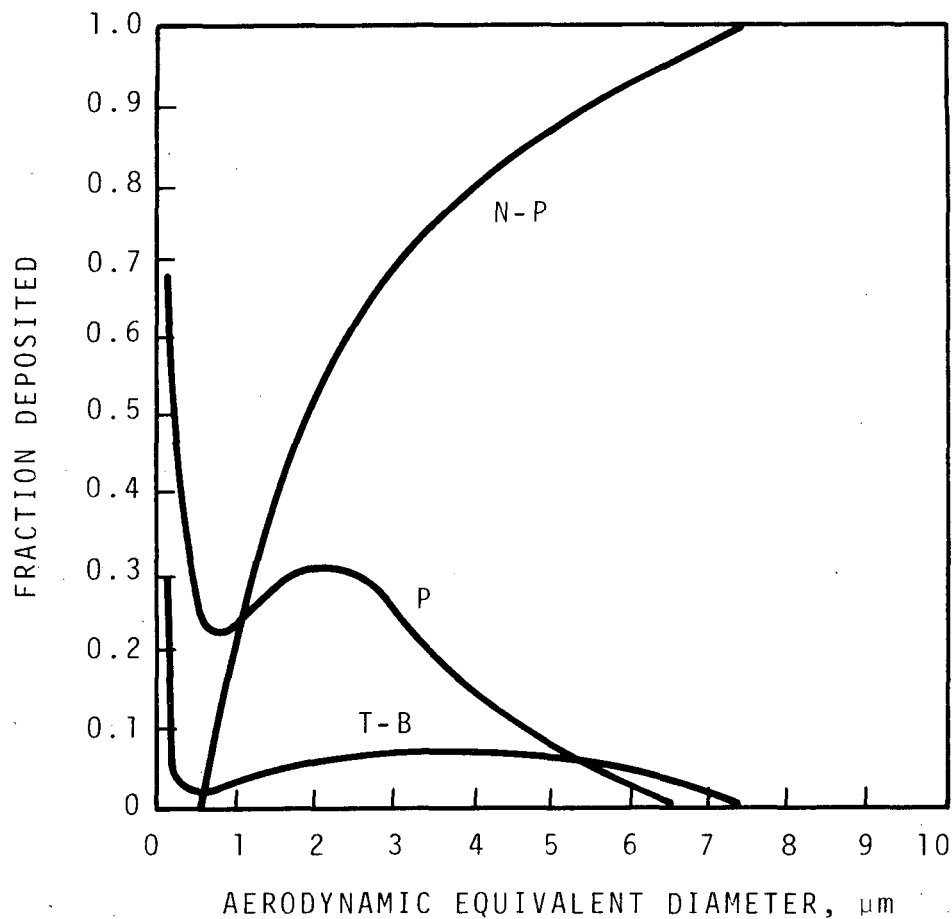


**FIGURE 42.** Calculated Deposition of Particles in Nasopharyngeal (N-P), Tracheobronchial (T-B), and Pulmonary (P) Compartments, Relative to Number Inhaled.<sup>(40)</sup>

Once in the lung, radioactive particles irradiate local tissue and adjacent organs. The particles may be dissolved and transferred to the blood and other organs, be swept out of the lung by the ciliated epithelium and delivered to the GI tract, or be engulfed in phagocytes and moved into the lymph system.

## 2. Particle Resuspension, Transport, Modification, and Removal by Atmospheric Processes

Between the accident site and man's location, atmospheric processes may markedly change the concentration and nature of particles released in an accident.

If a severe impact were to breach a waste container, material could be quickly sent into the air in the near vicinity. Dense and coarse particles ( $>20 \mu$ ) will soon settle back to the ground. Attempts to quantitatively assess entrainment in the initiating event will be frustrated by lack of information of particle behavior as well as the gross assumptions needed for the accident scenario.

Small particles airborne in the accidental release will remain airborne, at least for a period, and permit the wind to carry and diffuse them downwind. Particle concentration will decrease with distance due to turbulent diffusion. Models are available for estimating ground-level concentrations downwind.<sup>(41)</sup> Depending on atmospheric stability and windspeed, downwind concentrations can vary several orders of magnitude. It is therefore necessary to specify the location and atmospheric conditions prevailing at the time and place of the accident, and the distance downwind at which an individual is located.

Particles deposited on surfaces may subsequently become airborne and constitute a secondary source. Resuspension rates of  $10^{-8}$  to  $10^{-10}$  per second are typical, depending on windspeed.<sup>(42)</sup>

Precipitation will clean the air of particles and must be considered as a possible modifier of particle size and concentration. Other modifications in the atmosphere may involve gas-particle interactions, solution in

raindrops, condensation of moisture, particle-particle collisions, sublimation, and electrical charge effects.

Aerodynamic and other properties of particles at the source during an accident are important, yet the foregoing discussion shows that modifications will occur prior to contact with man. Measurement of glass particle sizes in this study provides essential information for the ultimate consequences assessment, but is only one of many necessary elements. Source particles larger than 10  $\mu$  can be largely ignored as an airborne hazard for physiological reasons and from recognition that particles larger than this are rapidly removed in atmospheric processes.

#### CONSIDERATIONS IN ANALYSIS OF THE GROUNDWATER PATHWAY

The groundwater pathway of radionuclides to man involves three phases which overlap in time. The first is contact of the waste by flowing groundwater after containment failure, with consequent leaching and dissolution. The second is migration of dissolved nuclides through the soil to surface water. The third includes pathways of nuclides from surface water to interaction with man.

##### 1. Leaching and Dissolution of Nuclides

A postulated incident may involve breach of containers of solidified waste deep within the earth. Groundwater contacts the waste and leaching begins. Alternatively, a container may be breached above ground, possibly in surface water. Leaching can then result from contact with the surface water or with precipitation and runoff. The dissolved nuclides find their way into the groundwater either by way of surface water or by flow down through the soil.

The leaching of nuclides from the waste material is governed by two mechanisms. The first, which accounts for a high initial leach rate, is diffusion of individual nuclides from the interior of the waste to the surface, where they are rinsed off and dissolved by water. This process soon slows due to formation of a surface boundary layer, deficient in free nuclide ions, which retards subsequent migration to the surface. When this

boundary layer has effectively halted nuclide diffusion, the second mechanism, dissolution of the waste material itself, controls the leach rate. For periods during which the relative change in surface area is small, the cumulative amount leached at time  $t$  is approximated by  $At^{1/2} + Bt$ , where  $A$  is considerably greater than  $B$ . The square root term represents diffusion; the linear term, dissolution. The required time for leaching of nuclides varies from a very short period to thousands of years. It depends on the groundwater composition, the waste incorporation material (borosilicate glass, calcine, etc.), and the degree of fracturing of the waste material prior to or during the incident. The particle size distribution and total surface area are thus important parameters.

The release rate of nuclides into groundwater may or may not significantly affect the intensity of exposure of man, depending on the second phase of the pathway.

## 2. Migration of Nuclides Through Soil to the Surface Water

Migration of nuclides through the strata and soil column to surface water is controlled by convection, dispersion, adsorption, and radioactive decay. Convection refers to bulk flow of nuclides dissolved in groundwater, at the same speed and direction as the water. Dispersion refers to mixing of the waste solution with the solution located ahead of and behind it in the soil column. Adsorption refers to ion-exchange interaction between the nuclides and the strata or soil particles. The nuclides are retained on the particle surfaces until displaced by further ion exchange and dissolved back into the groundwater. Radioactive decay occurs continuously throughout the entire process. Effective transport rates of radionuclides to surface water can be reduced significantly by retardation from adsorption and dispersion and by disappearance due to radioactive decay.

One dimensional migration of the  $i$ th member of a radionuclide chain is described by a set of  $i$  linear partial differential equations<sup>(43)</sup> based on a material balance of the  $i$ th chain member and of all preceding chain members  $j$  over a differential volume of the soil column. Each equation

$j$  (where  $1 \leq j \leq i$ ) of the set includes terms representing the net change in  $j$  inventory from dispersion, convection, adsorption, disappearance by decay and appearance from decay of the preceding chain member. The equations are solved subject to proper boundary conditions. The solution describes the inventory of nuclides at any time and at any point along the soil column, including the point of release to surface water.

### 3. Pathways of Nuclides from Surface Water to Man

Entrance of nuclides into surface water begins the third phase. This phase involves an intricate biological network of retention and concentration in plants and animals in man's food chain, as well as a direct route to man via consumption of surface or well water and via recreational activities such as swimming and boating.

## REFERENCES

1. A. M. Platt, compiler, Research and Development Activities, Waste Fixation Program, Quarterly Report, October through December 1973, BNWL-1809, Battelle, Pacific Northwest Laboratories, Richland, WA, January 1974.
2. J. E. Mendel, compiler, A Review of Leaching Test Methods and the Leachability of Various Solid Media Containing Radioactive Wastes, BNWL-1765, Battelle, Pacific Northwest Laboratories, Richland, WA, July 1973.
3. D. Walmsley et al., Volatility Studies of Glasses for the Fingal Process, AERE-R-5777, Harwell, Berkshire, England, 1969.
4. A. E. Albrethsen and L. C. Schwendiman, Volatilization of Fission Products from High-Level Ceramic Wastes, BNWL-338, Battelle-Northwest, Richland, WA, February 1967.
5. J. E. Mendel and J. L. McElroy, Waste Solidification Program, Volume 10, Evaluation of Solidified Waste Products, BNWL-1666, Battelle-Northwest, Richland, WA, June 1972.
6. D. F. Haskell, "Impact Failure Criterion for Cylindrical and Spherical Shells," Department of Defense, The Shock and Vibration Bulletin, No. 39, Part 5, pp. 21-26, December 1968.
7. C. W. Young, C. E. Stoneking, and J. L. Colp, Containment Capsule Impact Safety Study, Phase A, Progress Report, SC-RR-65-9, Sandia Corporation, July 1965.
8. L. W. Oline and C. E. Stoneking, A Study of Impact Effects on Spherical Shells - Part I. "A Theoretical Study of the Response of Hollow Cylinders to Impact Loads", SC-CR-66-2135, Sandia Laboratories, November 1966.
9. J. C. Simonis and C. E. Stoneking, A Study of Impact Effects of Spherical Shells - Part II. "A Theoretical and Experimental Study of the Response of Spherical Shells to Impact Loads", SC-CR-2540, Sandia Laboratories, December 1966.
10. R. E. Morris, Permanent Impact Deformation of Spherical Shells, NASA Technical Memorandum, NASA TM X-2067, Cleveland, OH, October 1970.
11. R. E. Morris, Empirical Correlation of Small Hollow Sphere Impact Failure Data Using Dimensional Analysis, NASA Technical Memorandum, NASA TM X-52874, Cleveland, OH, September 1970.

12. C. A. Bodenschatz, "On Optimized Design of Radioisotope Capsules for Impact," Proceedings of the Intersociety Energy Conversion Engineering Conference, pp. 181-188, 1968.
13. W. J. Dalby, Status Report: Impact Tests - Radioisotope Fuels and Simulants, Sandia Corporation, SC-DR-710218, April 1971.
14. A. W. Barsell, "Impact Considerations for Optimum Radioisotope Heater Designs," Donald W. Douglas Laboratories, Technical Memorandum, Richland, WA, September 1971.
15. A. W. Barsell, "Analytical Developments for Capsule Impact Deformation," Donald W. Douglas Laboratories, Technical Memorandum, Richland, WA, April 1972.
16. L. B. Shappert, A Guide for the Design, Fabrication, and Operation of Shipping Casks for Nuclear Operations, Oak Ridge National Laboratory, ORNL-NSIC-68, February 1970.
17. J. M. Steichen and M. M. Paxton, The Effect of Strain Rate on the Mechanical Properties of Austenitic Stainless Steels, Interim Report, Hanford Engineering Development Laboratory, HEDL-TME 71-56, May 1971.
18. Plutonium-238 Space Electric Power Fuel Development Program, Los Alamos Scientific Laboratory, Quarterly Progress Report, January 1 to March 31, 1971, LA-4819-MS, October 1971.
19. P. H. Bonnell, Particle Sizing of Plutonium Dioxide Microspheres After Impact, Mound Laboratory, MLM-1499, Miamisburg, OH, June 1968.
20. P. H. Bonnell, Fines Analysis of Plutonium Dioxide Microspheres After Impact, Mound Laboratory, MLM-1626, Miamisburg, OH, April 1969.
21. R. B. Goranson, Phase II Radioisotope Heater Development Program, Donald W. Douglas Laboratories Report, MDC-G3128, Richland, WA, April 1972.
22. P. J. Pelto and T. H. Smith, "Graphical Presentation of Impact Test Particle Size Data," Waste Fixation Program Monthly Task Report, WFP-74-3, Battelle, Pacific Northwest Laboratories, Richland, WA, pp. 51-64, March 1974.
23. F. C. Bond, "The Third Theory of Comminution," Mining Engineering, Trans. AIME, pp. 484-494, May 1952.
24. Y. M. Tsai and H. Kolsky, "A Study of the Fractures Produced in Glass Blocks by Impact," J. Mech. Phys. Solids, vol. 15, p. 263 (1967).
25. T. A. Duffey, Scaling Laws for Fuel Capsules Subjected to Blast, Impact and Thermal Loading, Intersociety Energy Conversion Engineering Conference, pp. 775-786, 1971.

26. Y. M. Tsai, Technical Memorandum to T. H. Smith, August 1974.
27. USAEC, The Safety of Nuclear Power Reactors and Related Facilities, WASH-1250 (Final Draft), Chapter 4, July 1973.
28. D. W. Larson et al., "Quantitative Characterization of the Environment Experienced by Cargo in Railroad Accidents," 4th International Symposium on Packaging and Transportation of Radioactive Materials, Miami Beach, FL, September 1974.
29. A. M. Platt, compiler, Quarterly Progress Report, Research and Development Activities, Waste Fixation Program, December 1972 Through March 1973, BNWL-1741, Battelle, Pacific Northwest Laboratories, Richland, WA, April 1973.
30. A. M. Platt, compiler, Quarterly Progress Report, Research and Development Activities, Waste Fixation Program, July Through September 1973, BNWL-1788, Battelle, Pacific Northwest Laboratories, Richland, WA, October 1973.
31. Retrievable Surface Storage Facility Alternative Concepts Engineering Studies, Atlantic Richfield Hanford Company, ARH-2888, Richland, WA, December 1973.
32. M. B. Volf, Technical Glasses, Pitman and Son, Ltd., London, p. 78, 1961.
33. T. A. Golding, Impact Testing of Simulated Radioactive Waste Samples, Final Report, Donald W. Douglas Laboratories Report DWDL-745-163, Richland, WA, May 1974.
34. J. L. McElroy, compiler, Quarterly Progress Report, Research and Development Activities, Waste Fixation Program - April through June 1974, BNWL-1841, July 1974.
35. J. L. McElroy, compiler, Quarterly Progress Report, Research and Development Activities, Waste Fixation Program - January through March 1974, BNWL-1826, April 1974.
36. J. P. Den Hartog, Advanced Strength of Materials, McGraw-Hill Book Company, Inc., New York, NY, 1952.
37. G. G. Brown, Unit Operations, John Wiley and Sons, Inc., New York, NY, 1950.
38. L. Silverman et al., Particle Size Analysis in Industrial Hygiene, Academic Press, New York, NY, 1971.
39. J. H. Perry, Ed., Chemical Engineers' Handbook, 4th ed. McGraw-Hill Book Co., Inc., New York, NY, 1963, p. 8-8.

40. T. T. Mercer, Aerosol Technology in Hazard Evaluation, Academic Press, 1973.
41. D. H. Slade, Ed., Meteorology and Atomic Energy, 1968, U.S. Atomic Energy Commission, 1968.
42. G. A. Sehmel and F. D. Lloyd. Particle Resuspension Rates, BNWL-SA-5124, to be issued in The Proceedings of the Atmosphere-Surface Exchange of Particulate & Gaseous Pollutants - 1974 Symposium, Richland, WA, September 4-6, 1974.
43. H. C. Burkholder, G. Jansen, and D. H. Lester, Migration of Radionuclide Chains Through an Adsorbing Medium, BNWL-SA-5079, Battelle, Pacific Northwest Laboratories, Richland, WA, December 1974.

APPENDIX A

PARTICLE SIZE DISTRIBUTION TABLE

APPENDIX A

PARTICLE SIZE DISTRIBUTION TABLE

LARGE SPECIMENS

Percent of Inventory < Stated Sieve Size

Sieve Size, $\mu$	Specimen Number					
	1	2	3(a)	4	5	6
1700	0.00377	1.35	-	0.071	0.027	0.112
841	-	0.87	-	-	-	-
420	-	0.51	-	-	-	-
210	0.00024	0.27	0.00056	0.00066	0.00059	0.016
149	0.00014	0.18	0.00029	0.00032	0.00034	0.010
74	0.000037	0.083	0.000137	0.000075	0.00011	0.0044
44	-	0.048	-	-	-	-
37	0.00000023	0.040	0.000024	0.0000021	0.000016	0.0018
20		0.013	0.0000027		0.0000029	0.00042
10		0.0025				0.000042
5		0.000065				0.0000017

SMALL SPECIMENS

Percent of Inventory < Stated Sieve Size

Sieve Size, $\mu$	Specimen Number							
	1	4	5	6	7	8	9	10
1651	-	15.3	19.9	23.3	-	-	-	-
841	-	10.2	13.0	13.6	-	-	-	-
420	-	7.6	9.7	8.5	-	-	-	-
210	0.0025	2.8	3.1	3.4	0.33	0.61	0.20	0.19
149	0.0019	2.2	2.2	2.3	0.22	0.43	0.14	0.13
74	0.0011	1.4	1.2	1.2	0.10	0.20	0.076	0.061
37	0.00057	0.49	0.36	0.44	0.029	0.054	0.024	0.015
20	-	0.17	0.12	0.18	0.0019	0.0051	0.0013	0.0008
10	0.000068	0.0022	0.017	0.0022		0.00092		
5		0.0012	0.00077	0.00030				

Sieve Size, $\mu$	Specimen Number							
	11	12	13	14	15	16	17	18
1651	-	-	-	-	-	-	-	-
841	-	-	-	-	-	-	-	-
420	-	-	-	-	-	-	-	-
210	0.047	0.030	0.00087	0.72	1.20	0.42	0.31	0.015
149	0.038	0.021	0.00084	0.56	0.94	0.35	0.24	0.011
74	0.026	0.010	0.00051	0.33	0.57	0.21	0.14	0.0052
37	0.017	0.0017	0.00033	0.13	0.24	0.088	0.052	0.00097
20	0.0072	0.000093	-	0.036	0.076	0.029	0.0098	
10	0.00041		0.00018	0.0028	0.0083	0.0017	0.00056	
5					0.00055			

Sieve Size, $\mu$	Specimen Number					
	19	20	21	22	23(b)	24(b)
1651	-	-	-	-	17.2	18.5
841	-	-	-	-	10.7	10.5
420	-	-	-	-	7.1	6.4
210	0.054	0.055	0.013	0.00076	4.6	3.5
149	0.036	0.037	0.0092	0.00047	3.6	2.5
74	0.015	0.016	0.0038	0.00014	1.8	1.3
37	0.0019	0.0012	0.00004		0.66	0.4
20	0.00062	0.00013			0.18	0.11
10	0.0001				0.025	0.018
5					0.0023	0.0026

- a. Results incomplete - fines at bottom end not included.  
 b. Large sieve sizes were 1700, 850, 425, and 212  $\mu$ , rather than 1651, 841, 420, and 210  $\mu$ .

A.1

APPENDIX B

DATA FROM SIZE SAMPLING WITH MICROSCOPE

APPENDIX B

DATA FROM SIZE SAMPLING WITH MICROSCOPE

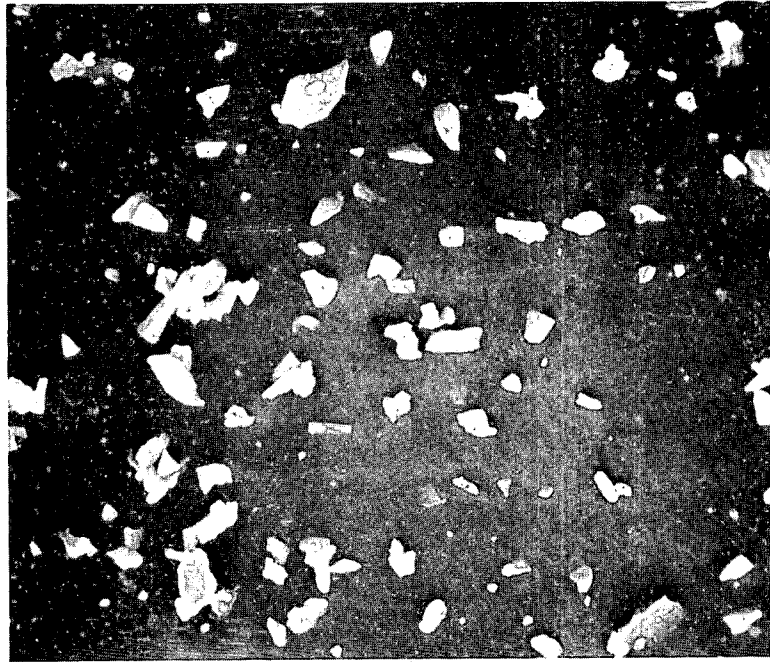
LARGE SPECIMEN 2, <5  $\mu$  SIEVE FRACTION

<u>Particle Size, (a) <math>\mu</math></u>	<u>Number of Particles</u>
>5	54
3-5	73
1-3	57
<1	<u>16</u>
	200

SMALL SPECIMEN 5, <5  $\mu$  SIEVE FRACTION

<u>Particle Size, (a) <math>\mu</math></u>	<u>Number of Particles</u>
>5	61
3-5	80
1-3	52
<1	<u>7</u>
	200

a. Equivalent circular dimension.

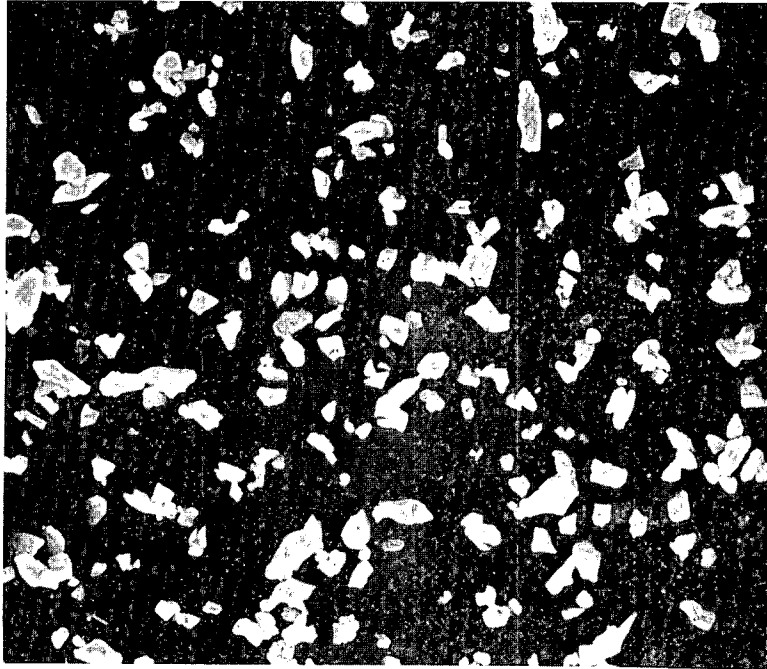


300X

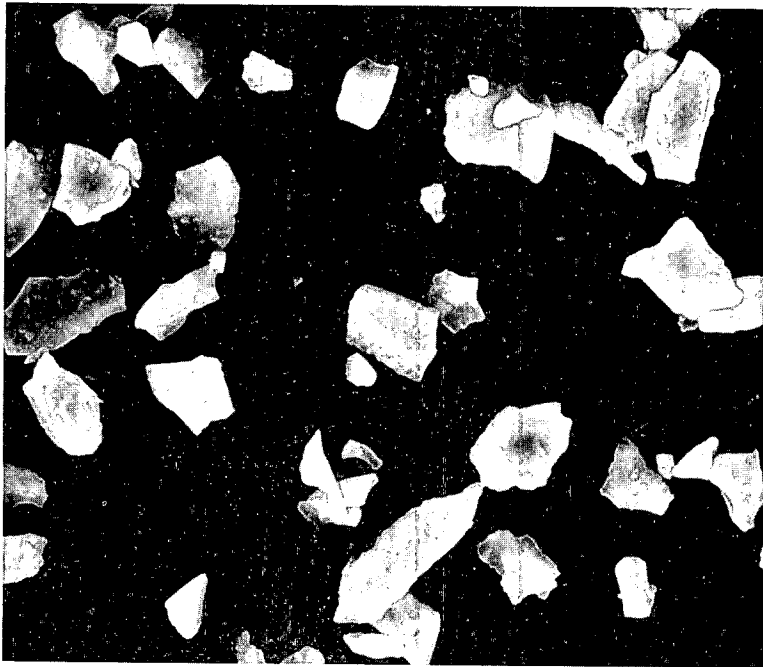


1000X

FIGURE B.1. Photomicrographs of a Sample from the  $<5 \mu$  Fraction of Large Test Specimen 2

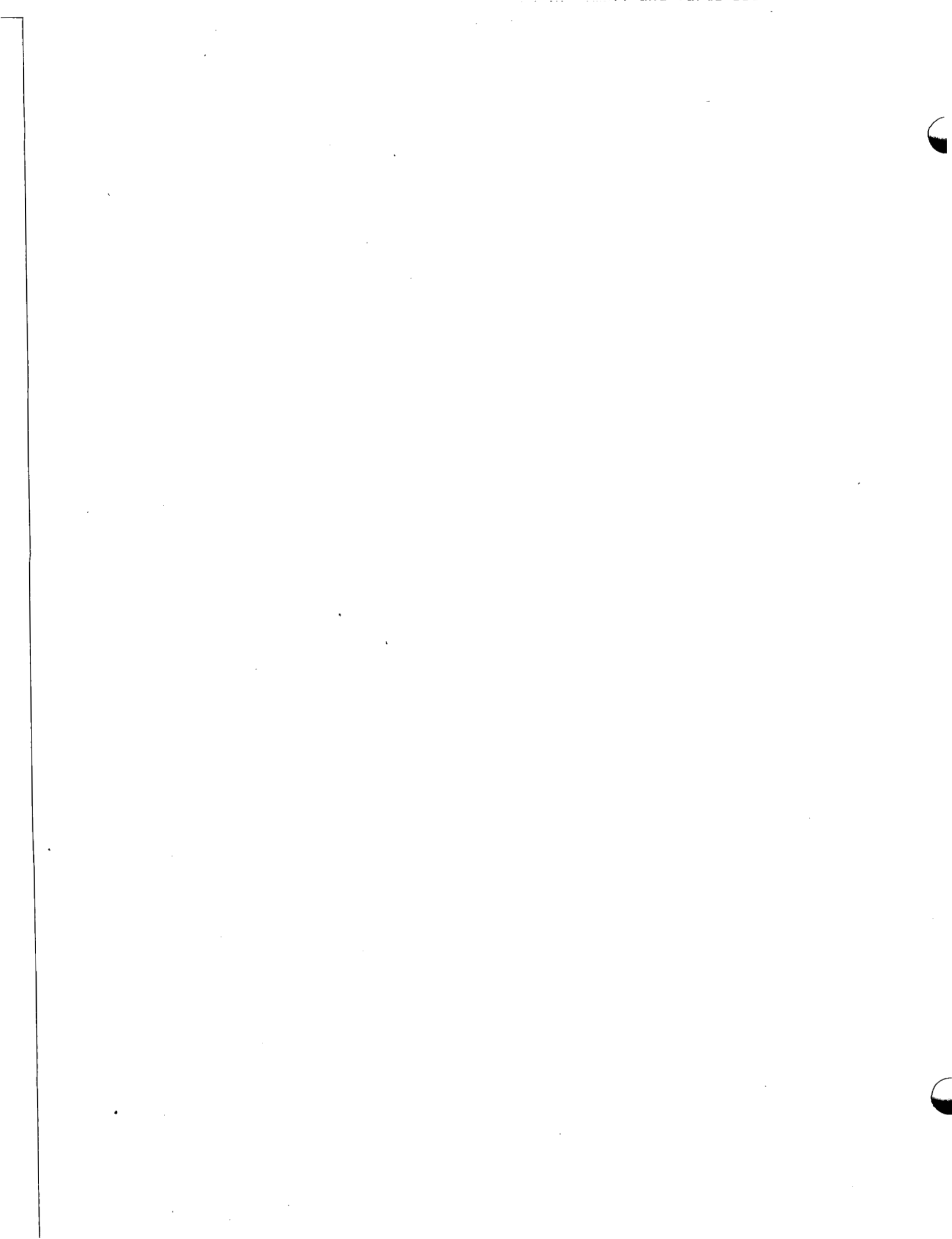


300X



1000X

FIGURE B.2. Photomicrographs of a Sample from the  $<5 \mu$  Fraction of Small Test Specimen 5



DISTRIBUTION

<u>No. of Copies</u>		<u>No. of Copies</u>	
<u>OFFSITE</u>		<u>OFFSITE</u>	
	<u>UNITED STATES</u>		<u>UNITED STATES (contd)</u>
1	<u>ERDA Chicago Patent Group</u> 9800 South Cass Avenue Argonne, IL 60439 A. A. Churm	1	<u>ERDA Idaho Operations Office</u> P.O. Box 2108 Idaho Falls, ID 83401 K. K. Kennedy
1	<u>ERDA Division of Biomedical and Environmental Research</u> Earth Sciences Branch Washington, DC 20545 W. G. Belter	1	<u>ERDA Oak Ridge Operations Office</u> P.O. Box X Oak Ridge, TN 37830 E. H. Hardison
2	<u>ERDA Division of Production and Materials Management</u> Washington, DC 20545 F. P. Baranowski R. K. Heusser	1	<u>ERDA Savannah River Operations Office</u> P.O. Box A Aiken, SC 29801 R. L. Chandler
2	<u>ERDA Division of Reactor Research and Development</u> Washington, DC 20545 Assistant Director for Reactor Technology E. E. Sinclair Chief, Fuel Recycle Branch W. H. McVey	212	<u>ERDA Technical Information Center</u>
		5	<u>Allied Chemical Corporation</u> 550 - 2nd Street Idaho Falls, ID 83401 J. A. Buckham B. R. Dickey E. W. Rhodes C. M. Slansky B. R. Wheeler
8	<u>ERDA Division of Waste Management and Transportation</u> Washington, DC 20545 W. A. Brobst G. H. Daly W. K. Eister O. P. Gormley A. F. Perge F. K. Pittman R. W. Ramsey R. D. Walton	3	<u>Allied-Gulf Nuclear Services</u> P.O. Box 847 Barnwell, SC 29812 B. M. Legler G. R. Bray A. Schneider
		1	<u>Argonne National Laboratory</u> 9700 South Cass Ave. Argonne, IL 60439

<u>No. of Copies</u>		<u>No. of Copies</u>	
	<u>UNITED STATES (contd)</u>		<u>UNITED STATES (contd)</u>
1	<u>Bechtel Corporation</u> 50 Beale Street San Francisco, CA 94119	4	<u>duPont Company, Aiken (ERDA)</u> E. I. duPont DeNemours and Co. Savannah River Laboratory Aiken, SC 29801  C. H. Ice A. S. Jennings L. H. Meyer R. W. Wallace
1	<u>Brookhaven National Laboratory</u> Research Library, Reference Section Information Division Upton, Long Island, NY 11973  M. Steinberg	1	<u>duPont Company, Wilmington (ERDA)</u> E. I. duPont DeNemours and Co. Wilmington, DE 19898  A. A. Johnson
1	<u>C-E Refractories</u> Box 828 Valley Forge, PA 19482  Alfred W. Allen	2	<u>Environmental Protection Agency</u> <u>Parklawn Building</u> 5600 Fishers Lane Rockville, MD 20852  C. G. Meyers
1	<u>Ceramic Engineering</u> University of Illinois Urban, IL 61801  Dr. Dennis O'Boyle	1	<u>Environmental Protection Agency</u> P.O. Box 15027 Las Vegas, NV 89114  B. Mann
1	<u>Combustion Engineering, Inc.</u> Combustion Division Windsor, CT 06095  Jack Parry	1	<u>Environmental Protection Agency</u> 5555 Ridge Ave. Cincinnati, OH 45213  R. E. Landreth
1	<u>Corning Glass Works</u> Technical Staffs Division Corning, NY 14830  M. G. Britton	1	<u>E. R. Johnson Associated, Inc.</u> Suite 317 910 17th N.W. Washington, DC 20006  J. P. McBride
1	<u>Desert Research Institute</u> University of Nevada System Reno, NV 89507  P. Senske	2	<u>Exxon</u> Richland, WA 99352  S. J. Beard L. T. Lakey
1	<u>Dow Chemical Company (ERDA)</u> Rocky Flats Division P.O. Box 888 Golden, CO 80401  D. L. Ziegler		

No. of  
Copies

- UNITED STATES (contd)
- 1 General Electric Company  
175 Curtner Ave.  
(M/C 160)  
San Jose, CA 95125  
R. G. Barnes
- 2 General Electric Company  
Midwest Fuel Recovery Plant  
Route 1, Box 219-B  
Morris, IL 60450  
R. Lambert
- 2 General Electric Company  
Vallecitos Nuclear Center  
Vallecitos Road  
Pleasanton, CA 94566  
W. H. Reas
- 1 Gibbs and Hill, Inc.  
393 Seventh Ave.  
New York, NY 10001  
P. P. DeRienzo
- 3 General Atomic Co.  
P.O. Box 81608  
San Diego, CA 92138  
L. H. Brooks  
J. J. Shefcik  
M. E. Spaeth
- 4 Holifield National  
Laboratory  
(ERDA)  
Central Research Library  
Document Reference Section  
Central Research Library, HNL  
Laboratory Records Dept., HNL  
Laboratory Records Dept.,  
HNL-RC  
P.O. Box X  
Oak Ridge, TN 37830

No. of  
Copies

- UNITED STATES (contd)
- 1 Los Alamos Scientific Laboratory  
(ERDA)  
P.O. Box 1663  
Los Alamos, NM 87544  
C. W. Christenson
- 1 National Academy of Sciences  
Committee of Radioactive Waste  
Management  
2101 Constitution Ave. NW  
Washington, DC 20418  
D. Cyrus Klingsberg,  
Technical Secretary
- 1 National Lead Company  
111 Broadway  
New York, NY 10006  
Stephen Brown
- 2 Nuclear Fuel Services, Inc.  
P.O. Box 124  
West Valley, NY 14171  
J. P. Duckworth,  
Plant Manager  
6000 Executive Blvd., Suite 600  
Rockville, MD 60852  
E. D. North, Director of  
Technical Administration
- 6 Nuclear Regulatory Commission  
Washington, DC 20555  
Division of Materials and Fuel  
Cycle Facility Licensing  
R. B. Chitwood  
Office of Nuclear Regulatory  
Research  
W. E. Vesely

<u>No. of Copies</u>		<u>No. of Copies</u>	
	<u>UNITED STATES (contd)</u>		<u>UNITED STATES (contd)</u>
	<u>Nuclear Regulatory Commission</u> (contd)	3	<u>Union Carbide Corporation (HNL)</u> <u>Chemical Technology Division</u> P.O. Box Y Oak Ridge, TN 37830
	Office of Standards		J. O. Blomeke F. Gera H. W. Godbee
	F. Swanberg		
	I. C. Roberts		
	R. J. Mattson		
	Office of Special Studies	1	<u>University of California</u> Los Angeles 6532 Boelter Hall Los Angeles, CA 90024
	S. H. Smiley		John D. MacKenzie
1	<u>Numec</u> 609 Warren Ave. Apollo, PA 15613		
	C. R. Woods		
1	<u>NYS Atomic and Space</u> <u>Development Authority</u> 230 Park Ave., Room 2425 New York, NY 10017	1	<u>Atomic Energy of Canada Ltd.</u> W.N.R.E. Pinawa, Manitoba, ROE 1LO CANADA
	J. G. Cline, General Manager		P. J. Dyne
1	<u>Penberthy Electromelt</u> 631 S. 96th Street Seattle, WA 98108	1	<u>Atomic Energy Research</u> <u>Establishment</u> Harwell, Didcot, Berks. ENGLAND,
	L. Penberthy		K. D. B. Johnson
1	<u>Pennsylvania State University</u> <u>Materials Research Laboratory</u> University Park, PA 16802	1	<u>United Kingdom Atomic Energy</u> <u>Authority</u> Risley, ENGLAND
	G. J. McCarthy		D. W. Clelland
3	<u>Sandia Laboratories</u> Albuquerque, NM 87107	2	<u>Centre de Marcoule</u> B. P. 106 30 - Bagnols S/Seze FRANCE
	R. L. Hagengruber		R. Bonniaud
	R. W. Lynch		
	A. C. Zuppero		
1	<u>Sandia Laboratories</u> <u>Division 1544</u> Albuquerque, NM 87115	2	<u>Centre d'Etudes Nucleaires</u> <u>de Fontenay-aux-Roses</u> Boite Postale 6 92 - Fontenay-aux-Roses FRANCE
	T. A. Duffee		J. Sauteron Y. J. Sousselier

No. of  
Copies

No. of  
Copies

<u>No. of Copies</u>	<u>FOREIGN (contd)</u>	<u>No. of Copies</u>	<u>FOREIGN (contd)</u>
1	<u>Bundesministerium für Bildung und Wissenschaft</u> D53 Bonn 12 Postfach 120124 GERMANY  R. P. Randl	1	<u>NUKEM</u> 6450 Hanau P.O. Box 869 W. GERMANY  Dr. Hartmut Witte
1	<u>Hahn-Meitner-Institut</u> 1 Berlin 39 Glienickerstr. 100 GERMANY  Hans W. Levi	1	Dr. H. F. Ramdohr c/o Friedrich Uhde GmbH 46 Durtmund Deggingstre 10-12 GERMANY
2	<u>Institut für Chemische Technologie</u> Kernforschungsanlage Julich GmbH D517 Julich Postfach 365 GERMANY  E. R. Merz K. H. Tattay	<u>ONSITE</u>	
1	<u>Laboratorio di Ingegneria Sanitaria</u> Via Anguillarese km 1 + 300 Roma, ITALY  Willy Bocola	1	<u>ERDA Richland Operations Office</u> Programs Division
2	<u>International Atomic Energy Agency</u> Kartner Ring 11 P.O. Box 590 A-1011, Vienna, Austria	2	<u>ERDA Richland Operations Office</u> Production and Waste Management Programs Division  O. J. Elgert R. B. Goranson
1	<u>MGH/GWK/Wiederacifurbeitung - Sanlage/WAK</u> Karlsruhe, GERMANY  W. A. Issel	1	<u>ERDA Richland Operations Office</u> Safety and Quality Assurance Division  J. H. Straub, Director
2	<u>Nuclear Research Center</u> Waste Management Dept. D75 Karlsruhe Weberstr. 5 GERMANY  W. Krause	11	<u>Atlantic Richfield Hanford Co.</u>  H. Babad L. E. Brownell R. E. Isaacson D. C. Nelson R. C. Rowles H. P. Shaw W. W. Shultz/M. J. Kupfer R. J. Thompson J. H. Warren D. D. Wodrich File Copy

No. of  
Copies

2 United Nuclear Industries, Inc.

2 Westinghouse Hanford Company

C. R. Cooley  
G. L. Richardson

58 Battelle-Northwest

E. L. Alpen  
W. Ambrose  
R. J. Bashor  
J. W. Bartlett  
J. L. Bates  
W. F. Bonner  
D. J. Bradley  
C. Burkholder  
J. R. Carrell  
N. E. Carter  
T. D. Chikalla  
O. Cloninger  
G. M. Dalen  
J. W. Finnigan  
A. Garrett  
T. A. Golding  
J. D. Kaser  
L. V. Kimmel

R. P. Marshall  
J. L. McElroy (4)  
J. E. Mendel  
E. S. Murphy  
R. E. Nightingale  
D. E. Olesen  
P. J. Pelto  
A. M. Platt  
W. A. Ross (4)  
K. J. Schneider  
L. C. Schwendiman  
T. H. Smith (10)  
S. L. Sutter  
J. M. Taylor  
E. C. Watson  
L. D. Williams  
W. K. Winegardner  
Technical Information (5)  
Technical Publications (3)